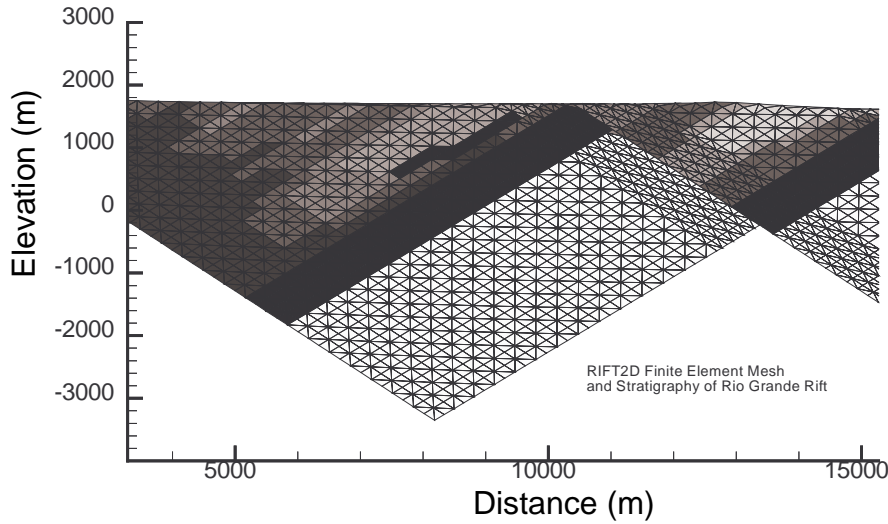


**RIFT2D: A FINITE ELEMENT MODEL FOR SIMULATING
TWO-DIMENSIONAL GROUND WATER FLOW, HEAT,
SOLUTE MASS TRANSPORT, AND PETROLEUM GENERATION
WITHIN EVOLVING SEDIMENTARY BASINS**



¹Mark Person, ²Chris Neuzil, ³ Paul Hsieh, ⁴Brian Mailloux,

⁵Elise Bekele, ⁶John Swenson, and ⁷Peter Eadington

¹The University of Minnesota, Department of Geology & Geophysics, Minneapolis, MN

²US Geological Survey, Reston, VA

⁴Princeton University, Department of Geological & Geophysical Sciences

³US Geological Survey, Menlo Park, CA

⁵CSIRO, Land & Water Division, Perth WA

⁶The University of Minnesota, Department of Geology, Duluth, MN

⁷CSIRO, Petroleum Resources Division, Perth WA

TABLE OF CONTENTS

TABLE OF CONTENTS	2
LIST OF FIGURES.....	4
LIST OF TABLES.....	6
ABSTRACT.....	8
ACKNOWLEDGMENTS.....	9
GUIDE TO USING THIS DOCUMENT.....	10
CHAPTER 1: INTRODUCTION.....	11
CHAPTER 2: MATHEMATICAL MODEL....	19
GROUND WATER FLOW	19
HEAT TRANSFER.....	24
SOLUTE TRANSPORT.....	26
PETROLEUM GENERATION.....	27
Vitrinite Reflectance.....	29
BASIN DEFORMATION.....	33
Sediment Deformation without Faulting..	36
Fault Block Rotation and Translation with Faulting....	36
CHAPTER 3: NUMERICAL METHODS.....	40
FINITE ELEMENT SOLUTION OF GROUND WATER FLOW AND HEAT TRANSFER EQUATIONS.....	40
FINITE DIFFERENCE SOLUTION OF SEDIMENT CONSOLIDATION EQUATION.....	44
MODIFIED METHOD OF CHARACTERISTICS SOLUTION OF SOLUTE TRANSPORT EQUATION..	51
NUMERICAL INTEGRATION OF PETROLEUM GENERATION EQUATIONS.....	54
NUMERICAL IMPLEMENTATION.....	56
RIFT2D PROGRAM STRUCTURE.....	57
CHAPTER 4: SYSTEM CONCEPTUALIZATION AND PROPERTIES FOR RIFT2D SIMULATIONS	61
INTRODUCTION.....	61
CONCEPTUALIZATION FOR RIFT2D.....	62
Hydrogeologic Architecture.....	62
SYSTEM PROPERTIES	63
Permeability.....	63
Deformation properties and porosity	73
Thermal response coefficient.....	79
Fluid-Density Variations in Basins, Thermal and Solute Mass Transport Parameters.....	81
Parameters for Petroleum Generation.	86
BOUNDARY CONDITIONS	86

List of Figures

Figure Number	Figure Caption	Page Number
1.1	Computed heads, groundwater flow vectors, and temperatures in an evolving basins using RIFT2D.	13
2.1	Schematic diagram depicting principal directions of permeability for sedimentary layers and fault zone.	23
2.2	Groundwater viscosity (A) and density (B) as a function of temperature and salinity calculated from equation of state used in RIFT2D model....	25
2.3	Observed and computed oil generation within organic rich sediments....	28
2.4	Changes in oil (A) and gas (B) density as a function of pressure and temperature.	31
2.5	(A) Schematic diagram illustrating fault and flexurally controlled subsidence and (B) ROTFLAG options for RIFT2D data files.....	34
2.6	Schematic diagram indicating how parameter ICASE is used by RIFT2D to control the erosion, uplift, and deposition of a sedimentary basin....	35
2.7	Schematic diagram depicting domino-style fault block rotation and imposition of specified heat flux boundary condition at base of solution domain.....	39
3.1	(A) Schematic diagram illustrating finite element discretization of fault blocks using three- and four-node triangular elements. (B) Shape functions for the three- and four-node elements.....	41
3.2	Schematic diagram illustrating changes in element thickness due to porosity changes along a nodal column of a RIFT2D finite element mesh	50
3.3	Schematic diagram illustrating particle tracking algorithm used in Modified Method Of Characteristics numerical scheme employed by RIFT2D to solve the solute transport equation.....	53
3.4	RIFT2D flow chart.....	58
4.1	Published range of permeability of sedimentary and crystalline rocks....	64
4.2	Effect of scale on permeability measurements made in fractured rocks...	68
4.3	Permeability verses porosity of carbonate (A), shales (B), and sandstones (C) rocks.....	69
4.4	Comparison of laboratory and in situ measurements of the moduli of compressibility of sedimentary rocks.....	76
4.5	Porosity-depth data for carbonates (A), shale (B), and sandstone (C)....	77
4.6	Effect of scale on longitudinal dispersion	85
4.7	Variations in salinity with depth in select North American Basins	91
6.1	(a) Jurassic Tank experimental strata and (b) RIFT2D mesh and (b) hydrostratigraphy at completion of example simulation.....	112
6.2	Evolution of RIFT2D finite element mesh at (a) 4.2 Ma and (b) and 12.7 Ma.....	114
6.3	Sea level fluctuations used in example simulation 1 to illustrate implementation of tectonic time periods in RIFT2D.....	120
6.4	Computed hydraulic heads (in m) from RIFT2D at 6.4 (A), 12.7 (B), and 17 (C) million years since start of simulation from first example simulation.....	121
6.5	Computed temperatures (°C) from RIFT2D at 6.4 (A), 12.7 (B), and 17 (C) million years since start of simulation.....	124
6.6	Computed vitrinite reflectance (%) and groundwater velocity vectors from RIFT2D at 6.4 (A), 12.7 (B), and 17 (C) million years since start of simulation.....	125
6.7	Computed solute concentration for example 1.....	126

6.8	RIFT2D Finite element mesh from example 2 at 2.5 (A) and 5.0 (B) million years after the onset of subsidence. In this example two fault blocks are separated by a vertical fault at 5000 m along the horizontal axis.....	129
6.9	Hydrologic and thermal boundary conditions used in example 2.....	133
6.10	Computed heads (m) and temperature (°C) from example 2.....	134
6.11	Computed solute concentration from example 2.....	135
6.12	Evolution of finite element mesh at 0, 20, and 35 million years using domino style fault block rotation.....	140
6.13	Calculated hydraulic heads and temperatures in example 2	141
7.1	Comparison of excess head generation (m) and porosity using RIFT2D and BASIN2 (Bethke and Corbet, 1988, Fig. 3C).....	145
7.2	Comparison of RIFT2D and analytic solution of Gibson (1958) using a hydraulic conductivity of 10-10 m/s, a specific storage of 0.0021 m ⁻¹ , and a sedimentation rate of 0.0005 m/yr.....	147
7.3	(A) Finite element mesh and (B) comparison of computed temperatures (oC) using RIFT2D (solid lines) to published hydrothermal model results from Smith and Chapman (1983, Fig4C; dashed lines).....	148
7.5	Comparison of simulated transformation ratio of Types I, II, and III kerogen using RIFT2D with published model results presented in Tissot et al. (1987; Fig 26A).....	151
7.5	Geometry and boundary conditions used in HYDROCOIN case 5.....	152
7.6	Comparison of simulated solute concentration (mass fraction) using MOCDENSE and RIFT2D. The simulations are intended to reproduce the HYDROCOIN Case 5 example reported in Konikow et al. (1997; Fig. 4).....	154
8.1	Window which appears on start-up of RIFT2D preprocessor.....	156

List of Tables & Plates

Table Number	Table Title	Page Number
1.1	Transport Processes Represented by Select Basin Models.....	16
Plate-1	Matrices for Finite Element Approximation to Flow Equation using three node triangular elements	45
Plate-2	Matrices for Finite Element Approximation to Flow Equation using four node triangular elements	46
Plate-3	Matrices for Finite Element Approximation to Heat Transfer Equation using three node triangular elements	47
Plate-4	Four Node Finite Element Approximation to Heat Transfer Equation using four node triangular elements	48
3.1	RIFT2D Subroutine Description.....	59
4.1	Rock Permeability Parameter Values used in Modeling Studies.....	72
4.2	Compressibility Coefficients for Sedimentary Rocks.....	80
4.3	Thermal Properties of Fluid and Solid Phase.....	82
4.4	Molecular Diffusivity of Chemical Components in Ground Water.....	84
4.5	Kinetic Parameters for Types I, II and III Kerogen.....	87
5.1	Description of RIFT2D Input/Output data files.....	94
5.2	RIFT2D Array Dimensions.....	96
5.3	Simulation Control Parameters used in RIFT2D Data Files.....	96
5.4	Graphical output parameters specified in RIFT2D data files.....	98
5.5	Material Properties assigned to a hydrostratigraphic Unit in RIFT2D Data File.....	100
5.6	Fault Block Rotation and Tectonic Time Period Data used by RIFT2D...	102
5.7	Subsidence Boundary Condition information for RIFT2D.....	104
5.8	Hydrologic, Thermal, and Solute Boundary Condition Information for First Tectonic Time Periods used by RIFT2D.....	106
5.9	New boundary condition information for Subsequent Tectonic Time Periods.....	110
6.1	RIFT2D subsidence data along select columns	116
6.2	Material tags used to represent sand and shale hydro-stratigraphic units in first example.....	118
6.3	Petrophysical and Geochemical Properties used to Represent Sand and Shale Hydrostratigraphic Units in Example 1.....	118
6.4	Simulation Control Paramters from Second RIFT2D Example Data File..	128
6.5	RIFT2D subsidence data along select columns for Example 2.....	128
6.6	Material tags used to represent sand and shale hydrostratigraphic units in second example.....	131
6.7	Petrophysical and Geochemical Properties used to Represent Fault Block And Fault Zone Units in Example 2.....	131
6.8	Rotation Information used in Domino-Model.....	136
6.9	Simulation Control Parameters used in Domino-Model.....	136
6.10	Material tags used to Represent Pre- and Syn-rift hydro-stratigraphic units in example 3.....	139
6.11	Petrophysical and Geochemical Properties used to Represent Fault Block and Fault Zone Units in Example 3 ..	140

Table Number	Table Title	Page Number
7.1	Validation Simulation Descriptions.....	141
8.1	RIFT2D variables used by TECPLOT.....	168

ABSTRACT

RIFT2D is a two-dimensional (cross-sectional) finite element model that simulates groundwater flow, heat transfer, solute transport processes such as brine migration, and petroleum generation within sedimentary basins. It can be used to simulate both mature and evolving basins over human (up to 10^3 years) or geologic (10^4 to 10^8 years) time scales. The model is capable of simulating fluid pressure patterns and flow due to sediment compaction and decompaction, fluid density variations, and gradients in water-table topography as well as fluid sources related to petroleum generation. RIFT2D solves coupled transport equations for ground water flow and heat transfer using the finite element method. Heat transfer by both conduction and convection are accounted for. For solute transport, a two-dimensional, advective-dispersive equation is solved using a modified method of characteristics algorithm. First-order rate-kinetic equations representing oil and gas formation are solved using numerical integration techniques. RIFT2D is also capable of computing the mass of oil, gas, H₂O, and CO₂ generated during burial from source rocks composed of types I, II, and III kerogen. For type III kerogen, vitrinite reflectance is also calculated. Oil migration can be inferred from computed oil heads and oil velocity vector maps. During compaction or decompaction RIFT2D is capable of representing vertical strain and the evolving grid can deform in response to porosity changes. Changes in porosity that accompany deformation, and the resulting changes in sediment permeability and compressibility are tracked. While RIFT2D is a powerful tool for simulating fluid flow within sedimentary basins of many types, it is uniquely suited to continental rift systems; basin evolution can be accommodated by vertical subsidence or uplift along nodal columns or by domino-style fault block rotation. When rift-style faulting is invoked, computational limitations prevent deforming the finite element grid during compaction and decompaction, but the effects of compaction and decompaction on pressure and basin properties are still accounted for.

This manual provides a detailed description of the model's governing equations and numerical solution methods, and provides a tutorial on implementing the model, model validation results, input file construction tips, and examples. Several sample-input files as well as graphical output from RIFT2D are provided in an appendix. RIFT2D can be used with an interactive graphical pre-processor/post-processor (RIFT2DI), available separately, to allow the RIFT2D user to quickly develop input files, run the model, and visualize the results. The code also can create output files formatted for TECPLOT visualization software.

ACKNOWLEDGMENTS

The development of RIFT2D has been supported by a number of grants from the Department of Energy (DE-AC22-9491008), the National Science Foundation (EAR-93-04873; OCE-9731494), The Petroleum Research Fund administered by the American Chemical Society (PRF 24184-AC8), and the Orpha & George Gibson Hydrogeology Endowment at the University of Minnesota. We thank Dan Hayba, Ming-Kuo Lee, and Alica Wilson for their review of this document.

GUIDE TO USING THIS DOCUMENT

This manual presents a detailed discussion of both the theory and implementation of the basin flow and transport simulator RIFT2D. *Chapter 1* provides background information, and an overview of both the transport and geochemical processes represented by RIFT2D and the model's intended use and limitations. *Chapter 2* presents the transport equations solved by RIFT2D. *Chapter 3* describes the finite element and finite difference solution algorithms used to solve the transport equations. *Chapter 4* gives a description of the input variables used in RIFT2D input files. *Chapter 5* discusses step by step instructions for constructing RIFT2D input files including guidelines for estimating basin-scale rock and fluid properties and choosing boundary conditions. *Chapter 6* discusses three RIFT2D input files, which explore different transport options available in RIFT2D. *Chapter 7* presents four additional RIFT2D simulations which are intended to reproduce results from published studies and therefore partially validate the numerical algorithms used in the code. Because many of the input files described in Chapter 7 reproduce results from published studies, they also serve to partially validate the RIFT2D transport algorithms. These along with the input files described in Chapter 6-7 can serve as templates to help users generate their own input files. The user can also generate RIFT2D input files using the public domain pre- and post-processor RIFT2DI, although some limitations regarding RIFT2D options which can be specified within the pre-processor exist. *Chapter 8* briefly describes how the preprocessor can be used to generate RIFT2D input data files and display results. In addition, this chapter provides tips for displaying RIFT2D output using TECPLLOT. *Appendix 1* presents a derivation of the ground water flow equations, as they are of a slightly different form than usually encountered. *Appendix 2* contains a description of variables used in the transport equations described in Chapter 2. *Appendix 3* describes the variables used in the input file to RIFT2D. Data files and source code described in this manual are available on a compact disk which accompanies this manual.

CHAPTER 1 – INTRODUCTION

Fluid flow and transport are now recognized as fundamentally important phenomena that affect, and in turn are affected by, processes occurring in sedimentary basins. As a result, numerical models that are capable of simulating subsurface fluid flow, heat transfer, and chemical mass transport are becoming increasingly important tools for Earth scientists studying a wide range of transport-limited geologic and hydrologic phenomena within sedimentary basins and elsewhere. These include heat flow anomalies, hydrothermal ore genesis, sediment diagenesis, faulting and deformation, and petroleum generation and migration as well as hydrodynamic phenomena such as anomalous fluid pressures. Groundwater hydrologists also are finding that many water-related problems, including some pertaining to water-supply and waste disposal, must be addressed by examining flow phenomena at large spatial and temporal scales, particularly in sedimentary basins. Because numerical models can represent geologic processes that occur over geologic time scales and continental length scales, they complement field- or laboratory-based investigations that are necessarily much more limited in their temporal or spatial scope.

We were motivated to release RIFT2D by a perceived need for a capable and broadly applicable basin flow simulator in the public domain. Moreover, there is an entire class of sedimentary environments, rift basins, in which the fluid flow regimes during their development could not easily be studied because the effects of ongoing fault displacement could not be incorporated into simulations. RIFT2D is intended to serve as a broadly applicable basin flow and transport simulator with the special capability of handling the complex geologic framework changes that occur in evolving rift basins.

RIFT2D was originally developed by Person and Garven (1992; 1994) but has been improved significantly by the co-authors to include fault block kinematics (Wieck et al. 1995; Mailloux et al., 1999), petroleum generation (Person et al. 1995; Toupin et al. 1996), and effects of compaction and decompaction due to sedimentary deposition and erosion. Some of the original ground water flow, heat transport and matrix inversion subroutines were modified versions of the steady-state basin model of Garven and Freeze (1984a,b).

RIFT2D is written in Fortran 90 and should run without modification on most computing platforms. Output from the model, including computed hydraulic heads, temperatures, ground water velocity vectors, and the mass of oil and gas generation can be displayed using the commercial software package TECPLLOT visualization software. A

public domain pre- and postprocessor (RIFT2D_INTERACTIVE) can also be used to generate RIFT2D data sets and graphically display model output.

Capabilities of RIFT2D. RIFT2D is a two-dimensional numerical model that can simulate topography-, density-, compaction-/decompaction-, and fluid source-generated fluid pressure and flow within evolving sedimentary basins and other subsurface environments. RIFT2D also simulates the transport of heat and solutes and tracks the changing temperature and concentration patterns that result. Fluid sources are computed as the mass of petroleum, gas, water, and CO₂ generated from kerogen with burial and heating. Changes in overburden from deposition and erosion as well as changes in effective stress brought on by evolving fluid pressures are tracked and used to deform the finite element mesh. The deformations feed back into the flow computations through corresponding changes in porosity, permeability, and porous matrix compressibility. Note, however, that *the finite element mesh is not permitted to deform when displacements are occurring along faults*. In this case, porosity, permeability, and compressibility are still varied as if the deformation occurred. This limitation is dictated by programming difficulties that arise if both deformation and active displacement along faults are permitted to occur.

A sense of the capabilities of RIFT2D can be obtained from inspection of Figure 1.1, which presents simulations of two different half grabens filling with sediment having significantly different permeability distributions. The basin on the left side of Figure 1.1 (Fig. A, C, and E) contains sediments which are relatively permeable (10^{-14} m^2), homogeneous and anisotropic. The basin simulation on the right side of Figure 1.1 (B, D, and F) has a permeability distribution which decreases from 10^{-14} m^2 near the basin margin (representing an alluvial fan) to 10^{-17} m^2 in the center of the basin (representing a lacustrine facies). Figure 1.1 displays computed heads (A, B), flow velocity vectors (C, D), and temperatures (E, F) in the two different half grabens. In these simulations, the half grabens were allowed to evolve over a period of 40 million years using an average subsidence/sedimentation rate of 10^{-4} m/yr . Note that hydraulic head rather than pressure is used. RIFT2D incorporates a variable density form of Darcy's Law written in terms of head to accommodate driving forces due to fluid density variation. Thus, for example, free convection can be simulated as seen in Figure 1.1C. Heat transfer by both conduction and convection is simulated (Figures 1.1E and 1.1F). Three flow types are apparent in Figures 1.1A through 1.1D: topographically-driven (often called "gravity-driven"), density-driven, and compaction-driven. Not shown in the simulations is flow driven by generation of petroleum and other fluids from kerogen, a process represented in RIFT2D using a suite of first-order rate-kinetic equations. All four of these driving

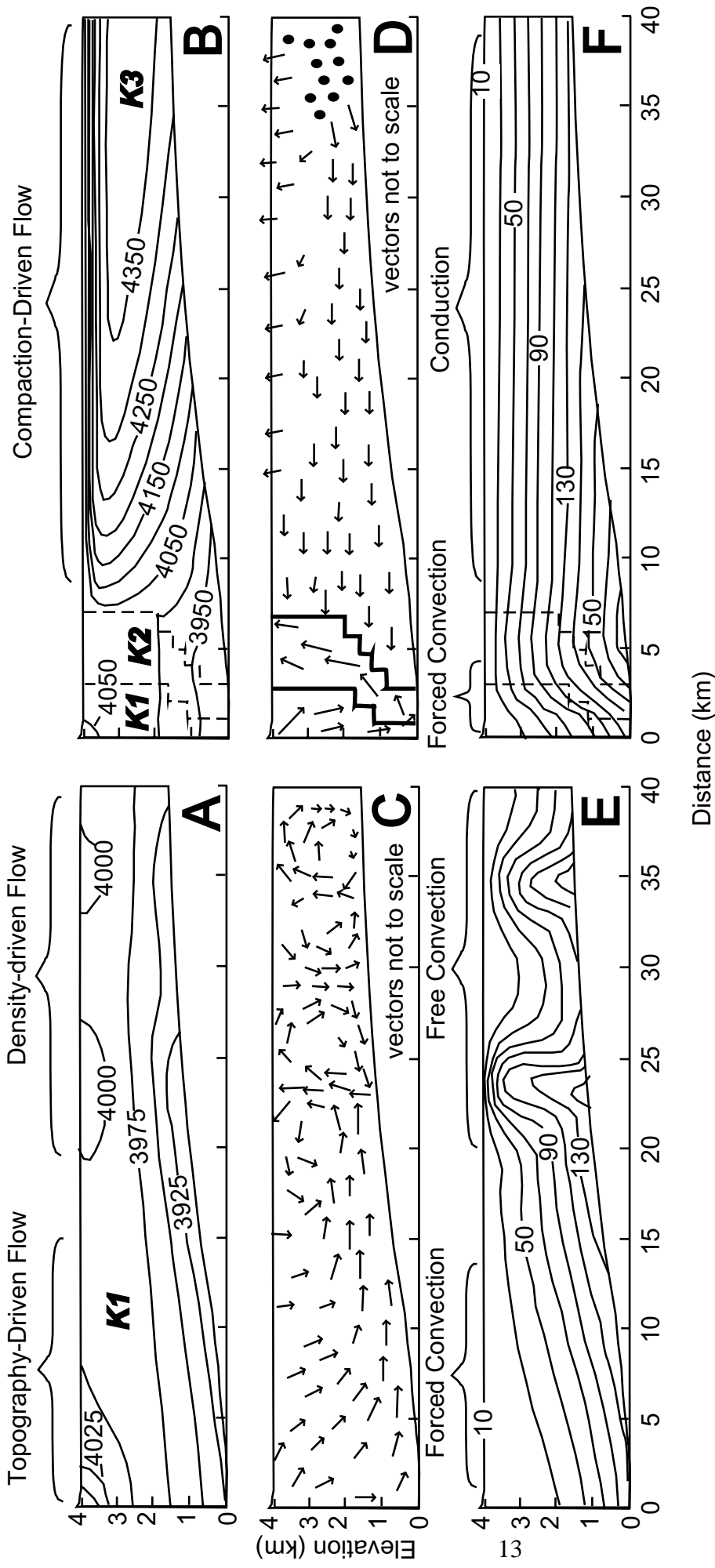


Figure 1.1 Computed heads (in m; A, B), groundwater flow vectors (not to scale; C, D), and temperatures (in °C; E, F) in two evolving basins with different permeability distributions. Both models were developed using an early version of RIFT2D (after Person and Garven, 1994). These output provide quantitative illustration of topography-, density-, and compaction driven flow systems induced by differences in permeability and sedimentation rates. The horizontal permeability of hydrostratigraphic units K1, K2, and K3 are 10^{-14} , 10^{-15} , and 10^{-17} m². K1 and K2 have a permeability anisotropy of 10. K3 has a permeability anisotropy of 100. The basin was formed over a period of 40 million years with an average subsidence rate of 0.0001 m/yr. A water table head boundary condition, which varied between 4100 and 4000 m, was imposed along the top of these basins. No fluid flow boundaries were imposed along all other edges. In this example, a specified temperature of 10 °C was specified along the water table while a heat flux of 60 mW/m² was imposed along the base of the sedimentary pile.

forces for flow may be present in a single system and each may dominate a different portion of the system. RIFT2D accounts for all simultaneously. Decompaction-driven flow, due to erosional unburdening in old basins, is also accounted for. Not illustrated in Figure 1.1 is RIFT2D's ability to simulate solute transport. The advective-dispersive transport equation for solute transport is solved using a modified method of characteristics algorithm.

In sum, RIFT2D accounts for and tracks subsidence and sedimentation, uplift and erosion, faulting, and petroleum generation as well as heat and solute transport. It computes deformation of the solid matrix (sediments or rocks), deforms the computational mesh (except in special cases) and varies porosity, permeability, and porous matrix compressibility accordingly.

A variety of boundary conditions can be specified in RIFT2D to best represent various subsurface environments in basins and other terrains. The upper and lower boundaries of the simulation domain can accommodate specified head or fluid fluxes, specified temperature or heat fluxes and specified solute concentrations. Side boundary conditions are specified as no flow because basin simulations frequently use lateral boundaries located by symmetry considerations, specify lateral boundaries far from the area of interest, or feather out laterally. Thus, RIFT2D can emulate most of the important flow, transport, and deformation processes that occur in sedimentary basins on time scales up to tens or hundreds of millions of years. The reader interested in learning more about the capabilities of RIFT2D and the types of hydrogeologic problems which it can be applied to should turn to Chapter 5 (Implementing RIFT2D).

Limitations of RIFT2D. Although RIFT2D is a broadly capable basin simulator, like all numerical models it has limitations that should be clearly understood. Creating a basin simulator that emulates all potentially important processes in basins would be difficult to do, and such a simulator would also be difficult to use. Thus all models simplify the processes of interest to make their analysis tractable and ignore others. The processes included in any model are chosen subjectively based on the authors' objectives. Before using any model, a user must carefully determine whether it describes the phenomena of interest in a particular problem. RIFT2D has three primary limitations that could preclude its use in certain studies. *First*, it is a single (liquid) phase model and does not simulate flow or transport in other liquid phases, such as petroleum, or in gas phases. Although petroleum generation and its effect (as a fluid source) on the flow system can be simulated, and the direction of movement of a petroleum phase can be inferred from computed oil heads and oil velocity vector maps, the flow of petroleum as a separate

phase cannot be simulated. Likewise, multiphase phenomena such as the trapping of oil or gas by capillary effects cannot be simulated. *Second*, transport of only single solutes or

TABLE 1: Transport Processes Represented by Select Basin Models

Model Name	Groundwater Flow				Solute Transport	Heat Trans-port	Oil Gen.	Two-Phase Flow	Fault Kine-matics
	Density -driven	Topography -driven	Compaction - driven	Oil Generation					
RIFT2D ¹	✓	✓	✓	✓	✓	✓	✓		✓
OILGEN ²	✓	✓			✓	✓			
BASIN2 ³	✓	✓	✓		✓	✓	✓		
MODFLOW ₄		✓							
THEMIS ⁵			✓			✓	✓	✓	
GBRN ⁶									
RIFTRTM ⁷									

¹Person and Garven (1992, 1994), Toupin et al. (1996), Person et al. (1995), Mailloux et al. (1999) ²

²Garven et al. (1993), Garven and Freeze (1984a,b), Garven (1985, 1989), Garven and Freeze (1984a,b), Garven (1985, 1989)

³Bethke et al. (1993), Bethke (1986a), Bethke et al. (1988), Harrison and Summa (1991), Bethke (1986b), Bethke et al. (1991)

⁴Bredehoeft and Belitz (1988)

⁵Burrus and Audebert (1988), Ungerer et al. (1990), Burrus et al. (1991)

⁶Roberts et al. (1995)

⁷Orteleva et al. (1987)

mixes of solutes is simulated; mixing of distinct dissolved constituents from different sources, for example, cannot be simulated. Similarly, reactions between dissolved constituents or with the porous medium are not determined. Chemical reactions involved in sediment diagenesis or ore deposition, for example, cannot be simulated. *Third*, RIFT2D assumes that only vertical deformation occurs in the porous medium. RIFT2D tracks vertical deformation and porosity changes associated with sedimentation/compaction or erosion/decompaction, but it cannot explicitly account for the effects of significant lateral deformation such as might occur in a tectonically active setting. Thus lateral deformation itself and resulting anomalous pressures are not simulated.

A number of basin simulators are now available, several of which are listed and compared with RIFT2D in Table 1.1. We have attempted to make Table 1.1 as complete as possible, however, some basin flow models may have been omitted. In addition, there are numerous more generic simulators for porous medium flow, transport, and related phenomena than can be used to study narrower aspects of basin hydrogeology and that are not listed.

Applying RIFT2D. While models such as RIFT2D are powerful tools for studying transport processes within basins, they are limited by the quality of information available about the geometry, properties and history of the systems they are applied to. It is important to keep in mind that basin-scale models of flow and transport processes are difficult, if not impossible, to fully calibrate due to the dearth of information on rock properties and stratigraphic architecture (Konikow and Bredehoeft, 1992; Oreskes et al., 1994) as well as uncertainty regarding present and past hydrologic, thermal and chemical boundary conditions. Thus extreme caution should be exercised in using RIFT2D model results in a predictive sense. More often than not, basin models such as RIFT2D are best suited for conceptualizing and for testing conceptual models.

There are a number of ways that numerical simulations of basin flow and transport can be constrained. For example, estimates of the permeability of various units in a basin should be refined, where possible, by permeability data from the region in question. The permeability of sediments and rocks of various types varies over a tremendous range. Even within a lithologic type, shales for example, permeabilities vary sufficiently to allow several very different interpretations of basin behavior. Where possible, basin models should also be used in conjunction with field and laboratory data that help constrain basin transport processes. Such data might include sediment remagnetization data (McCabe and Elmore, 1989), analysis of elemental and stable isotope patterns in diagenetic cements (Hay et al., 1988; Gregg et al., 1993), radioisotope dating of ore minerals (Brannon et al.,

1991) and authigenic clays (Elliot and Aronson, 1993), and apatite fission track analysis (Arne et al., 1990). These rock-based "paleoflow meters" can provide critical tests of conceptual models of basin processes.

CHAPTER 2 – MATHEMATICAL MODEL

The governing equations used by RIFT2D to represent transport processes, sediment compaction, decompaction, and petroleum generation within sedimentary basins are presented in this chapter. Because the groundwater flow equation used in RIFT2D is in a slightly different form than that typically seen, a more complete derivation of equation (1) is presented in Appendix 1. The transport equations are derived following a continuum approach, combining expressions of conservation of fluid mass, solute mass, and thermal energy with constitutive relationships such as Darcy's Law for ground water flow, Fourier's Law for heat transfer, and Fick's Law for solute transport (Turcotte and Schubert, 1982; de Marsily, 1986). A series of first-order rate kinetic equations are used to describe petroleum generation within organic rich sediments and are also presented here.

GROUND WATER FLOW

Energy that drives fluid flow within sedimentary basins is derived from a number of mechanisms that include sediment loading, topography in the water-table elevation ("gravity-driven" flow), lateral variations in fluid density, tectonic deformation, the production of petroleum and other fluids, and diagenetic processes. The importance of various flow-driving mechanisms usually varies during basin evolution, depending on which geologic processes are active and on system properties such as permeability, porosity, and lithology. Reviews of the roles of different flow-driving mechanisms are provided by Bethke (1989), Garven (1995), Neuzil (1995), and Person et al. (1996).

Ground water flow systems within sedimentary basins often have hydrodynamic, mechanical, thermal, and chemical mass transfer processes that are all closely coupled. For example, within rapidly subsiding basins near lithostatic fluid pressures often support a significant proportion of the overlying sediment load, maintaining relatively high porosities at depths of several km (Hart et al., 1995). In other settings, increases in temperature with depth in permeable sediments and sedimentary rocks create density instabilities that induce free convection (Evans and Nunn, 1989). Interactions like these necessitate greater complexity in basin-scale hydrogeological models than in those typically required to simulate ground water flow in shallow aquifers over human time scales.

The ground water flow equation solved by RIFT2D considers the effects of sediment loading or unloading, water-table topography (or hydraulic head at the upper boundary), and fluid-density differences resulting from spatial variations in either salinity or temperature. It can be written as

$$\nabla_x [K\mu_r \rho_f \nabla_x (h + \rho_r)] = S_s \rho_o \frac{\partial h}{\partial t} - \frac{\rho_f}{K' \rho_s g} \frac{\partial \sigma_v}{\partial t} - \phi \rho_f \Lambda \frac{\partial T}{\partial t} + (\rho_k - \rho_{oil}) \frac{\partial T_r}{\partial t} \quad (2.1)$$

where ∇_x is the gradient operator, \mathbf{K} is the hydraulic conductivity tensor, h is hydraulic head, T is temperature, Λ is a thermal response coefficient, T_r is the kerogen transformation ratio, ρ_{oil} is oil density, ρ_k is the density of kerogen, σ_v is the vertical total stress, K' is the one-dimensional deformation modulus of the medium, μ_f is the viscosity of water, ρ_o is the density of water at the standard state (10 °C, 0.0 mg/l, and 0.0 MPa), ρ_s is the sediment density, ρ_r is the relative density (defined below), μ_r is the relative viscosity (also defined below), S_s is the specific storage, ρ_f is the density of ground water, and ϕ is porosity. Specific storage is defined by

$$S_s = \rho_f g \left[\frac{1}{K'} + \frac{\phi}{K_f} \right] \quad (2.2)$$

where K_f is the fluid modulus of compressibility. The specific storage is discussed in more detail in Appendix 1. Note that the porous medium deformation modulus K' controls both storage behavior through 2.2 and the response to depositional loading and erosional unloading through the loading term (second on r.h.s.) of 2.1. In essence, 2.1 is a multi-dimensional, variable-density equation for deforming media of the type originally derived by Gibson (1958) to describe compaction and fluid flow in earthen structures. Equation 2.1 can account for transient, variable-density groundwater flow in heterogeneous and anisotropic porous media. It accounts for deformation of the porous framework, but assumes that all deformation is vertical.

The fact that equation 2.1 is written in terms of the deformation modulus K' rather than compressibility (the reciprocal of the modulus) is merely a matter of convenience and results from using a linear-elasticity to derive 2.1. Linear elasticity assumes that deformation is fully reversible and that K' is constant and, as such, cannot describe the behavior of sediments which become "stiffer" with compaction and never recover their former porosity when unloaded. However, RIFT2D emulates the non-elastic behavior of sediments and rocks by allowing K' to vary. In essence, the deformation within each time step is assumed to be elastic (constant K'), but over multiple time steps K' is varied to mimic actual compaction and decompression. This provides a close approximation of actual behavior because the deformation within any time step is generally small and closely

approximated by a linear elastic description. K' is recalculated at each node for every time step using the prevailing effective stress and a relation between porosity and effective stress. The latter is user-chosen in RIFT2D simply by specifying an Athy's Law type porosity-depth relationship (Athey, 1930) that is written in terms of effective stress. An Athey-type relation is specified for each lithologic unit in the simulation.

In RIFT2D the Athey's Law type relationship takes the form

$$\phi = \phi_o \exp \left(-\beta \frac{\sigma_e}{g(\rho_s - \rho_f)} \right) + \phi_{ir} \quad (2.2)$$

where ϕ_o is porosity at the sediment/water interface (or land surface), ϕ_{ir} is irreducible porosity, σ_e is the effective stress, and β is a compressibility coefficient relating changes in porosity to changes in effective stress for loading (compaction) conditions. Equation 2.2 uses effective stress σ_e as a surrogate for depth. Effective stress is computed in RIFT2D using

$$\sigma_e = \sigma_T - P = \int_z^L (1 - \phi) g \rho_s (L - z) + \phi g \rho_f (L - z) dz - P \quad (2.3)$$

where P is fluid pressure, L is the total length of the sedimentary column, and σ_T is the total load (sediments plus pore water) on a sedimentary layer at depth. Equation 2.2 is applied when the sediment is experiencing increasing overburden loads that are larger than experienced in the past, such as in active basins that have never experienced uplift and erosion. During periods of erosion when overburden loads are decreasing, RIFT2D uses another form of Athey's Law written as

$$\phi = [\phi_{min} - \phi_{ir}] \exp \left(-\beta_{ul} \frac{\sigma_e - \sigma_{max}}{g(\rho_s - \rho_f)} \right) + \phi_{ir} \quad (2.4)$$

where β_{ul} is a compressibility coefficient relating changes in porosity to decreases in effective stress, ϕ_{min} is the minimum porosity attained before unloading begins, and σ_{max} is the maximum effective stress attained before unloading occurs. The choice of porosity-depth parameters in 2.2 and 2.4 has important implications for storage and loading/unloading behavior. The assumptions inherent in this approach should therefore be clearly understood; see Chapter 4 for a discussion.

Hydraulic head in equation 2.1, originally derived by Hubbert (1940), is given by

$$h = \frac{P}{\rho_0 g} + z \quad (2.5)$$

where P is fluid pressure, g is gravitational acceleration and z is elevation above some datum. The fluid flux can be related to the gradient in hydraulic head through Darcy's law. A variable density form of Darcy's law that is written in terms of head (see Garven and Freeze, 1984a) is used, namely

$$\vec{q} = -\mathbf{K} \mu_r \nabla_x (h + \rho_r) \quad (2.6)$$

The relative density (ρ_r) and viscosity (μ_r) used in equations 2.1 and 2.3 are given by

$$\rho_r = \frac{\rho_f - \rho_0}{\rho_0} \quad (2.7)$$

$$\mu_r = \frac{\mu_0}{\mu_f} \quad (2.8)$$

where μ_0 is the viscosity of water at standard state.

The principal components of the hydraulic conductivity tensor \mathbf{K} are assumed to align with and normal to sedimentary layering. The tensor components K_{xx} , K_{zz} , K_{zx} , and K_{xz} are thus calculated using the dip of the sedimentary layering (see Fig. 2.1) as

$$\begin{aligned} K_{xx} &= K_{\max} \cos(\theta) + K_{\min} \sin(\theta) \\ K_{zz} &= K_{\max} \sin(\theta) + K_{\min} \cos(\theta) \\ K_{xz} &= K_{zx} = (K_{\max} - K_{\min}) \sin(\theta)\cos(\theta) \end{aligned} \quad (2.9)$$

where K_{\max} is the maximum hydraulic conductivity, K_{\min} is the minimum hydraulic conductivity, and dip (θ) is measured relative to horizontal. The maximum conductivity is usually assumed to be in the direction of bedding (or the fault plane in fault zones). The minimum conductivity is typically assumed to be perpendicular to bedding. Dip

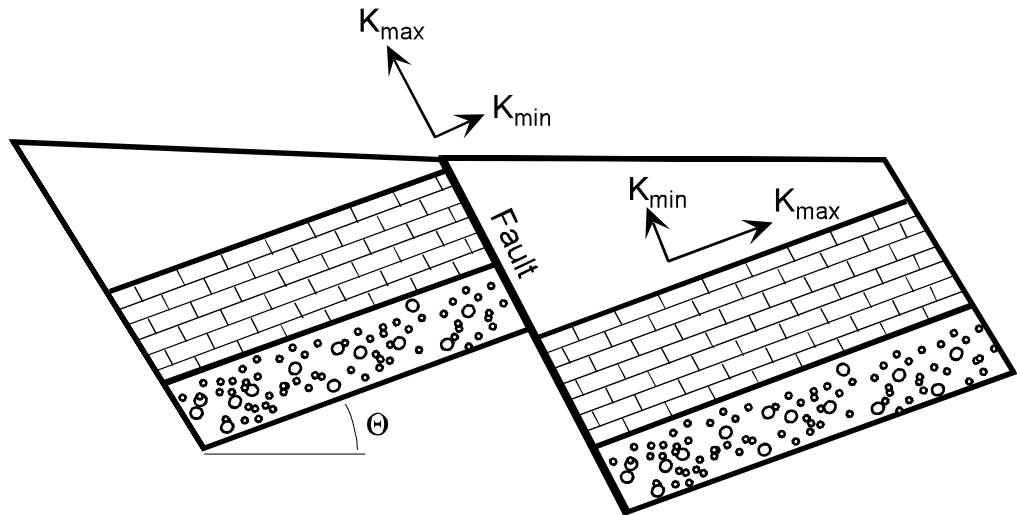


Figure 2.1. Schematic diagram depicting principal directions of permeability for sedimentary layers and fault zone. In RIFT2D the maximum permeability of the fault zone is assumed to be parallel to the fault plane while the maximum permeability of the sedimentary layers is assumed to be in the direction of bedding.

angle θ is automatically calculated in RIFT2D. Hydraulic conductivity, in turn, depends on the properties of both the medium and the fluids as

$$K = \frac{\rho_f g k}{\mu_f} \quad (2.10)$$

where k is the medium permeability, which is also a tensor quantity. RIFT2D allows the user to specify either constant k values for each lithologic unit or to specify a log-linear relation between k and porosity for each lithologic unit.

Thermodynamic equations of state are required to compute the density and viscosity of ground water at elevated temperature, pressure, and salinity conditions. RIFT2D uses fitted polynomial expressions presented by Kestin et al. (1981), which are given by

$$\frac{1}{\rho_f} = a(T) + b(T)P + c(T)P^2 + Cd(T) + C^2e(T) \quad (2.11)$$

$$-\rho_f Cf(T) - C^2 Pg(T) - \frac{h(T)}{2} P^2 \\ \mu_f = \mu_o [1 + B(T,C)P] \quad (2.12)$$

where $a(T)-h(T)$ and $B(T,C)$ are the 3rd and 4th order temperature and concentration dependent polynomials defined by Kestin et al. (1981). These polynomial expressions are valid for temperature ranges between 10° and 150°C and salinities between 0 and 6 molal NaCl (represented in the equation of state as solute mass fraction; see Fig. 2.2). In general, fluid density is not as sensitive to changes in fluid pressure as changes in temperature and salinity for the range of conditions encountered in sedimentary basins.

HEAT TRANSFER

Heat transfer in basins occurs by conduction and advection. Conductive heat transfer, enthalpy transfer resulting from Brownian motion in the solid and fluid phases, is governed by Fourier's Law. Advective heat transfer results from enthalpy transport in moving fluid. Thermal dispersion results from mechanical mixing during advective transport. Advective heat transfer effects are especially important in recharge and discharge areas where vertical fluid motion is important. However, advective thermal effects are sometimes difficult to distinguish from the effects of variations in thermal conductivity with depth or between different lithologic units.

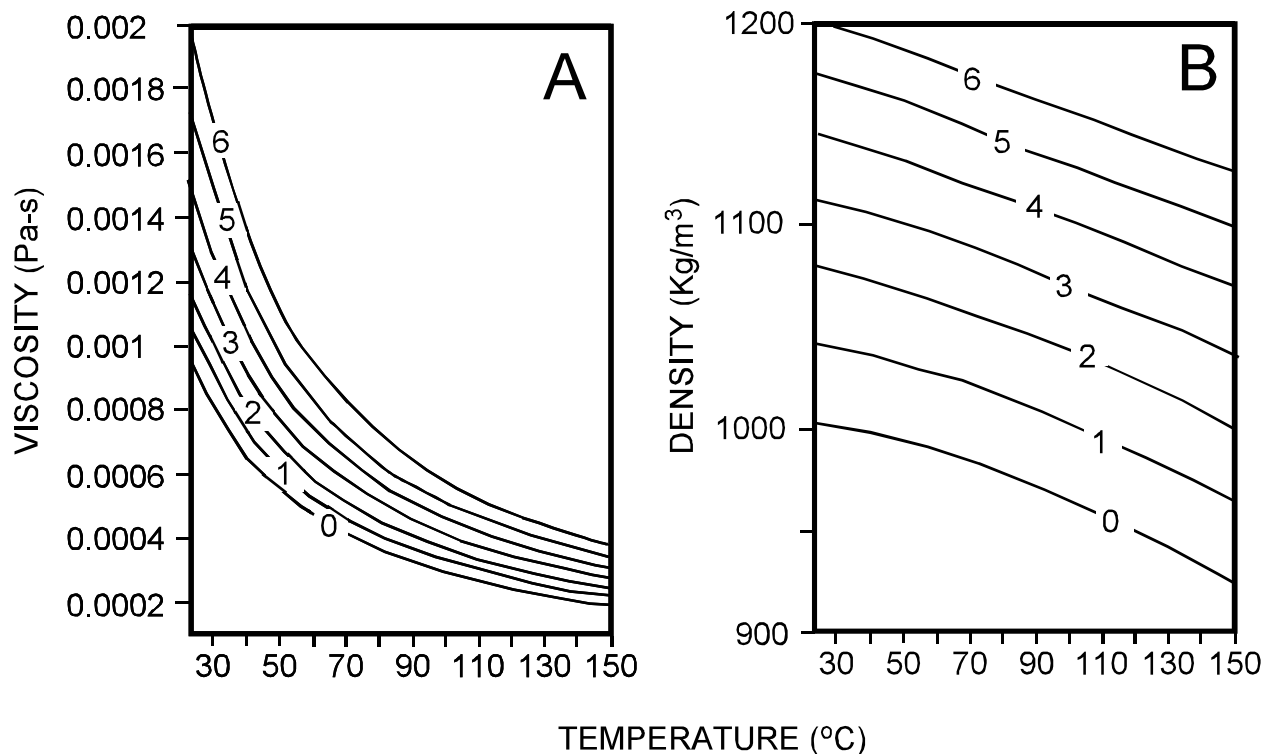


Figure 2.2. Groundwater viscosity (A) and density (B) as a function of temperature (horizontal axis) and salinity (numbered curves) calculated from equation of state used in RIFT2D model. The numbers on the curves indicate moles of NaCl/kg H₂O. The density and viscosity data is calculated at 10 MPa or about 1 km depth.

RIFT2D accounts for both conductive and advective-dispersive heat transfer. The governing equation is given by (Bethke, 1985)

$$[c_f \rho_f \phi + c_s \rho_s (1-\phi)] \frac{\partial T}{\partial t} + \frac{\rho_f h_f}{(1-\phi)} \frac{\partial \phi}{\partial t} = \nabla_x [\nabla_x T] - \vec{q} \rho_f c_f \nabla_x T \quad (2.13)$$

where \mathbf{l} is the thermal dispersion-conducton tensor, T is temperature, c_s is the specific heat capacity of the solid phase, c_f is the specific heat capacity of the fluid phase, and ρ_s is the density of the solid phase. Effects of differing transverse and lateral thermal dispersivity as well as heterogeneity in thermal properties are accounted for in \mathbf{l} , the components of which are given by

$$\begin{aligned} \lambda_{xx} &= \rho_f c_f \frac{q_x^2}{|q|} \alpha_L + \frac{q_z^2}{|q|} \alpha_T + \lambda_f^\phi \lambda_s^{1-\phi} \\ \lambda_{zz} &= \rho_f c_f \frac{q_x^2}{|q|} \alpha_T + \rho_f c_f \frac{q_z^2}{|q|} \alpha_L + \lambda_f^\phi \lambda_s^{1-\phi} \\ \lambda_{xz} &= \lambda_{zx} = (\alpha_L - \alpha_T) \frac{q_x q_z}{|q|} \rho_f c_f \end{aligned} \quad (2.14)$$

where λ_{xx} , λ_{zz} , λ_{xz} , λ_{zx} are the components of the thermal conduction-dispersion tensor, α_L and α_T are the longitudinal and transverse dispersivities, q_x and q_z are Darcy fluxes in the x- and z-directions, and λ_f and λ_s are the thermal conductivity of the fluid and solid phases which are assumed to be isotropic scalar quantities. $|q|$ is the absolute value of the Darcy flux, given by $|q| = \sqrt{q_x^2 + q_z^2}$. Equation 2.13 implicitly assumes that the solid phase is in thermal equilibrium with the fluid phase, which is reasonable for most basin environments.

SOLUTE TRANSPORT

Solute transport through porous media in basins is controlled by both diffusion and hydrodynamically dispersive advection. At small flow velocities ($< 10^{-5}$ m/yr), solute transport is dominated by diffusion, while dispersive advection becomes important at larger flow velocities. To represent solute transport RIFT2D uses an advective/dispersive solute transport equation of the form:

$$\frac{\partial C}{\partial t} + \frac{C}{\phi} \frac{\partial \phi}{\partial t} = \nabla_x [\mathbf{D} \nabla_x C] - \vec{v} \cdot \nabla_x C \quad (2.15)$$

where \mathbf{D} is the hydrodynamic dispersion-diffusion tensor, \vec{v} is the groundwater velocity ($\vec{v} = \vec{q}/\phi$), and C is solute concentration. As reflected by the similarity between 2.15 and the heat transport equation (2.13), solute and heat transport are governed by similar processes. However, while environments dominated by diffusion (conduction) of heat are common, diffusion dominated solute transport is restricted to environments with relatively small groundwater velocities, especially low-permeability environments. Note that effects of porosity changes can be neglected in 2.15 because of the dominant role advection plays in solute transport processes. The hydrodynamic dispersion-diffusion tensor can be separated into components (Bear, 1972) of the form

$$\begin{aligned} D_{xx} &= \frac{v_x^2}{|v|} \alpha_L + \frac{v_z^2}{|v|} \alpha_T + D_d \\ D_{zz} &= \frac{v_x^2}{|v|} \alpha_T + \frac{v_z^2}{|v|} \alpha_L + D_d \\ D_{xz} = D_{zx} &= (\alpha_L - \alpha_T) \frac{v_x v_z}{|v|} \end{aligned} \quad (2.16)$$

where D_{xx} , D_{xz} , D_{zx} , D_{zz} are the components of dispersion-diffusion tensor, v_x and v_z are components of seepage velocity in the x- and z-directions (q_x/ϕ and q_z/ϕ), D_d is the diffusion coefficient, and $|v|$ is the absolute value of the groundwater velocity defined by $|v| = \sqrt{v_x^2 + v_z^2}$. Readers wishing more background on equation 2.15 should refer to Bear (1972) or other treatments of solute transport theory.

PETROLEUM GENERATION, VITRINITE REFLECTANCE, AND PETROLEUM MIGRATION

Petroleum generation. RIFT2D uses first-order rate-kinetic equations to mimic petroleum generation from kerogen. Laboratory experiments and field observations indicate that these provide accurate descriptions of kerogen decomposition upon burial and heating (Fig. 2.3); first-order kinetics have been successfully used by petroleum geologists for

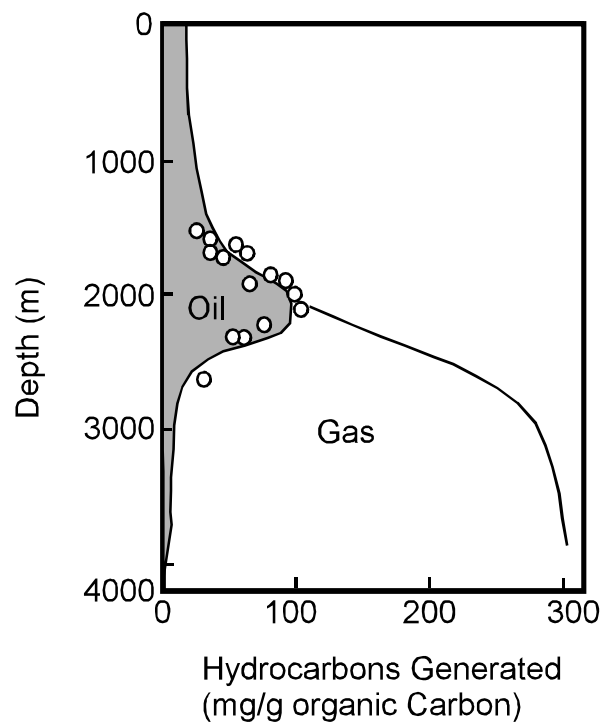


Figure 2-3. Observed (bullets) and computed (lines) oil generation within organic rich sediments from the Douala basin, Cameroon (from Tissot et al., 1987).

over two decades to describe decomposition reactions, and particularly the thermal cracking of kerogen (Tissot et al., 1987). A first-order kinetic relationship implies that the rate of kerogen transformation is proportional to the initial amount of kerogen. Kerogen is insoluble organic matter composed of organic molecules with a variety of C-O, H-O, and H-C chemical bonds. When heated, kerogen degrades to form petroleum, with variable amounts of energy required to rupture the different bonds. The amount of energy required to break a chemical bond is referred to as its activation energy. These decomposition reactions take place in a parallel fashion, and thus require a set of parallel kinetic equations of the form

$$\frac{dx_i}{dt} = -K_i x_i \quad (2.17)$$

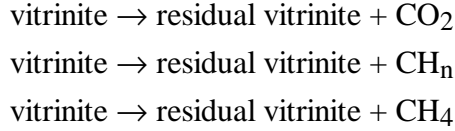
where x_i is the petroleum potential of kerogen involved in reaction i , and K_i is the rate constant for the i^{th} reaction. K_i is defined by Arrhenius' law which relates it to the absolute temperature and the energy required to break the chemical bonds with an equation of the form

$$K_i = A \exp\left(\frac{-E_i}{RT}\right) \quad (2.18)$$

where A is the pre-exponential coefficient, E_i is the activation energy for the i^{th} component of kerogen, R is the gas constant, and T is temperature. Theoretical considerations and the derivation of these equations are discussed by Tissot (1969), Tissot and Espitalie (1975), Ungerer (1984), and Ungerer et al. (1986). Equations (2.17) and (2.18) describe the primary cracking reactions for all three types of kerogen, as well as the secondary cracking of oil to gas. Secondary cracking generally occurs once much of the original kerogen has been transformed to oil. These reactions are not reversible (Tissot and Welte, 1984).

Vitrinite reflectance. Vitrinite reflectance ($\%R_o$) is one of the most commonly-used and most reliable indices for the thermal maturity of source rocks. To help constrain basin flow simulations, RIFT2D can compute $\%R_o$ using first-order rate kinetics. Degradation of type III kerogen (vitrinite) can be described using four parallel reactions that follow the first-order rate kinetics described by equations (2.15) and (2.16) (Burnham and Sweeny, 1989). These reactions are





Thus, type III kerogen generates water, carbon dioxide, higher hydrocarbons (CH_n or oil), and methane gas (CH_4). RIFT2D relies on a model provided by Burnham and Sweeney (1989) that uses the computed amounts of H_2O , CO_2 , CH_n , and CH_4 generated from type III kerogen to determine $\%R_o$. The model assumes that the increase in reflectance of vitrinite is due to changing elemental composition of the vitrinite and involves relating $\%R_o$ to H/C and O/C ratios in a polynomial expression given by

$$\%R_o = \left(12 \exp \left[-3.3 \frac{H}{C} \right] - \frac{O}{C} \right) \quad (2.19)$$

The constants in equation (2.19) were fitted using published measurements of $\%R_o$, H/C, and O/C. The H/C and O/C ratios in equation (2.19) can be computed by knowing the relative fractions of H_2O , CO_2 , oil (CH_n), and CH_4 evolved from the original genetic potential for each of these kerogen products (computed using equations 2.17 and 2.18). The model predicts published reflectance values quite well, agreeing within 0.1 at low rank and within 0.4 at high rank. Details of calculating the ratios of H/C, and O/C are presented in Burnham and Sweeney (1989).

Petroleum migration. At present, RIFT2D does not simulate primary oil migration from source rocks. However, it does permit determining whether oil is likely to have been expelled from source rocks and the direction of flow after expulsion. The pressure-dependent density of oil and gas is calculated using equations of state derived from data presented by England et al. (1987) (Fig. 2.4). The best-fit polynomials through the data are

$$\rho_{oil} = h(P) + i(P)T + j(P)T^2 + k(P)T^3 + l(P)T^4 \quad (2.20)$$

$$\rho_{gas} = m(P) + n(P)T + o(P)T^2 + p(P)T^3 + q(P)T^4 \quad (2.21)$$

where $h(P)$ through $q(P)$ are fitted, pressure-dependent polynomial coefficients. Using these relationships, the volume of oil and gas in each finite element (in m^3) is compared

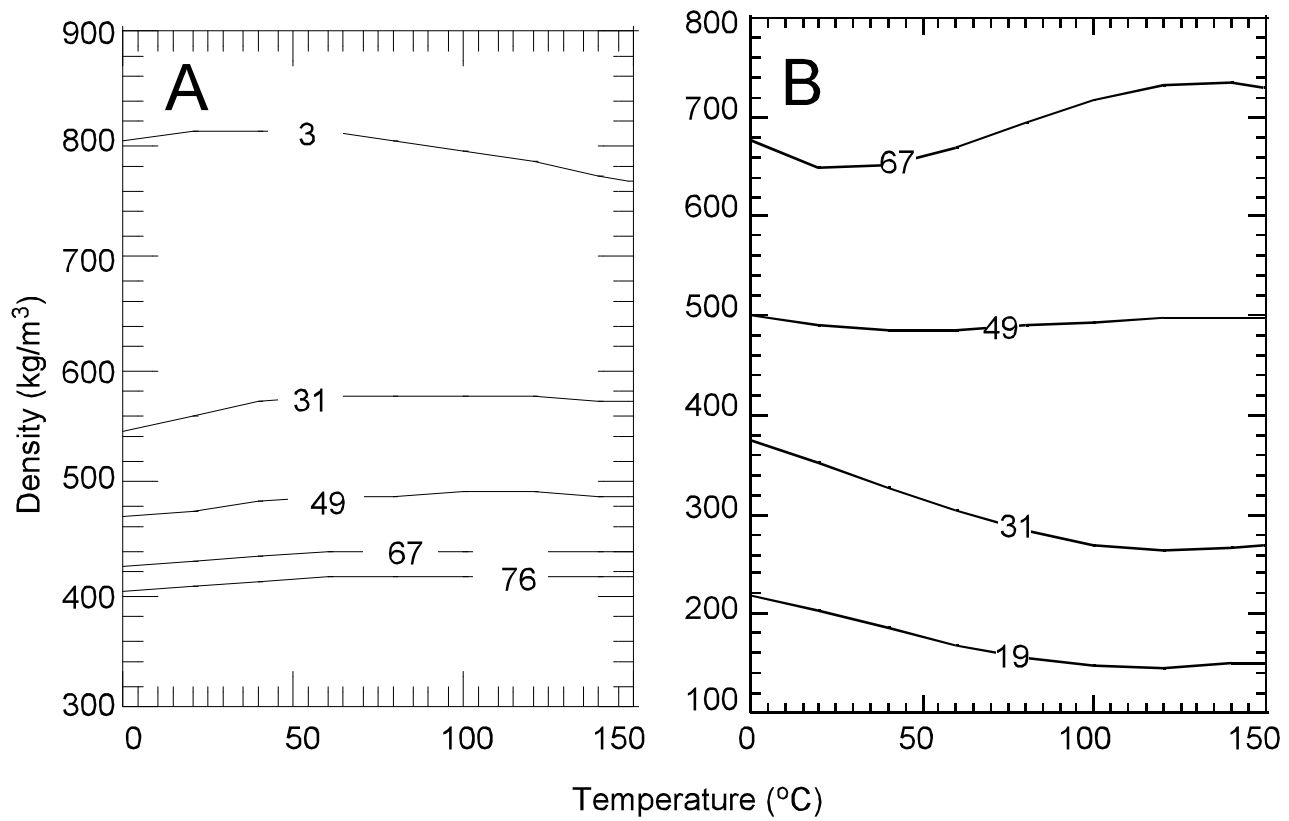


Figure 2.4. Changes in oil (A) and gas (B) density as a function of pressure and temperature. Oil density is calculated using fourth order polynomial equation of state. The numbers on the lines represent pressure in MPa.

to the elemental porosity and a "percent saturation" value for each element is computed. Because RIFT2D represents petroleum generation as a closed system, oil and gas saturations in excess of 100% will occur. In the subsurface, fluid hydrocarbons are expelled from source rocks before this occurs; England et al. (1987) indicate that expulsion occurs at saturations between 8 and 91%. The next logical step in the development of RIFT2D, therefore, will be to describe first the expulsion, and then possibly the migration of the petroleum fractions.

Oil flow directions and fluxes can be inferred from oil head patterns. RIFT2D calculates oil heads (Hubbert, 1953) as

$$h_o = \frac{\rho_f}{\rho_{oil}} h + \left(\frac{\rho_{oil} - \rho_f}{\rho_{oil}} \right) z \quad (2.22)$$

where h_o is the head in the oil phase. If petroleum migration is assumed to occur near the top of coarse-grained formation under oil-saturated conditions, then Darcy's Law can be used to estimate oil migration rates and directions. In this case Darcy's Law is written as

$$\vec{q}^o = \frac{\mu_f}{\mu_{oil}} \vec{q} + \mathbf{K} \left(\frac{\rho_{oil} - \rho_f}{\rho_{oil}} \right) \nabla_x z \quad (2.23)$$

where μ_{oil} is the viscosity of oil. Petroleum researchers have frequently adopted this approximation for representing long-range oil migration (Garven, 1989; Bethke et al., 1991; Toupin et al., 1996) because of the inherent difficulties involved in solving a system of non-linear, multi-phase transport equations on a basin scale with a relatively coarse grid. However, it must be clearly understood that while equations 2.22 and 2.23 provide quantitative estimates of oil migration directions and rates due to the effects of buoyancy and hydrodynamic impelling forces, they do not account for capillary forces. The latter are significant in fine-grained sedimentary units. However, even if a more sophisticated treatment of oil migration were implemented in RIFT2D, it is inherently a three-dimensional process that can only be approximated in cross-sectional representations.

BASIN DEFORMATION

Sedimentary basins subside by either fault block motion or flexure (Fig. 2.5A). Distinguishing between the two is important for fluid flow because faulting can change the configuration and connectedness of permeable units and thus control the evolution of ground water flow patterns. RIFT2D can emulate both fault block motion and flexure. If faulting is simulated, movement along faults with or without fault block rotation can be selected using the variable ROTFLAG (Fig. 2.5B). Grid displacement actually occurs across the faults, but the grid elements are not allowed to change volume (area in two dimensions) as porosity changes. This operational simplification is necessary to ensure that no 5 or 6 node elements develop along faults. As an illustration, consider a system comprised of two fault blocks subsiding at different rates. One fault block containing relatively compressible shale subsides past an adjacent fault block comprised of less compressible sandstone. If volume deformation is allowed, the shale block elements will compress more rapidly than the adjacent sandstone elements. The node density within the shale will be greater than in the sandstone, presenting the possibility of generating 5 and 6 node elements, a situation that presents computational problems. RIFT2D avoids this by not permitting elements to deform when faulting occurs. Note, however, that porosity changes and accompanying changes in permeability k and porous medium deformation modulus K' are still tracked and used in the computations.

Basin sedimentation, erosion, and uplift (without erosion) is specified using the parameter ICASE (Fig. 2.6). While ICASE is specified for each nodal column, it is highly recommended that the user select a single value of ICASE for all nodal columns during a given tectonic time period. For ICASE=0 or 1, subsidence will occur along subsurface nodes provided that a negative values is assigned to VBASE for that column. If VBASE is positive, erosion will occur. In either case, nodes below the land surface (or sediment water interface) are moved while the top node is pinned. If ICASE is set to 0 the grid does not deform with changes in effective stress. If ICASE is set to 1, then the grid elements compact or expand due to sediment loading or unloading. If ICASE is set to 2, then the entire column is moved up or downward with no changes in pore pressure (although head will change due to changes in position relative to datum). If ICASE is set to 3, then the top node is denuded provided that VER is set to some positive value.

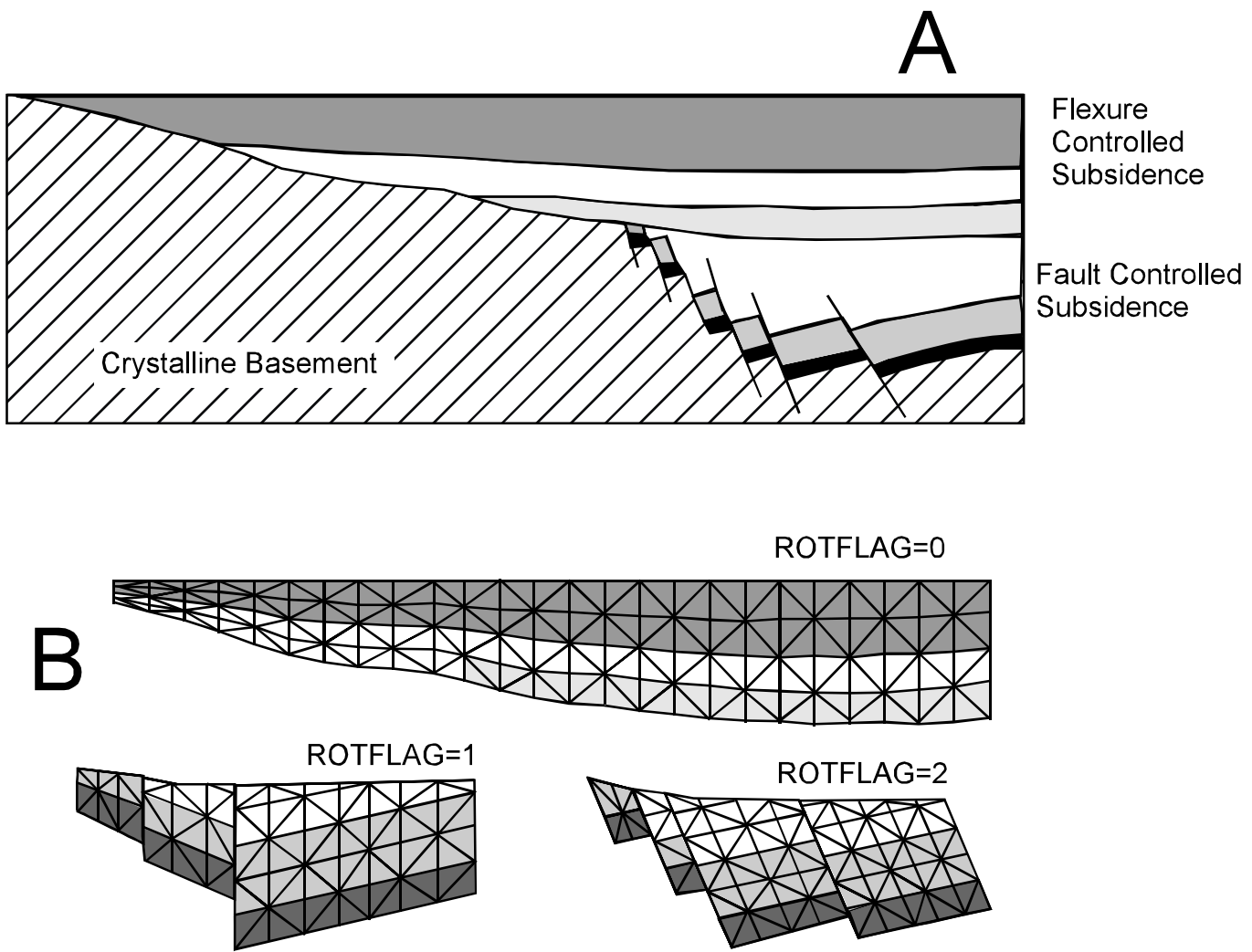


Figure 2.5. (A) Schematic diagram illustrating fault and flexurally controlled subsidence within a "steers head rift basin". Both styles of subsidence can be represented using RIFT2D by varying the parameter ROTFLAG between 0-2 as illustrated in B (after White and McKenzie, 1988). Note that for ROTFLAG=0, the vertical mesh discretization can vary across the basin. For ROTFLAG>0, the vertical discretization (DELZ) is constant everywhere.

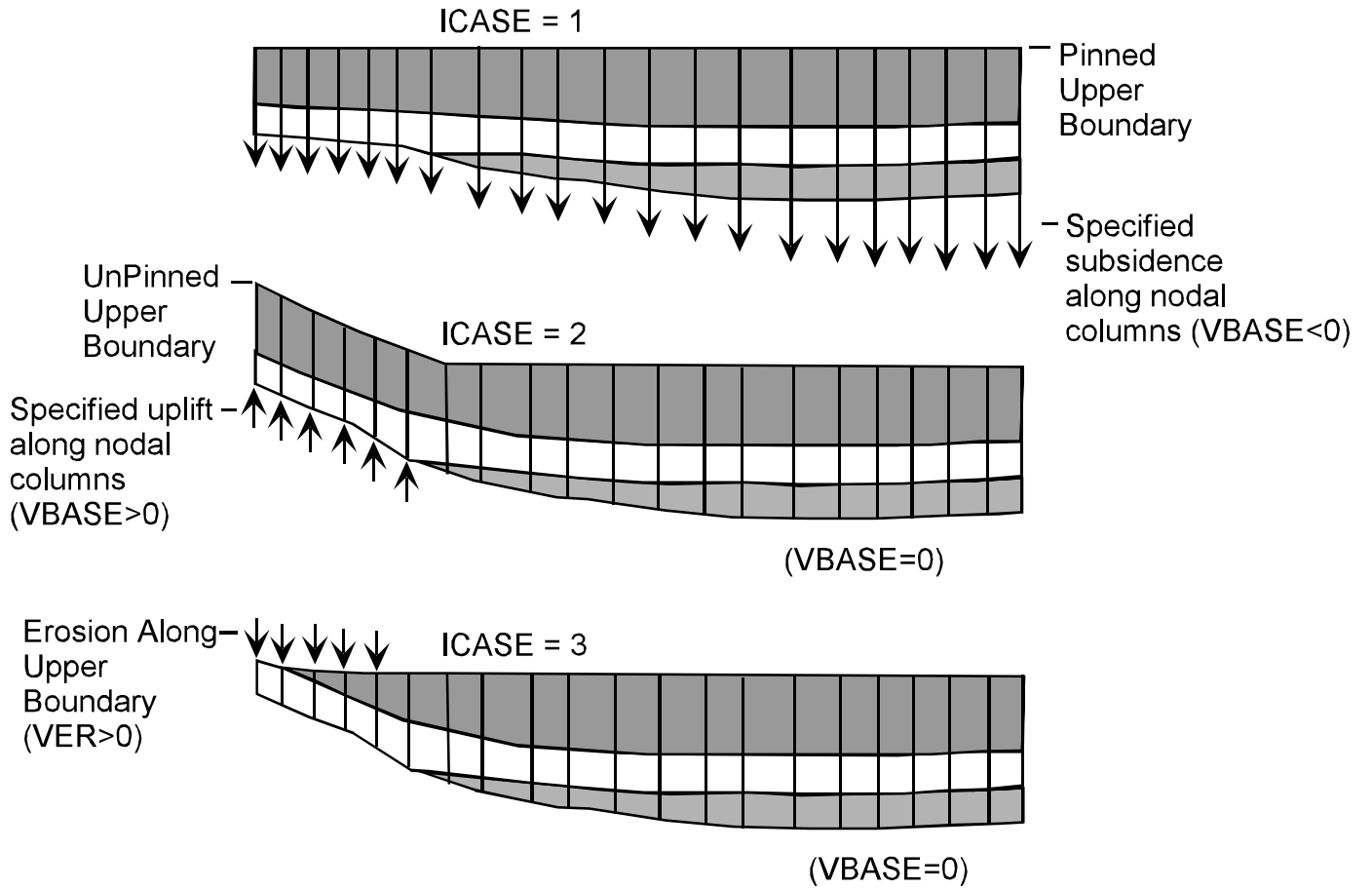


Figure 2.6. (A) Schematic diagram indicating how parameter ICASE is used by RIFT2D to control the erosion, uplift, and deposition of a sedimentary basin. These parameters are discussed in more detail in appendix 3 and Chapter 4 and 5.

Sediment deformation without faulting. When no faults are specified, RIFT2D allows elements of the computational grid to deform vertically in response to changes in vertical effective stress. The amount of deformation is determined from the change in porosity, which in turn is computed, from equations 2.2 and 2.4. (Refer to Chapter 4 for a discussion of the rationale for this approach, inherent assumptions, and practical guidelines for selecting a porosity-depth parameters). For these computations it is assumed that the medium solids (sediment grains) are incompressible and all deformation is vertical. Under these assumptions, the relationship between the vertical velocity of the solids and the rate of porosity change is given by a statement of solid mass conservation for a deforming control volume, or

$$\frac{\partial v_{s_z}}{\partial z} = \frac{1}{1-\phi} \frac{\partial \phi}{\partial t} \quad (2.24)$$

where v_{s_z} is the vertical rate of displacement of medium solids. Equation 2.24 is used by RIFT2D in each timestep to compute the vertical compaction and decompression in each element in the simulation domain.

Fault Block Rotation and Translation with Faulting. During basin evolution, fault displacements can exceed several kilometers and produce large elevation differences between border fault scarps and basin centers. In continental rifts, this displacement is accommodated by either domino-style or listric-style faulting (Jackson and McKenzie, 1983; Gibbs, 1983; Jackson and White, 1989; Reiter, et al., 1992). RIFT2D represents extensional fault block rotation using a simple domino-style kinematic model. While kinematic approaches fail to represent the relationship between stress and strain rigorously, they provide a useful approximation of the changing arrangement of basin sedimentary layers during basin evolution. More rigorous models which couple two- and three-dimensional mechanical deformation and fluid flow (e.g. Ge and Garven, 1993) generally cannot represent large displacements except in rather idealized scenarios.

Fault block rotation in RIFT2D is either maintained at zero to obtain piano key tectonics (ROTFLAG=1) or is represented as domino-style fault block motion (ROTFLAG=2). During rotation, the kinematic equations used to translate nodes within the i^{th} fault block are

$$\begin{bmatrix} x^{m'} \\ z^{m'} \end{bmatrix} = \sum_{i=0}^{\text{Blocks}} \sum_{m=0}^{\text{nodes}(i)} \left[\begin{bmatrix} x^m \\ z^m \end{bmatrix} - \begin{bmatrix} X_c^i \\ Z_c^i \end{bmatrix} \right] * \begin{bmatrix} \cos(\alpha) & \sin(\alpha) \\ -\sin(\alpha) & \cos(\alpha) \end{bmatrix} + \begin{bmatrix} X_c^{i'} \\ Z_c^i \end{bmatrix}$$

(2.25)

RIFT2D can apply 2.25, which rotates the computational grid between faults with no internal deformation, to an arbitrary number of fault blocks. Each fault block rotates around its respective centroid and fault surfaces remain parallel (Fig. 2.6). The resulting nodal location ($x^{m'}$, $z^{m'}$) is a function of the previous nodal position (x^m , z^m), the incremental rotation (α), and the position of the fault block's centroid (X_c^i , Z_c^i). The location of the nodes in each fault block (x^m , z^m) are subtracted from the centroid's position (X_c^i , Z_c^i) thus converting to a local fault block coordinate system with the centroid of the fault block at the origin (0,0). These coordinates are then multiplied by a rotation matrix. The depth (Z_c^i) of the fault block's centroid is held constant in RIFT2D for each tectonic time period (a predesignated portion of the total simulation time generally comprised of several timesteps). Extension, fault block width, and the new centroid locations are represented in our model through geometric relationships:

$$W_n^i = W_o^i * \left(\cos(\delta) + \frac{\sin(\delta)}{\tan(\gamma + \delta)} \right)$$

(2.26)

$$X_C^{i'} = X_C^{i-1} + W_n^{i-1} - \left[(Z_C^i - Z_C^{i-1}) \tan(\gamma + \delta - 90^\circ) \right] \quad i > 1 \quad (2.27)$$

Equation 2.26 calculates the new horizontal half-width of a fault block (W_n^i), from the original fault block half-width (W_o^i), the original fault dip (γ), and the total amount of rotation (δ) (see Fig. 2.7). In this model the fault block half-width is the horizontal distance from the centroid to the fault or one-half the total width. Equation 2.27 calculates the new horizontal location of the centroid ($X_C^{i'}$). Note that the superscript term i' is greater than or equal to 2. The position of the first (that is, the leftmost) fault block's

centroid is a constant value (X_c^I , Z_c^I) for a given tectonic time period; however, the horizontal position of each subsequent fault block (equation 2.27) is a function of its half-width, its vertical location relative to the previous centroid position, and the fault dip minus 90 degrees ($\gamma+\delta-90$). Calculation of the location of the centroids enables calculation of the new nodal positions ($x^{m'}, z^{m'}$) for the finite element grid used to calculate groundwater flow, heat, and solute transport. Rotation will move some nodes into negative space. The maximum negative horizontal location is subtracted from each node to maintain the western edge of the basin along the zero vertical axis.

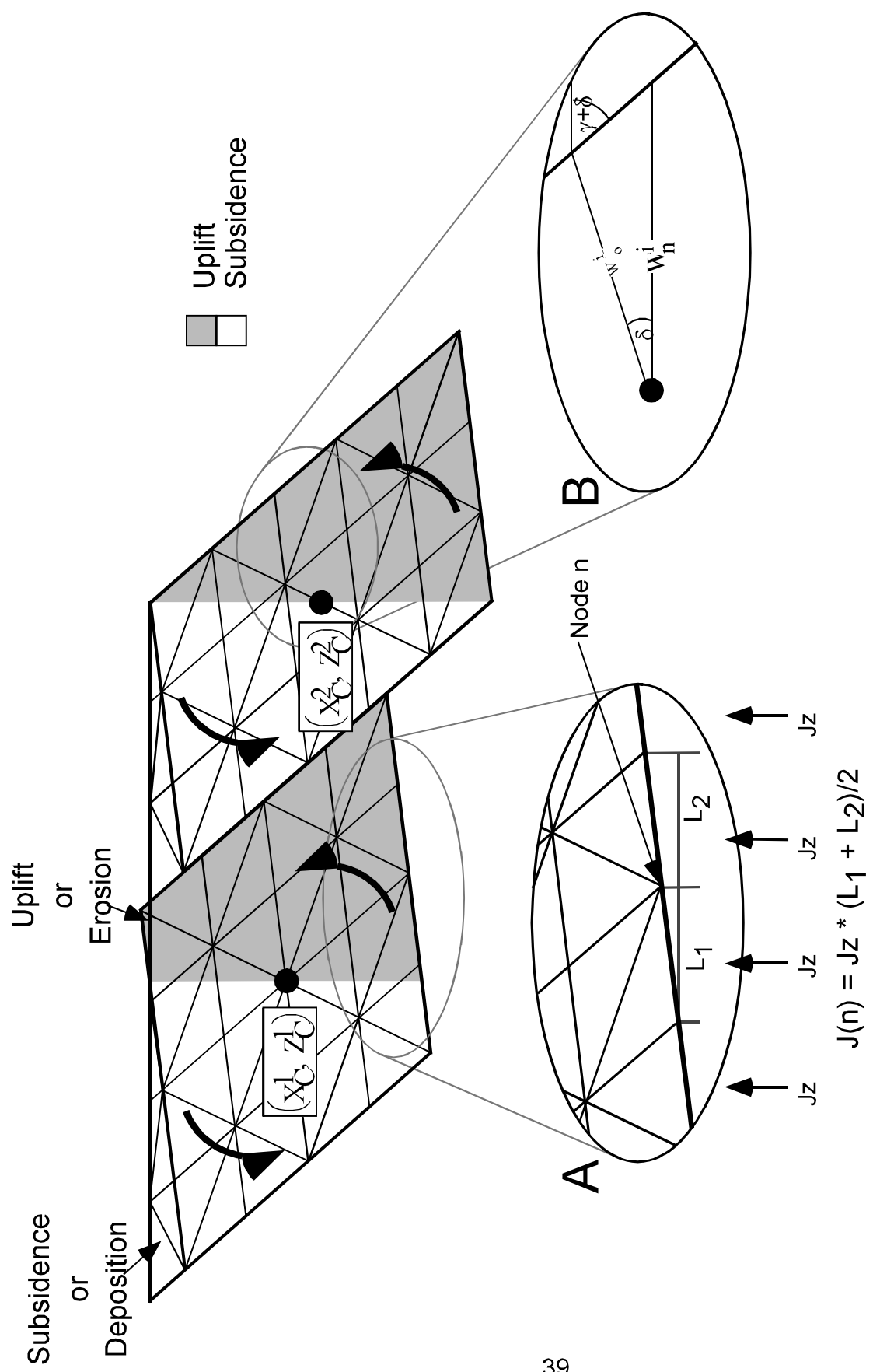


Figure 2.7. Schematic diagram depicting domino-style fault block rotation and imposition of specified heat flux boundary condition at base of solution domain.

CHAPTER 3 – NUMERICAL METHODS

FINITE ELEMENT APPROXIMATION OF GROUND WATER FLOW AND SOLUTE TRANSPORT EQUATIONS

A finite element method is utilized in RIFT2D to solve equations (1.1) and (1.11) because of its advantages over the finite difference method in representing mesh discontinuities associated with fault block movement. In RIFT2D fault blocks are represented by a series of three- and four-node triangles (Fig. 3.1A) whose vertices are defined by the nodal grid points. Porous media properties are defined for each element.

For three-node elements, the unknown hydraulic heads (and temperatures) are required to vary linearly across each triangular element using the standard Galerkin approach (Reddy, 1984):

$$\hat{h} = \sum_{m=1}^3 \psi_m^o h_m = \psi_1^o h_1 + \psi_2^o h_2 + \psi_3^o h_3 \quad (3.1)$$

where \hat{h} is the trial solution and ψ_m^o are the standard Lagrange shape functions:

$$\psi_m^o = \frac{\alpha_m + \beta_m x + \gamma_m z}{2A_e} \quad (3.2)$$

The coefficients in equation (3.2) are calculated using the nodal coordinates of the vertices of the triangular elements:

$$\alpha_1 = x_2 z_3 - x_3 z_2, \quad \alpha_2 = x_3 z_1 - x_1 z_3, \quad \alpha_3 = x_1 z_2 - x_2 z_1 \quad (3.3)$$

$$\beta_1 = z_2 - z_3, \quad \beta_2 = z_3 - z_1, \quad \text{and} \quad \beta_3 = z_1 - z_2 \quad (3.4)$$

$$\gamma_1 = x_3 - x_2, \quad \gamma_2 = x_1 - x_3, \quad \text{and} \quad \gamma_3 = x_2 - x_1 \quad (3.5)$$

$$A_e = \frac{\beta_1 \gamma_2 - \beta_2 \gamma_1}{2} \quad (3.6)$$

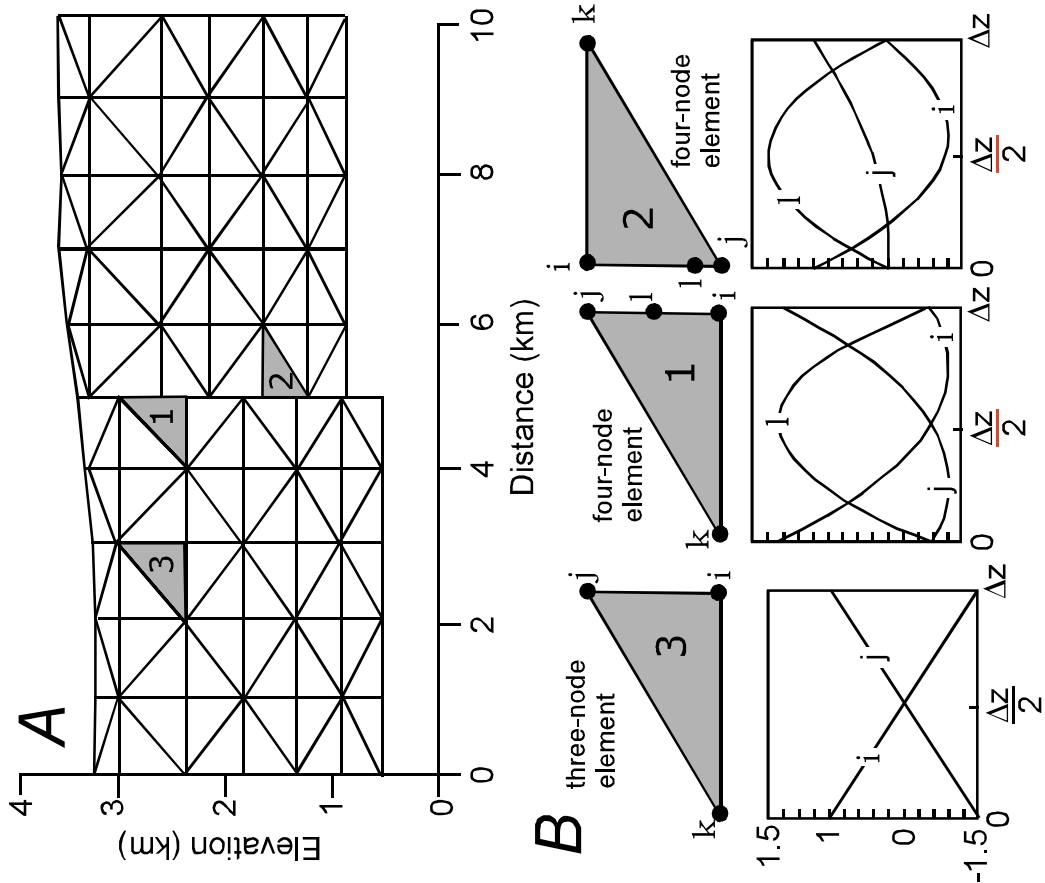


Figure 3.1. (A) Schematic diagram illustrating finite element discretization of fault blocks using three- and four-node triangular elements. (B) Shape functions for the three- and four-node elements. Note that only nodes which lie on the vertical edge of the element are depicted in B.

As usual the values of the Lagrange shape functions must be equal to one at the node they refer to and equal zero at all other nodes. In addition, all three shape functions must sum to 1 everywhere across the element (Fig. 3.1B). Unknown hydraulic heads within the four-node elements vary linearly along the element edges which have two node sides. Hydraulic heads vary quadratically along the third side which contains the extra pinch node. For a four-node element, hydraulic head is given by:

$$\hat{h} = \sum_{m=1}^4 \psi_m h_m = \psi_1 h_1 + \psi_2 h_2 + \psi_3 h_3 + \psi_4 h_4 \quad (3.7)$$

The shape functions for the fourth node or pinch node ($n=4$) and vertices of each triangular element (nodes 1–3) are given by:

$$\begin{aligned} \psi_1 &= \psi_1^0 \\ \psi_2 &= \psi_2^0 - C_2 C_1 (\psi_2^0 \psi_3^0) \\ \psi_3 &= \psi_3^0 - C_3 C_1 (\psi_2^0 \psi_3^0) \\ \psi_4 &= C_1 (\psi_2^0 \psi_3^0) \end{aligned} \quad (3.8)$$

where the coefficients $C_1 – C_3$ are constants at any time step and are given by:

$$\begin{aligned} C_1 &= \frac{1}{C_2 C_3} \\ C_2 &= \psi_2^0(x_4, z_4) \\ C_3 &= \psi_3^0(x_4, z_4) \end{aligned} \quad (3.9)$$

The fourth node may be located at any position (x_4, z_4) along the edge of an element except at one of the vertices. The shape functions along the fault surface are presented in Figure 3.1B for two different positions of the fourth node. In the finite element method, the trial solution, \hat{h} , is substituted into an integral form of the ground water flow equation

represented by equation (2.1). The integrand is multiplied by a weighting function, v , given by:

$$v = \sum_{n=1}^3 \psi_n = \psi_1 + \psi_2 + \psi_3 \quad (three-node-elements; 3.10)$$

$$v = \sum_{n=1}^4 \psi_n = \psi_1 + \psi_2 + \psi_3 + \psi_4 \quad (four-node-elements; 3.11)$$

Upon substitution of \hat{h} and v and integration, the ground water flow is transformed into a set of "n by m" algebraic equations. The resulting system of algebraic equations take the form:

$$\hat{A}_{nm} \hat{h}_m + P_{nm} \frac{\partial h}{\partial t} = B_n \quad (3.12)$$

The vector, B_n , and the matrices A_{nm} and P_{nm} are listed in Plates 1 and 2 for three- and four-node elements, respectively. A finite difference approximation of the temporal derivative is used to approximate the $\partial h / \partial t$ term. Using a time weighting scheme, equation (3.12) is recast as follows:

$$\begin{aligned} (\theta - 1) A_{nm} \hat{h}_m^k + \theta A_{nm} \hat{h}_m^{k+1} + P_{nm} \frac{h_m^{k+1} - h_m^k}{\Delta t} &= B_n \\ \theta A_{nm} \hat{h}_m^{k+1} + P_{nm} \frac{h_m^{k+1}}{\Delta t} &= B_n + (1 - \theta) A_{nm} \hat{h}_m^k + P_{nm} \frac{h_m^k}{\Delta t} \end{aligned} \quad (3.13)$$

where θ is the time weighting parameter (fully implicit, $\theta=1$; fully explicit, $\theta=0$; Crank-Nicholson method, $\theta=0.5$). Solving equation (3.13) using an implicit or Crank-Nicholson time weighting scheme guarantees that the solution to the flow equation will be unconditionally stable (Huyakorn and Pinder, 1983).

Once \hat{h} is found, the elemental fluid fluxes can be calculated using a finite element approximation of Darcy's Law (equation 2.6):

$$q_x = -\frac{K_{xx} \mu_f}{2 A_e} [h_1 \beta_1 + h_2 \beta_2 + h_3 \beta_3] - \frac{K_{xz} \mu_f}{2 A_e} [h_1 \gamma_1 + h_2 \gamma_2 + h_3 \gamma_3] + \frac{K_{xz} \rho_r \mu_f}{3} \quad (3.14)$$

$$q_z = -\frac{K_{zx}\mu_f}{2A_e}[h_1\beta_1 + h_2\beta_2 + h_3\beta_3] - \frac{K_{zz}\mu_f}{2A_e}[h_1\gamma_1 + h_2\gamma_2 + h_3\gamma_3] + \frac{K_{zz}\rho_r\mu_f}{3} \quad (3.15)$$

Following the approach outlined above, the heat transfer equation (2.13) can be approximated using the finite element method as:

$$\theta S_{nm} \hat{T}_m^{k+1} + C_{nm} \frac{\tilde{T}_m^{k+1}}{\Delta t} = R_n + (1 - \theta)S_{nm} \hat{T}_m^k + C_{nm} \frac{\hat{T}_m^k}{\Delta t} \quad (3.16)$$

where \hat{T}_n is the nodal temperature. The vectors, R_n , and the matrices S_{nm} and C_{nm} from equations (3.16) are listed in Plate 3 and 4 for three- and four-node elements, respectively.

FINITE DIFFERENCE APPROXIMATION OF SEDIMENT CONSOLIDATION EQUATION

When no faults are present in the solution domain, the sediment consolidation of individual nodes within a column is solved in RIFT2D by relating the change in porosity between the old and new time steps along nodal columns (Fig. 3.2). In RIFT2D, equation (2.24) is approximated using an explicit finite difference scheme:

$$\frac{v_{sj+1}^{k+1} - v_{sj}^k}{\Delta z} = \frac{1}{(1 - \phi_{j+1/2}^k)} \frac{\phi_{j+1/2}^k - \phi_{j+1/2}^{k-1}}{\Delta t} \quad (3.17)$$

where k denotes time and j denotes the position along a nodal column moving upward. The porosity terms in equation (3.17) are given by:

$$\begin{aligned} \phi_{j+1/2}^k &= \frac{\phi_{j+1}^k + \phi_j^k}{2} \\ \phi_{j+1/2}^{k-1} &= \frac{\phi_{j+1}^{k-1} + \phi_j^{k-1}}{2} \end{aligned} \quad (3.18)$$

Plate 1

Plate 2

Plate 3

Plate 4a

Plate 4b

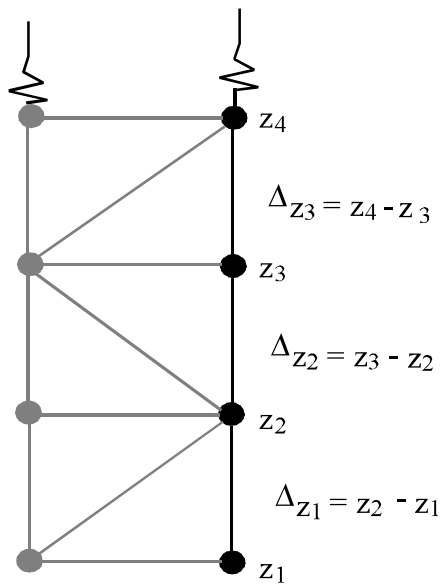


Figure 3.2. Schematic diagram illustrating changes in element thickness due to porosity changes along a nodal column of a RIFT2D finite element mesh.

A backward difference approximation is used to approximate the porous medium velocity because the porosity at the new time level is not known. Solving for the porous medium velocity up the column yields:

$$v_{s,j+1}^{k+1} = v_{s,j}^k + \frac{\Delta z}{(1 - \phi_{j+1/2}^k)} \frac{\phi_{j+1/2}^k - \phi_{j+1/2}^{k-1}}{\Delta t} \quad (3.19)$$

The position of the base of the sedimentary pile is also adjusted to account for subsidence. Sediment consolidation can only be represented in a rigorous fashion in RIFT2D when no faults are represented in the data file. When fault blocks are specified, a sedimentary layer thickness is constant once it has been deposited at the top of the solution domain. This simplification is necessary to prevent the formation of five and six node elements across fault blocks.

MODIFIED METHOD OF CHARACTERISTICS SOLUTION TO SOLUTE TRANSPORT EQUATION

The modified method of characteristics (MMOC) algorithm was used to solve the solute transport equation (Zheng and Bennet, 1994). In the MMOC method, the governing advective/dispersive solute transport equation is recast using the total derivative:

$$\frac{DC}{Dt} = \frac{\partial}{\partial x} \left[D_{xx} \frac{\partial C}{\partial x} + D_{xz} \frac{\partial C}{\partial x} \right] + \frac{\partial}{\partial z} \left[D_{zx} \frac{\partial C}{\partial x} + D_{zz} \frac{\partial C}{\partial z} \right] \quad (3.20)$$

where $\frac{DC}{Dt}$ is the total derivative ($\frac{DC}{Dt} + \vec{v}_f \nabla C$). This algorithm has some decisive advantages over classical finite difference and finite element solutions of the advection/dispersion equation. No numerical oscillations are generated with this method, even at high (<1 m/yr)

ground water flow rates because advective transport is removed from the spatial derivative terms. The total derivative is approximated as follows:

$$\frac{DC}{Dt} = v_x \frac{\partial C}{\partial x} + v_z \frac{\partial C}{\partial z} + \frac{\partial C}{\partial t} \cong \frac{C_n^{k+1} - C_p^k}{\Delta t} \quad (3.21)$$

where C_p^k is the particle concentration upwind of the node C_n^{k+1} and Δt_p is the particle time step size (must be smaller than or equal to the flow and heat transport time step size). This derivative is approximated using a *reverse* particle tracking algorithm to estimate the changes in concentration of the solute along the flow path between the nodes at the upwind particle positions (Fig. 3.3). The particles are initially located at nodes and then moved upstream along the flow path using the following expressions

$$\begin{aligned} x_p^k &= x_p^{k+1} - \Delta t_p v_x^k \\ z_p^k &= z_p^{k+1} - \Delta t_p v_z^k \end{aligned} \quad (3.22)$$

where x_p^k, z_p^k denote the upwind position of the mathematical particles at the old time level, x_p^{k+1}, z_p^{k+1} are the particle positions at the nodal locations (before they are moved). Unlike the method of characteristics algorithm (Konikow and Bredehoeft, 1978) this method only requires placing one particle at each node. The concentration is estimated by interpolation of nodal concentrations at the old time level:

$$C_p^k = \sum_{n=1}^4 \Psi_n C_n^k(x_p^k, z_p^k) \quad (3.23)$$

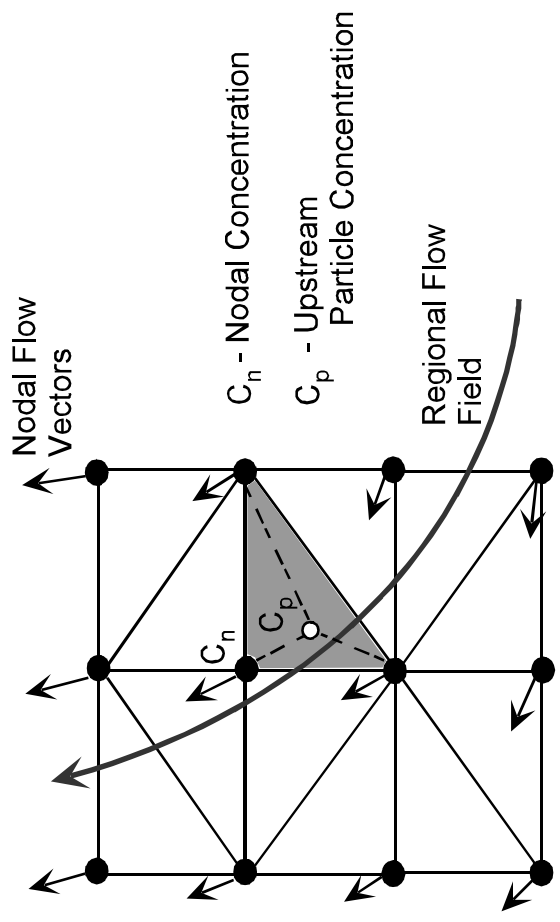


Figure 3.3. Schematic diagram illustrating particle tracking algorithm used in Modified Method Of Characteristics (MMOC) numerical scheme employed by RIET2D to solve the solute transport equation. The regional flow field is depicted by the large curvilinear arrow. The nodal velocity vectors are indicated by the smaller arrows at each node (black circle). A particle (open circle) is moved "upstream" in the MMOC approach using the local velocity vector. The shaded element indicates the triangle "home" for the particle. The surrounding nodes are used to determine the particle (C_p) by employing a standard finite element weighting scheme.

The time step criteria is calculated by requiring the particles travel by less than the distance of each element:

$$\Delta t_p \leq \min \left[\frac{\omega v_x^m}{\gamma_m^e}, \frac{\omega v_z^m}{\beta_m^e} \right] \quad (3.24)$$

where γ_m^e is the characteristics length of the element in the x direction, β_m^e is the characteristic length of the element in the z direction, and ω is the time step weighting parameter. Solving the solute transport equation is numerically intensive, requiring many iterations within a single flow and heat transport time step. Equation (3.20) is approximated in RIFT2D using the finite element method outlined above for the fluid flow and heat transport equations.

NUMERICAL INTEGRATION OF PETROLEUM GENERATION EQUATIONS

The first order rate kinetic equation for petroleum generation is approximated using numerical integration. First, separating variables in equation (2.17) yields:

$$\frac{dx_i}{x_i} = -K_i dt \quad (3.25)$$

Next, integrating both sides:

$$\int_{x_i^k}^{x_i^{k+1}} \frac{1}{x_i} dx_i = \int_k^{k+1} -K_i dt \quad (3.26)$$

Substituting in the value of the Arrhenius rate constant, K:

$$\int_{x_i^k}^{x_i^{k+1}} \frac{1}{x_i} dx_i = -A \int_k^{k+1} \exp\left(\frac{E_i}{RT}\right) dt \quad (3.27)$$

The integral on the RHS of equation (3.27) can be evaluated numerically using Simpson's Rule:

$$\int_A^B f(x)dx = \frac{B-A}{6} \left[f(A) + 4f\left(\frac{A+B}{2}\right) + f(B) \right] \quad (3.28)$$

Applying Simpson's Rule to the situation, $f_i(t) = \exp\left(\frac{-E_i}{RT(t)}\right)$; A is the value of the function at the k time level, B is the value of the function at the k+1 time level, and B-A is therefore equal to Δt . Thus, using Simpson's Rule to evaluate the integral on the RHS of equation (3.28):

$$G^{k+1/2}(T) = \frac{\Delta t}{6} \left\{ \left[\exp\left(\frac{-E_i}{RT^k}\right) \right] + \left[4 \exp\left(\frac{-E_i}{R\left(\frac{T^k + T^{k+1}}{2}\right)}\right) \right] + \left[\exp\left(\frac{-E_i}{RT^{k+1}}\right) \right] \right\} \quad (3.29)$$

Now, evaluating both integrals in equation (3.30), we have:

$$\ln(x_i^{k+1}) - \ln(x_i^k) = -A * G^{k+1/2}(T) \quad (3.30)$$

Rearranging to solve for $\ln(x_i^{k+1})$:

$$\ln(x_i^{k+1}) = \ln(x_i^k) - (A * G^{k+1/2}(T)) \quad (3.31)$$

Exponentiating both sides:

$$\exp(\ln(x_i^{k+1})) = \exp(\ln(x_i^k) - (A * G^{k+1/2}(T))) \quad (3.32)$$

or

$$x_i^{k+1} = \exp(\ln(x_i^k) * \exp(A * G^{k+1/2}(T))) \quad (3.33)$$

Thus, the final expression reduces to:

$$x_i^{k+1} = x_i^k * \exp(A * G^{k+1/2}(T)) \quad (3.34)$$

Equation (3.34) is used to compute the progressive degradation of the i^{th} phase of kerogen in RIFT2D with increasing time and temperature. In this final equation, x_i^{k+1} is the amount of genetic potential for the i^{th} reaction remaining at the $k+1$ time level. At the initial time, the full genetic potential values are used in the calculation. Equation (3.34) is used to calculate the thermal degradation of type I and II kerogen to form oil, the degradation of type III kerogen to form H_2O , CO_2 , oil and CH_4 , and the thermal cracking of the oil to gas at higher temperatures. If the source rock assigned to a triangular element contains more than one type of kerogen, the relative masses of the end products is weighted by the fractional composition of the source rock. For elements containing type III kerogen, once the relative fraction of water, carbon dioxide, oil, and methane are determined, the progressive increase in vitrinite reflectance through time is calculated using equation (2.19).

NUMERICAL IMPLEMENTATION

The nodes within each fault block are arranged in columns and rows (Fig. 3.1A). For basins with multiple fault blocks, two nodal columns must be defined along the bounding fault surface separating the fault blocks. Within a fault block, the number of nodes in adjacent nodal columns may vary by up to two nodes (or less). Elements and their constituent nodes are added or removed at the land surface to account for sedimentation and erosion. Unless domino-style rotation is specified, the positions of the nodes in the x -direction are fixed, while the positions of the nodes in the z -direction are determined by the uplift or subsidence rate plus or minus the amount of local consolidation due to sediment compaction. The position of the uppermost node in each nodal column can be either pinned at the land surface or allowed to move. The four-node slip-elements allow one fault block to move past another by requiring that two nodal columns be specified at the fault surface; one column for each fault block. The two nodal columns occupying the fault block are treated separately for calculations of vertical displacements (one column moves upwards; the other downwards), but are treated as a single column in the finite element approximations of the flow, heat, and solute transport equations. This will result in a series of four-node elements. An operational problem arises when a node from one column on the fault surface occupies the same position as a node from the other column. This violates one of the underlying assumption of the Lagrange family of shape functions (all shape functions must be zero at adjacent nodes) and one of the offending nodes is removed. As long as the fourth node is

separated by a distance of $\frac{1}{10,000}$ of the element height, an accurate numerical approximation of the heat and flow equations will result (Wieck, 1993). One shortcoming with this method is that a discontinuity develops in computed heads and temperatures in four-node elements sharing the same fourth node along a fault surface. Because each of the adjacent elements have one node that is not shared in common, small differences in the trial solution occur along the fault edge.

RIFT2D PROGRAM STRUCTURE

The sediment compaction, ground water flow, heat, and solute transport equations are evaluated by RIFT2D in a sequential fashion in arriving at a numerical solution of coupled ground water flow and heat transfer in compacting sedimentary basins. Figure 3.4 outlines the solution procedure taken in solving this system of equations with the code RIFT2D. Because the hydrologic, thermal, and chemical boundary conditions change slowly, no iterative scheme is used in RIFT2D to find coupled solutions to ground water flow and heat transport within the sedimentary basin. Rather, the system of equations are solved in a sequential fashion (one transport equation at a time) to achieve coupling (Huyakorn and Pinder, 1983).

The algebraic equations that result from the finite element approximation of the ground water flow and heat transport are all solved directly in RIFT2D using a matrix inversion technique. The summation of the local matrix coefficients for all of the elements results in a set of sparsely filled banded matrices. A reduced band-width Gaussian elimination method (Bathe and Wilson, 1976) is used in RIFT2D to solve equations (3.13) and (3.16) and the matrices resulting from the finite element approximation of equation (3.20). For the ground water flow equation, only the upper-half of the banded matrices have to be stored because the matrices are symmetric. For the two-dimensional conductive/ convective heat transfer equation, the resulting matrix is asymmetric and thus the full band width had to be stored in the matrix inversion procedure. A bandwidth of 1000 is assigned to the A matrix for Gaussian elimination.

RIFT2D is written in a modular subroutine structure for easy modification. All subroutines are called by the MAIN program. Each subroutine completes one or more distinct tasks. The subroutines used in RIFT2D are described in Table 3.1.

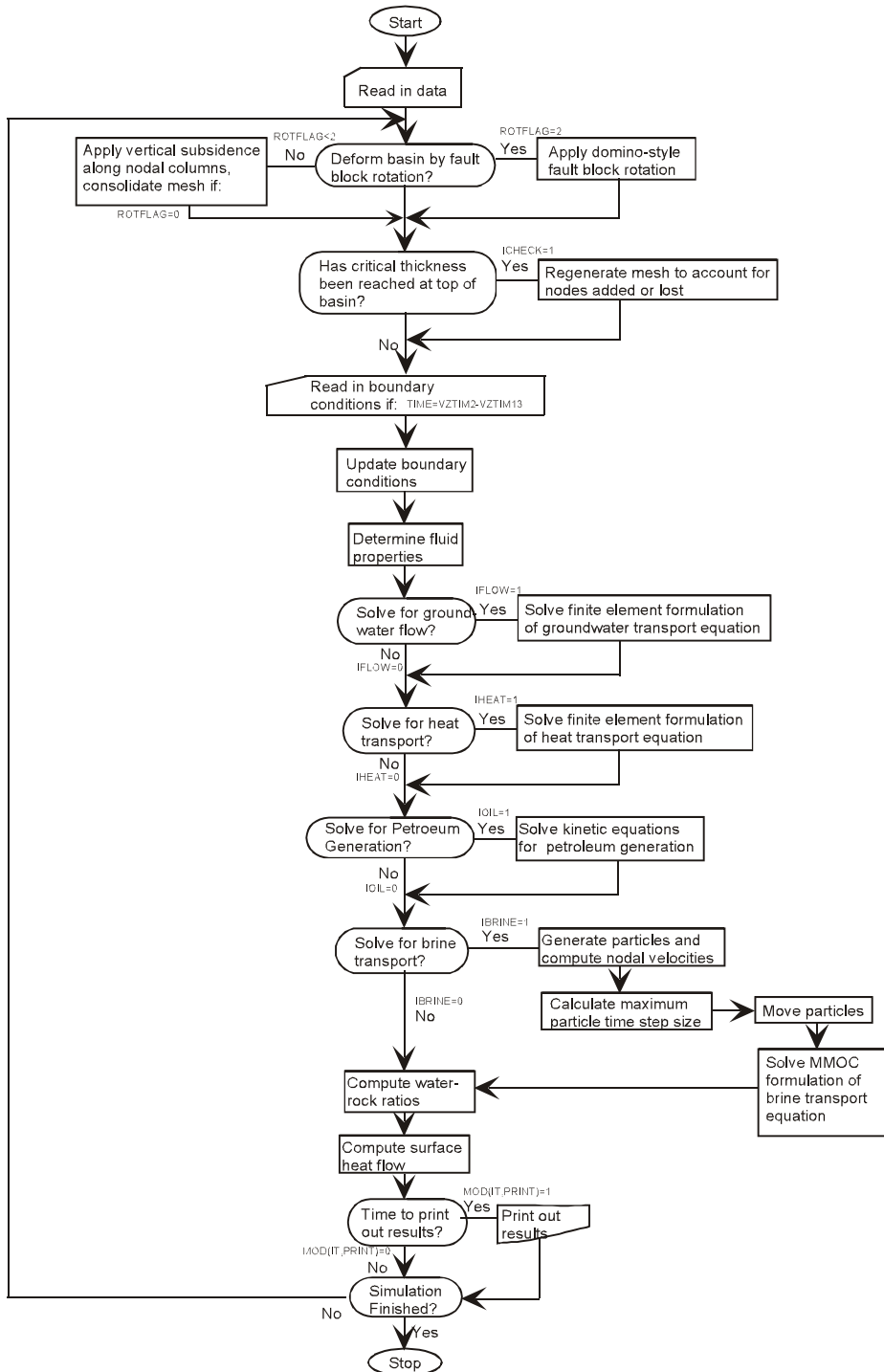


Figure 3.4. RIFT2D flow chart.

Table 3.1 RIFT2D Subroutine Description

Subroutine Name	Description
READIN	Reads in the RIFT2D input data file from UNIT 7. The input data is echoed to an output file (rift.out; UNIT 8). READIN also initializes the positions of the nodes (X,Z arrays) and assigns initial porosity (PHI).
FBSEP	Determines the node numbering when more than one fault block exists. The subroutine removes any nodes which occupies same location along fault blocks. Node positions of individual fault blocks are stored in XSP, and ZSP arrays. The global node locations (overlapping nodes removed) are stored in the X and Z arrays.
SET_ZMAX	For ROTFLAG=2, sets the elevation of the top node of each column equal to the boundary head value (HDBASE + HDINC).
SUBSID	Adjusts the vertical position of nodes along their respective columns due to tectonic subsidence and erosion. The code also adjusts nodal heads due to changes in elevation of the top node of a column.
ROTATE	Rotates fault blocks when ROTFLAG=2
DEPTH5	Determines depths of nodes below land surface when ROTFLAG=2
GRDCHK	Determines thickness of elements at land surface or sediment/water interface to determine whether or not it is time to generate new elements
GENSIS	Renumbers nodes if nodes are added or lost due to sedimentation or erosion.
MESH	Develops element connectivity matrix for both three- and four-node elements. Called when nodes are added or removed from basin.
BOUND	Determines new boundary condition node numbers when nodes are added or removed from basin.
BCREAD	Reads in boundary condition and material tag data a for new tectonic time period
BCTIME	Imposes boundary conditions for ground water flow, heat, and brine transport equations as well as tectonic subsidence. Adjusts boundary condition values if specified.
AREAS	Calculate elemental areas and derivatives of shape functions
ZERO, ZERO1	Zeros matrices (A) and vectors (B) used in Gaussian elimination routines
DENSITY	Calculates fluid density
VISCOS	Calculates fluid viscosity
PRSCAL2	Calculates effective stress, lithostatic pressure, hydrostatic pressure, and nodal fluid pressures,

Subroutine Name	Description
PORPERM	Calculates porosity and permeability during basin evolution
COMPACT	Solves sediment consolidation equation
FLOW	Forms global and local stiffness and capacitance matrices and load vectors for ground water flow equation.
UPDATE	Saves temperatures calculated at old time level
FEBND, HEBND, BEBND	Applies specified value boundary conditions along the land surface for the ground water flow (FEBND), heat transfer (HEBND), and brine transport (BEBND) equations.
FGAUSS, HGAUSS, BGAUSS	Gaussian elimination subroutines for flow (FGAUSS), heat (HGAUSS), and brine (BGAUSS) matrices
VELO	Calculates elemental ground water and oil velocity vectors.
HEAT	Forms global and local stiffness and capacitance matrices and load vectors for heat transport equation.
HNBND	Applies basal heat flow to load vector for heat transport equation.
KINETIC	Calculates petroleum generation within source rock elements
PETPOT	Calculates oil heads and oil density
PARGEN	Places particles at node locations. Determines nodal velocities from using surrounding elements.
CONCST	Imposes user specified concentration gradients with depth along nodal columns.
TSTEP	Determines maximum time step size for solute transport (DTP).
PARMOV	Moves particles upstream from original nodal locations. Determines what element particle resides in.
PARINTERP	Determines particle concentrations using nodal concentrations of element particle resides in.
BRINE	Forms A matrix and B vector for brine transport
WRRATIO	Calculates elemental water-rock ratios
HEAT_FLOW	Calculates surface heat flow
TECOUT	Produces TECPLOT formatted plot file (rift_tec.dat)
OUTPUT	Generates printed output file (rift.out)

CHAPTER 4 – SYSTEM CONCEPTUALIZATION AND PROPERTIES FOR RIFT2D SIMULATIONS

INTRODUCTION

Simulating flow and transport processes in sedimentary basins and other subsurface environments requires various levels of conceptualization. At one level, the researcher must decide how to represent natural processes. In RIFT2D, for example, transient fluid flow through a deformable porous medium is described using a formulation based on elastic theory. At another level, the researcher must select an appropriate method for solving the resulting equations, such as the finite element technique utilized by RIFT2D. Using RIFT2D to simulate flow and transport implies a decision, whether conscious or not, to accept the conceptualization and the corresponding assumptions that it relies upon. These were described in the previous chapters.

An entirely different and in many ways more difficult level of conceptualization is required to implement RIFT2D (or any other simulator). Three broad questions must be answered. First, which processes must be simulated in order to understand the system or answer the questions of interest? For example, is the behavior of interest steady-state or transient, is it affected by deposition or erosion, do variations in fluid density affect flow? These and similar questions must be considered during the conceptualization stage. Indeed, it is in this phase that the applicability or inapplicability of a simulator like RIFT2D to the problem at hand is determined. Second, what is the most appropriate way to simplify the actual geologic framework in order to make analysis tractable? This seemingly innocuous task is one of the most important and difficult steps in constructing a useful model. Third, what are the physical and chemical properties of the system, and how do they vary in space and through time? Models results are no better than one's description of the system being modeled. In addition to the considerations enumerated above, there are practical questions related to each simulation that must be answered, in particular one must determine what level of discretization is necessary to accurately represent the transport and geochemical processes of interest. In this chapter we offer some insights and tips for addressing all of these issues.

The mechanics of implementing the conceptualizations discussed below are addressed in Chapter 5. There we develop three RIFT2D input files to illustrate some of the points made in this chapter and the features and limitations of the model. Chapter 5 also discusses constructing input files for simulations with and without active faults, deposition, and erosion.

CONCEPTUALIZATION FOR RIFT2D

Subsurface environments are tremendously complex. Sediment accumulations can be divided into distinct units on scales ranging from millimeters to kilometers. It is impossible to fully account for this rich complexity because we have no practical way of gathering the data that would be necessary to specify it, and incorporating such detail into a conceptual model would make it impractical to use for simulations. Thus we must judiciously simplify these complex systems in a manner that will capture the character of the system and permit useful conclusions to be drawn from the analysis. Unfortunately, there is no standard approach or technique for doing this. Each situation is different; different hydrogeological processes are important in each problem, and the objectives of every analysis are different. Every situation therefore requires hydrogeological experience and judgment.

Hydrogeologic Architecture. At a minimum, nearly every simulation requires lumping or grouping numerous small geologic units together to make fewer large ones. This involves judgments about the similarity or disparateness of properties as well as a sense of the scale at which a set of heterogeneous units can be lumped into a larger, representative unit. This process is, in fact, a common geological task that has always been practiced by geologists for purposes of mapping and description. Mapped geological units, for example, always incorporate some lithologic variation such as small-scale stratification, minor lenses and stringer, and so on. However, for hydrogeological investigations, the task is somewhat different than it is for traditional geology. It is necessary to perform the aggregation with an eye to the roles played by various units in fluid flow. Hydrogeological units are composed of smaller units that can be reasonably lumped together for purposes of computing flow, transport and other aspects of the fluid regime that are of interest. By implication, this means that it must be possible to represent the hydrologic behavior of the various small subunits using representative values of permeability, specific storage, porosity, dispersivity and so on. In practice, this usually boils down to lumping sedimentary strata into sequences of "high" and "low" permeability units representing fluid transporting reservoirs or aquifers and confining units. Generally, hydrogeological units correspond to one of the major sedimentary types, namely shales, sandstones, carbonates, or evaporites. In practice, this means that boundaries are chosen so that the units are dominated by one of these lithologies. However, because hydrogeological units generally include lesser amounts of other lithologies (typically as finer scale strata), their properties are often different from those of a single lithologic type on a small scale. A good example is permeability anisotropy, which tends to be small in cores but large in major hydrogeologic units. Once again, there are no formal techniques or cookbook approaches

to this problem. Rather, training, experience, and a working knowledge of the subsurface environment in question are what counts.

The most fundamental property of any subsurface environment, once it has been rendered into workable hydrogeologic units, is the geometry of those units. In other words, what are the size and shape of those units or equivalently, where are their common boundaries? In simulations that unfold over geologic time scales, there is the added complication of determining how this architecture changes as units compact and deform over the course of the simulation. In sedimentary sequences, stratigraphic timelines help establish how the geometry of the system changed over its history. However, portions of the stratigraphy may be missing because of erosion between periods of deposition. In other cases one may wish to analyze a basin that has experienced significant uplift and erosion, with little hard information concerning the nature or dimensions of the system prior to erosion. This is a difficult problem, because typically one can only speculate on the properties of the missing material. Similar considerations apply when faulted systems are simulated. The locations of faults and the timing and magnitude of displacement along them are often difficult to ascertain. Care should be taken when interpreting or presenting the results of such simulations that their speculative nature is recognized and acknowledged.

SYSTEM PROPERTIES AND SIMULATION PARAMETERS FOR RIFT2D

Permeability. Perhaps the most fundamental and critical control of ground water flow and transport is permeability and its variation in the subsurface. The importance of permeability is due to its dramatic range, with measured values for different geologic media spanning at least 17 orders of magnitude. The spatial permeability variation that results from this dramatic heterogeneity creates the "plumbing" of the subsurface. In sedimentary environments, high permeabilities are associated with coarse-grained sediments and with carbonates that have solution widened fractures. Low permeabilities, in contrast, are associated with fine-grained sediments and evaporites. Clays and shales typically have small but measurable permeabilities while evaporites (particularly pure halite) can have unmeasurably small permeabilities and may, in some cases, actually be impermeable (Beauheim et al., 1991). Various authors have compiled summaries of permeability values for various rock and sediment types. The summary presented by Freeze and Cherry (1979) and shown here as Figure 4.1 is still quite useful for indicating the permeability ranges associated with various geologic media. Unfortunately, such compilations are of limited use for flow simulations because the permeability ranges

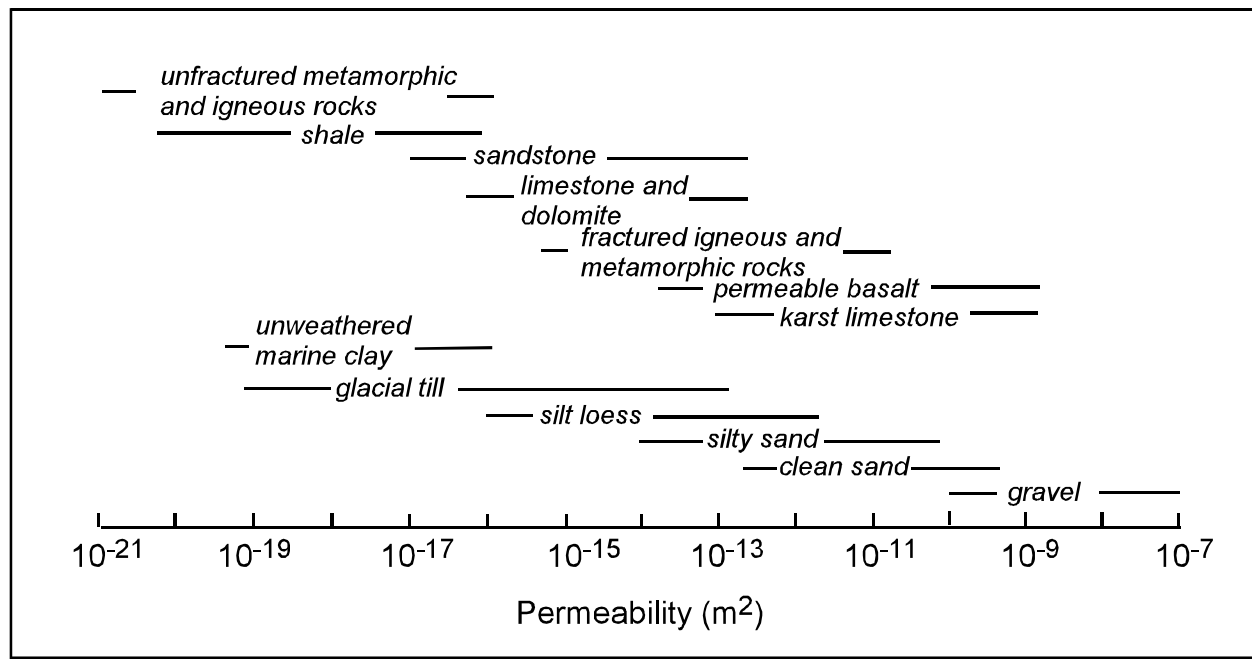


Figure 4.1 Published range of permeability of sedimentary and crystalline rocks
(From Freeze and Cherry, 1979).

associated with each lithologic type are typically several orders of magnitude. Ranges this large permit a number of completely different simulation outcomes. The large ranges are partly due to the significant variability within accepted definitions of rock and sediment types. However, they are probably mostly caused by two very important controls of permeability, namely compaction and diagenetic effects and scale or heterogeneity effects.

Compaction and related diagenetic processes in sedimentary basins cause a loss of porosity, rearrangement of the pore structure, and a decrease in permeability; sediments typically become progressively less porous and permeable with depth. This is of great importance for simulating flow over geologic time scales in sedimentary environments because the permeability of a unit can change dramatically during burial and compaction. Failure to account for these permeability changes, which can amount to several orders of magnitude, can produce misleading simulation results.

Porosity loss in sediments, discussed at greater length in the section on deformation properties, results from mechanical compaction as well as diagenetic processes such as pressure solution and mineral precipitation. The resulting relation between porosity and permeability is complex, but in many cases measurements suggest that it is roughly log-linear. A good example is a compilation of clay and shale permeability data by Neuzil (1994) that shows a distinct log-linear trend between permeability and porosity for porosities from 0.9 to less than 0.1. Several researchers (Mercer et al., 1982; Garven, 1989; Sanford and Konikow, 1989; Corbet and Bethke, 1992) have assumed a log-linear relation between the permeability and porosity of lithologic units of various types in their simulations. Evidence for rather broad applicability of such log-linear relations plus ease of use prompted their inclusion in RIFT2D. Thus, as described in Chapter 2, the user can choose to compute permeability in RIFT2D using

$$\log_{10}(k_{\max}) = PM1 + PM2f \quad (4.1)$$

where k_{\max} is maximum permeability in a lithologic unit in m^2 and PM1 and PM2 are fitting coefficients. Plots of permeability-porosity data for various lithologic types that can serve as a guide to selecting appropriate values of PM1 and PM2 as well as estimates of PM1 and PM2 used by other researchers are presented below.

Some permeability models have included sediment grain size as well as porosity. These models are based on the Kozeny-Carman equation (Bear, 1972; Scheidegger, 1974) or a similar relationship. Most have met with limited success, in part because the mixtures

of grain sizes in most natural sediments create difficulties. However, Koltermann and Gorelick (1995) have developed a so-called "fractional packing Kozeny-Carman model" and an approach for arriving at the appropriate representative grain size and porosity for mixtures of sediment sizes. This model is most appropriate before sediments are "lithified" by significant diagenesis. Because it shows promise, RIFT2D permits using this model as an alternate to equation 4.1. Maximum permeability is then calculated using

$$k_{\max} = \frac{dF^3}{180(1-F)^2} \quad (4.2)$$

where representative grain size d and initial porosity ϕ_0 are determined as described by Koltermann and Gorelick (1995).

Permeability scale effects are the other important consideration because simulations typically consider flow at relatively large scales and, as described above, minor stratigraphic units must be lumped together, producing hydrogeologic units that are somewhat heterogeneous. Much of our knowledge of the permeability of various geologic media, such as that represented in the compilation in Figure 4.1, comes from relatively small volumes of rock such as cores or, for borehole tests (including DSTs), the formation near the borehole. Tests on small volumes of rock exclude large-scale heterogeneities that can control permeability. They also tend to yield biased samples if only intact portions of core (as opposed to those sampling fracture zones, for example) are used for permeability determinations. This can cause small-scale permeabilities and their directional properties, or anisotropy, to be quite different from those in large volumes of rock or sediment. For example, Brace (1980, 1984) has presented evidence suggesting that permeability tends to increase as progressively larger scales are considered. Garven (1986) has also argued that the permeability of hydrogeologic units at basin scales can be orders of magnitude larger than the permeabilities measured from core samples or in borehole tests. Increases in permeability with scale are usually thought to result from the progressive incorporation of fractures, faults, and stratigraphic heterogeneity. These features may not be encountered in boreholes and, as already noted, are sometimes purposely excluded.

There are no hard and fast rules regarding the relationship between permeability and scale. Trends can be subtle and obscured by scatter in the data, as seen in the case of data for crystalline rock collected by Clauser (1992) and shown in Figure 4.2. Changes in permeability with scale are usually viewed as most significant in media that have intrinsically low permeabilities, such as clays, shales, and crystalline rocks, because fractures and faults can easily increase permeability many orders of magnitude above the

low matrix values. In some cases, however, there appears to be no permeability scale effect in these media. The data assembled by Neuzil (1994) for clays and shales, for example, suggest that permeability can be quite independent of the scale of observation. Fractures in clays and shales may tend to close with depth except, as suggested by the work of Gupta and Bair (1997), in regions of intense faulting. Evaporites are usually considered to have low permeabilities that are scale independent because fractures are very difficult to maintain in these deformable media. In sandstones, fractures may only marginally increase already high matrix permeabilities. Carbonate rocks on the other hand, often have rather low matrix permeability and usually seem to owe their status as highly permeable units to fractures that are subsequently widened by solution. In summary, permeability scale effects can be very important but are difficult to generalize. In view of Figure 4.2 this, evidence for or against scale dependency should be examined in each case, and it may be wise to examine the effect of various degrees of scale dependency.

Permeability anisotropy may also change dramatically with scale. This is particularly true in lumped hydrogeologic units in which strata of differing permeabilities are intermingled more or less intimately. Continuum-based basin simulators such as RIFT2D require assignment of uniform properties to grid cells that often have dimensions of several kilometers laterally and tens to hundreds of meters vertically, so hydrogeologic units may have to be fairly coarse and heterogeneous. Flow along bedding in these units, with permeabilities arranged in parallel, is facilitated by the most permeable units, while flow across bedding, with permeabilities arranged in series, is limited by the least permeable. Because of this, interbedding of strata must be accounted for by assigning relatively high anisotropies to represent parallel and series flow.

Core-scale permeability anisotropies are commonly smaller than 10, but the presence of low permeability strata or lenses can produce effective anisotropies many orders of magnitude larger. Bethke (1989) has discussed how shale lenses or stringers within sandstone sequences can increase the basin scale anisotropy of sandstone by several orders of magnitude over that of the small-scale. This should not be surprising in

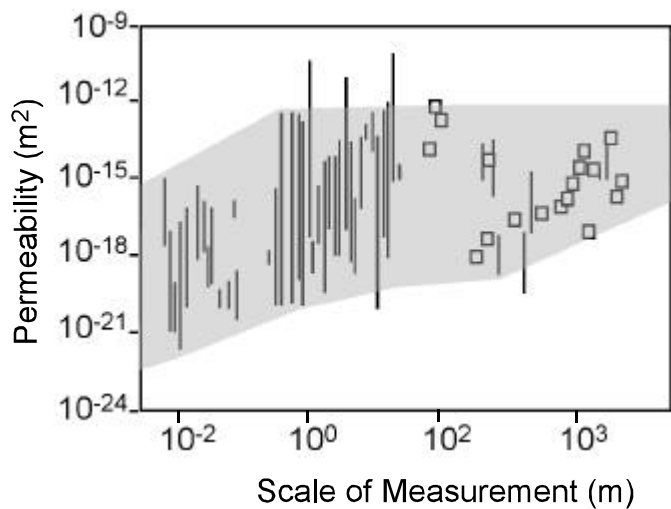


Figure 4.2. Effect of scale on permeability measurements made in fractured rocks (From Clauser, 1992).

view of the large permeability contrasts that exist in sediments. Determination of the appropriate anisotropies at the scale of discretization must be made by considering the mix of permeabilities that occur in the strata at smaller scales and their lateral continuity, or lack of it. In practice this is rather uncertain and it may be desirable to consider a range of possible anisotropies.

Permeability data, when available, typically consist of relatively few small-scale measurements, often of dubious quality. In many cases little or no actual permeability data are available. In addition, we can only estimate the permeabilities that prevailed in the geologic past. As a result, a rather significant level of uncertainty in permeabilities (and thus in simulation results) must be accepted as an inherent part of most basin simulations. Usually there is sufficient uncertainty in the permeability of certain units to allow several very different interpretations of flow and transport. In order to constrain a simulation as much as possible, one must utilize all available permeability data. Where such data are not available, it is necessary to estimate permeability and permeability anisotropy from a knowledge of these properties in similar lithologies and environments. In such an endeavor, there is no substitute for experience. Below we present some very general guidelines for estimating permeability properties of major lithologic types.

When considering published permeability values and other types of permeability information, it is well to carefully distinguish between measured and assumed values. Actual permeability data is obtained in a number of ways, generally by tests on core samples, outcrop faces, and in boreholes. Large-scale permeability values are generally obtained by simulating large scale systems and "backing out" permeabilities of certain units. In the latter, the system is treated like a large natural experiment that can be constrained by knowing other system properties. A good example of this is Bethke's (1986) inverse analysis of the Gulf Coast. In contrast, many studies (particularly studies of paleohydrology) have been done using only assumed permeabilities. As valuable as these studies are, the permeability values they use reflect the researcher's intuition (or bias) rather than observations. When estimating permeability, the geologic environment and history as well as the lithology must be carefully considered. With these caveats, we consider a sampling of permeabilities measured or estimated by other workers.

Three major sedimentologic/lithologic families, clays and shales, sands and sandstones, and carbonate sediments and rocks, dominate basin environments. Permeability-porosity data for each family are displayed in Figure 4.3. Sandstone permeability-porosity measurements from the Dead Sea Rift Helez Formation compiled by Shenhav (1971) are presented in Figure 4.3A. These data show a reasonably good correlation between log permeability and porosity. The porosity-permeability data for

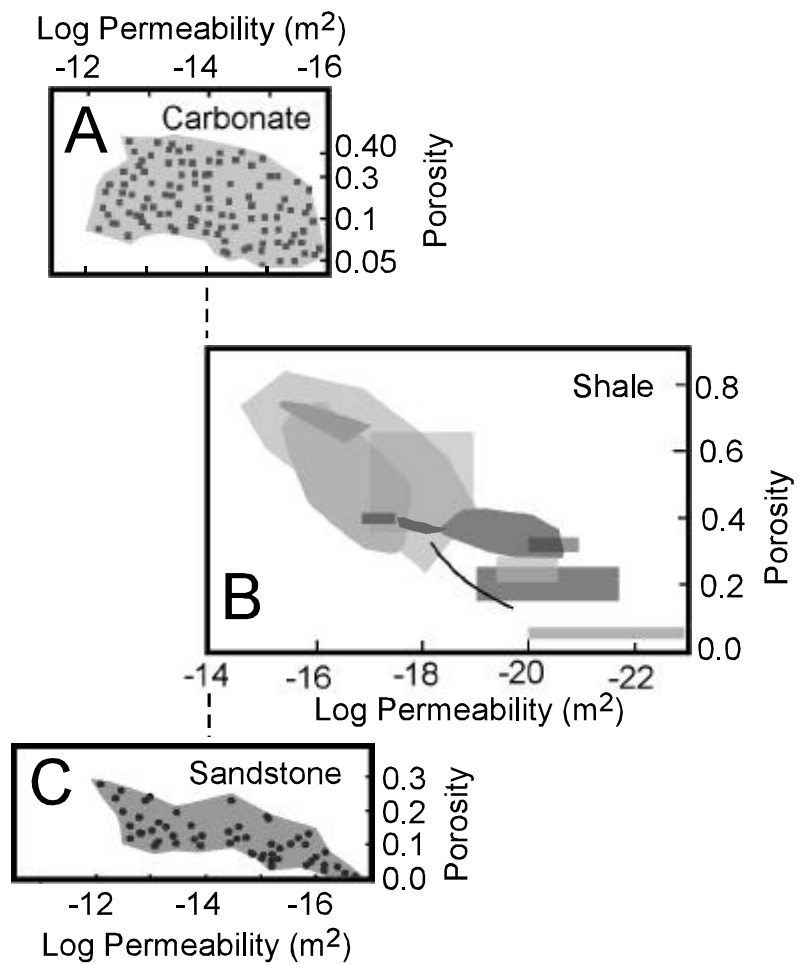


Figure 4.3. Permeability verses porosity of carbonate (A), shales (B), and sandstones (C) rocks. Data is based on measurements and inverse analysis (after Neuzil, 1994; Shenhav, 1971; and Lucia, 1995).

clays and shales compiled by Neuzil (1994) and alluded to earlier are shown in Figure 4.3B. Although clays and shales volumetrically dominate most sedimentary sequences relatively few data are available for them. Figure 4.3B incorporates measurements from laboratory, borehole and regional scales, showing that shale permeability is not necessarily scale-dependent. It should be noted, however, that instances can also be found where shale permeability increases with scale, apparently when transmissive fractures or faults are present. As discussed earlier, fracture permeability in shale seems to be important mostly in the upper one or two kilometers of the crust. Additional discussion of fracture permeability in shales can be found in Bredehoeft et al. (1983) and Belitz and Bredehoeft (1989). Note that for comparable porosities one might expect a factor of $\sim 10^6$ difference in permeability between sandstones and intact shales.

The permeability of carbonate rocks is somewhat problematical because it can be grossly affected by fractures, especially when they are widened by solution. In carbonate sediments and rocks that are not affected by secondary permeability, such as those at significant depths, Lucia (1995) has presented an exhaustive study of measured permeability-porosity relationships. His data are presented in Figure 4.3C. Note that the relationship between permeability and porosity in carbonate rocks is not as clear-cut as in sandstones and shales. Note also that for a given porosity carbonates rocks like sandstones tend to be several orders of magnitude more permeable than intact shales. Lucia (1995) also considered the drastic effects that secondary permeability can have and calculated the permeabilities that might be associated with fractured carbonates.

It is also instructive to consider some of the permeability values that researchers have adopted or assumed in studies of various basins. Several studies have used a log-linear relationship to represent permeability versus porosity so that values of PM1 and PM2 for different lithologies can be compared directly. Table 4.1 does just this and includes assumed anisotropy values as well. Note that the parameter values for marine shale from Corbet and Bethke (1992) were constrained by the large-scale behavior of their system and are actually a large-scale "measurement."

TABLE 4.1 Rock Permeability Parameter Values used in Modeling Studies

Rock Type	K_h (m^2)	$\frac{K_h}{K_v}$	PM1	PM2	Reference
Sandstone	3.47E-14	2.5	-15	15	1
Marine Shale	2.04E-15	10	-21	8	1
Limestone	6.5E-11	2	-16	20	2
Evaporite	3.33E-18	100	NA	NA	3
Congomerate	1.0E-14	10	-14	NA	5
Siltstone	2.14E-13 to 2.86E-14	NA	NA	NA	4

References:

- 1 - Corbet and Bethke (1992).
- 2 - Sanford and Konikow (1989). Modeling parameters for a carbonate formation.
- 3 - Garven (1989). Modeling parameters for the Middle Devonian evaporites in the Western Canada Sedimentary Basin.
- 4 - Mercer et al. (1982) Table 2.1.22, from Golder Associates (1977).
- 5 - Mailloux et al. (1999)

Deformation properties and porosity. All transient flow phenomena in basins, including the generation, maintenance, and dissipation of anomalous pressures, are controlled by porous medium deformation in response to changes in effective stress and diagenetic processes. Over human time scales, when overburden loads and other external stresses are usually constant, porosity changes and deformation occur only as fluid is stored or released from storage during transient flow. On longer time scales, additional porosity changes and deformation occur if external loads change due to ongoing deposition, erosion, or tectonic squeezing, or if diagenesis alters the pore structure. Active deposition, for example, tends to decrease porosity and raise fluid pressures by compaction. Pressure solution and other diagenetic processes that cause changes in porosity and increase fluid pressure also occur in basins on these time scales. Although deformation is crucial to so many aspects of basin flow, the difficulty of determining appropriate deformation properties for flow simulations is largely unappreciated. In this section we discuss the deformation parameters used by RIFT2D and offer guidelines for determining values for them. Because deformation properties in RIFT2D are closely related to porosity evolution, the latter is an integral part of the discussion.

Deformation of geologic media in response to stress changes and diagenesis is quite complex. Although the groundwater flow equation in RIFT2D derives its form from poroelastic theory (and thus is based on the notion of a linearly-elastic porous medium and small deformations), RIFT2D is, as noted in Chapter 2, able to account for large deformations that are not elastic. This is accomplished by letting K' , the modulus of vertical deformation, vary in space and time. An "elastic" or constant K' is applied only over a single time step and thus for small deformation increments that can reasonably be represented as linear. In addition, because of its poroelastic basis, RIFT2D can be used in engineering applications where the deformation behavior of the porous medium may in fact be approximated as elastic.

In elastic media, deformation moduli can be measured in a relatively straightforward manner with laboratory tests. However, basin analyses present a rather different problem. Even testing geologic samples over the range of loads encountered in a basin is not sufficient to determine K' because we cannot duplicate the long-term physical and diagenetic deformation processes that can be quite significant over geologic time. Effective values of K' that apply over geologic time and include diagenetic effects simply cannot be measured directly. Fortunately, basins themselves can be viewed as natural, long-term deformation experiments, and by accepting certain assumptions they can provide estimates of effective, long-term values of K' . The change in porosity with depth

provides the measure we seek, because it aggregates all the deformation processes at work in the basin as overburden loads increase and temperatures climb during burial.

Porosity-depth plots graphically demonstrate the complexity of deformation behavior. In nearly every case, the rate of porosity loss can be seen to decrease with depth, showing that geological media become "strain hardened" (that is, the deformation modulus K' becomes larger with increasing overburden loads). This simple observation is, in fact, the basis for the approach RIFT2D uses to estimate K'; in essence, the observed porosity loss (assumed to indicate vertical deformation) over a particular depth interval is related to the change in effective stress over the same interval to compute K'. Some form of this approach is adopted by most basin simulators, such as BASIN2 (Bethke et al., 1993). Indeed, short of attempting to simulate complex rheologies and diagenetic processes directly, which is impractical at present, this seems to be the best approach available for representing deformation on geologic time scales.

Although tying deformation properties to porosity profiles solves many problems, there are important assumptions implicit in this approach that are rarely discussed and not widely appreciated. In order to gain an appreciation of the pitfalls inherent in this approach, *it is crucial that these assumptions be clearly understood*. The main assumption underlying the approach is that porosity variation in a sedimentary sequence at a moment in time can be used as a surrogate for porosity changes in a packet of sediment over a long period of time. In effect, it is assumed that

$$\frac{D\mathbf{f}}{Dt} = \frac{D\mathbf{s}_e}{Dt} \frac{d\mathbf{f}}{d\mathbf{s}_e} \quad (4.2)$$

The left hand term is the information of interest, namely the porosity loss in a packet of sediment over a time step. It is determined in RIFT2D by the terms on the right hand side of 4.7 (although the calculations are not done in exactly this form). The change in \mathbf{s}_e over the time step (the first term on the right hand side) is calculated from changes in total stress and fluid pressure, while the change in porosity \mathbf{f} with \mathbf{s}_e (the last term), is computed from the porosity-depth (or, equivalently, the porosity-effective stress) relationship. Thus, by invoking 4.2 *one is assuming that all porosity loss can be uniquely tied to effective stress \mathbf{s}_e* . However, porosity loss in basins clearly does not depend only on \mathbf{s}_e . Diagenetic porosity loss also depends on temperature, pressure, chemical environment, and time. Diagenetic porosity changes are therefore included in RIFT2D as reflected in a particular porosity-depth curve; they are not controlled (as in real basins) by the actual temperature, pressure, and chemical changes the sediment experiences.

Because they include diagenetic effects, values of K' computed from porosity profiles are generally much smaller (that is, the compressibility is much larger) than those measured in laboratory tests on the same materials. This can be seen in Figure 4.4, taken from Neuzil (1986), which compares vertical compressibilities ($1/K'$) computed from porosity-depth profiles with a large number of laboratory-measured compressibilities. Figure 4.3 shows that laboratory compressibilities are generally about two orders of magnitude smaller than long-term *in situ* compressibilities (that is, media appear ~ 100 times stiffer in the laboratory than *in situ*). Short-term analyses, for example those involving engineering problems, would more appropriately use laboratory-determined moduli. Constant porosity can be represented in RIFT2D by setting the vertical compressibility to zero and assigning the desired porosity to ϕ_o .

Using porosity-depth data to estimate deformation properties is greatly simplified if the data can be represented with an analytical expression. Such an expression was developed by Athy (1930) who, guided by field observations, proposed an exponential relationship between porosity and depth. As noted in Chapter 2, RIFT2D uses a form of Athey's expression written in terms of effective stress. For burial and compaction it is

$$\phi = \phi_o \exp \left(-\beta \frac{\sigma_e}{g(\rho_s - \rho_f)} \right) + \phi_{ir} \quad (4.3)$$

while for erosion and decompression it is

$$\phi = [\phi_{min} - \phi_{ir}] \exp \left(-\beta_{ul} \frac{\sigma_e - \sigma_{max}}{g(\rho_s - \rho_f)} \right) + \phi_{ir} \quad (4.4)$$

In these expressions ϕ_o is the porosity at the sediment surface, ϕ_{ir} is the irreducible porosity, σ_e is the effective stress, and β and β_{ul} are deformation coefficients for loading and unloading conditions respectively. The quantity ϕ_{min} is the minimum porosity a sedimentary layer attains before unloading begins, and σ_{max} is the maximum effective stress applied before unloading occurs. The current version of RIFT2D does not allow for the seamless treatment of multiple cycles of deposition and erosion using equations (4.3 and 4.4). That is, following an initial phase of erosion, RIFT2D implements equation 4.3 regardless of whether or not σ_v is less than σ_{max} . The variable β_{ul} is invariably smaller than β so that only part of the porosity lost with burial is regained when the porous medium is unburdened by erosion.

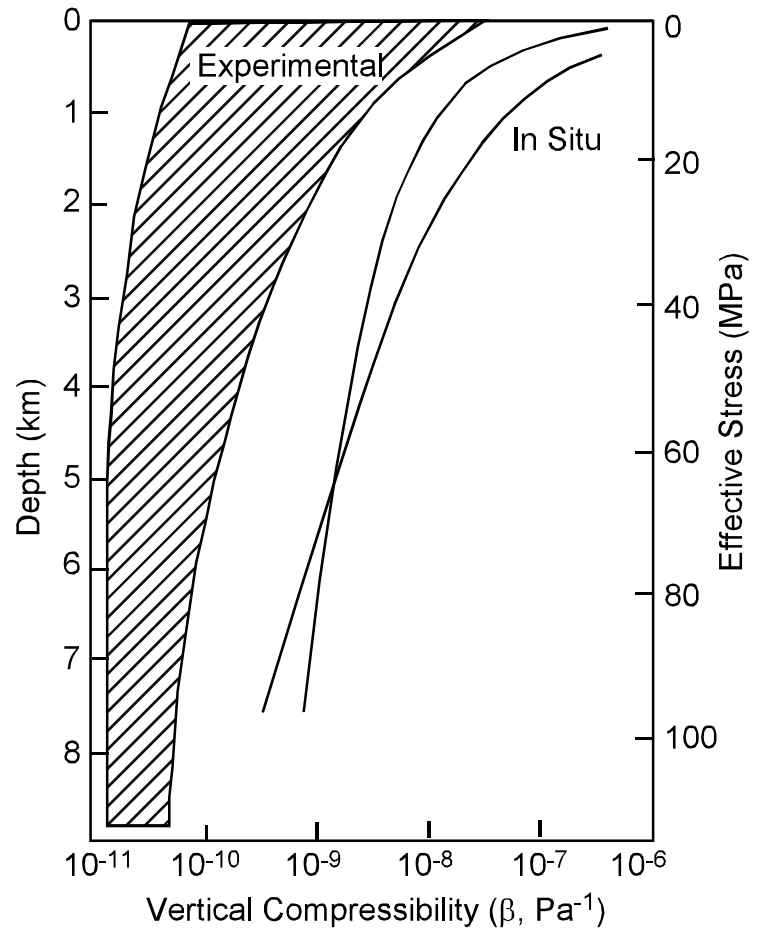


Figure 4.4. Comparison of laboratory and in situ measurements of the moduli of compressibility of sedimentary rocks (from Neuzil, 1986).

In Appendix 1 we show that if equation 4.3 applies, the modulus of vertical deformation K' is given by

$$\frac{1}{K'} = \beta \left[\phi_o \exp \left(-\beta \frac{\sigma_e}{g(\rho_s - \rho_f)} \right) \right] \quad (4.5)$$

In a similar fashion, if equation 4.4 applies, K' is given by

$$\frac{1}{K'} = \beta_{ul} \left[(\phi_{min} - \phi_{ir}) \exp \left(-\beta_{ul} \frac{\sigma_e - \sigma_{max}}{g(\rho_s - \rho_f)} \right) \right] \quad (4.6)$$

Thus the parameters that determine K' and control deformation in RIFT2D are β , β_{ul} , ϕ_o , and ϕ_{ir} . Except for β_{ul} , these are estimated by fitting 4.3 to an appropriate porosity-depth relation. Appropriate values for β_{ul} are somewhat problematic because, as noted above, compaction deformation is not fully recovered when sediments are unloaded. Most analysts have adopted the simple rule-of-thumb that roughly 10% of compactional deformation is recovered during decompression. Because β and β_{ul} represent the natural log of the rate of change of porosity with effective stress, the 10% rule-of-thumb equates to setting the value of β_{ul} at half the value of β . This broad generalization seems to fit what is known of rock deformation over long time scales but clearly oversimplifies the complex behavior of geologic media. In studies where decompression behavior is important better estimates of β_{ul} should be obtained or the consequences of uncertainty in the values of β_{ul} should be considered.

Because different sediment and rock types tend to deform differently, the most general approach is to specify these parameters for each unit in the simulation. While there are rarely sufficient data to permit this level of specificity, it is often reasonable to define parameters for each of the major sediment/rock types, namely clays and shales, sands and sandstones, and carbonate sediments and rocks. Giles (1997) has performed a valuable service by compiling a number of published porosity-depth relations for each of these lithologic families; these can guide estimates of β , β_{ul} , ϕ_o , and ϕ_{ir} . His compilations, summarized in Figure 4.5, show that there are definite differences in patterns of porosity loss in different lithologies and also a rather wide range of behavior within each lithologic type. Clays and shales tend to lose porosity relatively easily, carbonates maintain porosity to greater depths, and sands and sandstones seem to be, on the whole, most resistant to compaction and porosity loss. The variation within a

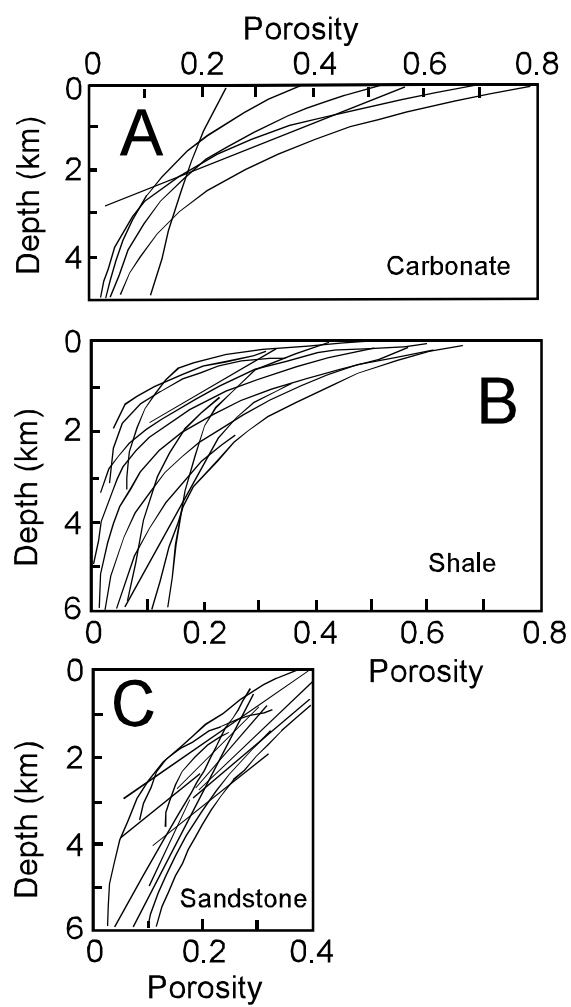


Figure 4.5. Porosity-depth data for carbonates (A), shale (B), and sandstone (C) (From Giles, 1997).

lithologic type is due to differences in the media themselves and their histories. Generally speaking, the most rapid porosity loss with depth is found in uplifted, eroded basins while porosity is maintained to the greatest depths in active, subsiding basins. Like generic permeability-porosity relations discussed in the previous section, there is great deal of "slop" within each lithologic type and rather different simulation outcomes are possible depending upon the relation that is selected. It is therefore always desirable to use system-specific data if available and to consider a range of behaviors if it is not. Table 4.2 presents a compilation of compressibility coefficient data.

A final word is in order about the fact that equations 4.3 and 4.4 are written in terms of effective stress σ_e rather than depth. This is because porosity-depth data are derived from basins with a variety of fluid pressure regimes so there is no single relationship between depth and effective stress. Thus, when fitting equation 4.3 to observed porosities such as those in Figure 4.5, depths must be converted to effective stress by accounting for the prevailing fluid pressures. In practice, it is usually sufficient to use a representative constant fluid pressure gradient and porous medium density to convert depth to effective stress. Unfortunately, published porosity-depth profiles (including those in Fig. 4.4) do not routinely include information about prevailing fluid pressure regimes making the conversion from depth to effective stress uncertain.

Thermal response coefficient. In equation 2.1 the thermal response coefficient Λ accounts for the effect of temperature changes on fluid pressure. For example, when sediments are buried and heated, both the pore water and the porous medium tend to expand. Λ is defined as $a_{Tf} - a_{Tp}$, the difference between the thermal expansivities of the pore water and the porous framework itself. If the pore water expansivity is the greater of the two, Λ is positive and increasing temperatures would tend to increase the fluid pressure. If, on the other hand the pore expansivity is greater, Λ is negative and rising temperatures would tend to decrease fluid pressure.

There are relatively few data from which to estimate Λ . Palciauskas and Domenico (1982) suggest that in well-compacted rocks a_{Tp} is on the order of $10^{-5} \text{ }^{\circ}\text{C}^{-1}$, while Neuzil (1993) reports that it is as large as $5 \times 10^{-4} \text{ }^{\circ}\text{C}^{-1}$ in compressible shale. Experimental data presented by Somerton (1992) indicates that, in sandstones at least,

TABLE 4.2 Compressibility Coefficients for Sedimentary Rocks

Rock Type	ϕ_o	ϕ_{ir}	β (1/m)	β_{ul} (1/m)	Reference
Sandstone	0.4	0.05	5.0E-04	1.0E-04	1
Shale	0.55	0.05	8.3E-04	1.67E-04	1
Limestone (Chalk)	0.7	NA	7.1E-04	NA	2
Evaporite	0.05	NA	NA	NA	3
Conglomerate					
(Dense sandy gravel)	NA	NA	6.8E-05 to 1.4E-04	NA	4
Siltstone					
(Shaley-Sandstone)	0.56	NA	3.9E-04	NA	2
Argillaceous					
Sediments	0.5	NA	6.0E-04	NA	5
Rock, fissured	NA	NA	4.2E-06 to 9.0E-05	NA	4
Rock, sound	NA	NA	=4.2E-06	NA	4

References:

- 1 - Corbet and Bethke (1992). This study expresses b and b_{ul} as exponential terms without $g(r_s-r_f)^{-1}$.
- 2 - Allen and Allen (1990). The compressibility coefficient is from Athy's equation.
- 3 - Garven (1989). Modeling parameter for the Middle Devonian evaporites in the Western Canada Sedimentary Basin.
- 4 - Domenico and Palciauskas (1979) Table 1 (after Domenico and Mifflin, 1965).
- 5 - Luo and Vasseur (1995). The compressibility coefficient is from Athy's equation.

α_{Tp} can actually have negative values of approximately $-2 \times 10^{-4} \text{ }^{\circ}\text{C}^{-1}$ indicating that the pores become smaller as temperature increases. This is apparently due to the solid grains preferentially expanding into the pore space. Water thermal expansivity α_{Tf} ranges from $10^{-4} \text{ }^{\circ}\text{C}^{-1}$ at $10 \text{ }^{\circ}\text{C}$ to $10^{-3} \text{ }^{\circ}\text{C}^{-1}$ at $150 \text{ }^{\circ}\text{C}$. In view of this, it appears that Λ probably varies from values somewhat greater than water expansivity to values that are near zero or even small negative values. Fortunately, although Λ is not very well constrained, thermal pressuring is usually a second-order effect in basin flow systems. In active, compacting basins, for example, thermal pressuring is usually overwhelmed by the effects of compaction. Thermal effects *are* sometimes of particular interest, however, because they can increase fluid pressure sufficiently to raise it above the lithostatic (overburden) stress and cause natural hydrofracturing. In analyses where thermal effects on fluid pressure are an important consideration it is probably advisable to consider a range of values, both positive and negative, for Λ .

Thermal and solute transport properties. Heat transfer, which is described by equation (2.18), occurs by both advection and dispersion/conduction. The dispersive-conductive component of heat transport (analogous to the dispersive-diffusive component of solute transport) is governed by the thermal dispersion-conduction tensor which in turn depends on the longitudinal and transverse thermal dispersivities, the conductivities of the grains and water, the heat capacity of the water, and the porosity. Longitudinal and transverse dispersivities for both heat and solute transport have been shown to be the same, so RIFT2D uses the same variables for both. (See the discussion of solute transport below for tips on estimating dispersivity values.) The thermal conductivity of the solid phase is typically several times larger than that of the fluid phase, so the magnitude of the thermal conduction-dispersion tensor will increase with decreasing porosity; these changes are calculated by RIFT2D (see equation 2.19). Typical values of thermal properties of geologic media and water are presented in Table 4.3. Values of these quantities are compiled by Mercer et al. (1982), Garven and Freeze (1984a), and de Marsily (1986). Except at high ($>1 \text{ m/yr}$) flow rates, thermal conduction is a more important heat transfer mechanism than thermal advection and dispersion.

Solute transport in RIFT2D is described with equation 2.20, which requires specifying components of the hydrodynamic dispersion-diffusion tensor. The dispersion-diffusion tensor components depend on the longitudinal and transverse dispersivities, which are properties of the porous medium, and the diffusion coefficient, which is also largely a medium property (see equations 2.21). In relatively permeable formations groundwater flow velocities are usually large enough that advective-dispersive transport

TABLE 4.3 Thermal Properties of Solid Phase

Rock Type	λ (W/m-°C)	c_r (cal./kg°C)
Siltstone	0.8-1.25	
Shale	1.05-1.45	
Sand	1.7-2.5	
Quartzite	4.2-6.3	
Lithic sand	1.23-2.1	
Graywacke	2.7-3.35	
Limestone	2.5-3.1	
Dolomite	2.5-3.1	
Salt	4.8-6.05	
Anhydrite	4.9-5.8	
Coal	<0.5	
Granite	2.5-3.35	
Basalt	1.45-2.1	
Rhyolite Glass	1.25-1.45	
Rhyolite Ash	0.6-1.05	
Welded Tuff	1.7-2.1	
Water	0.59	

dominates and diffusion is unimportant. However, in shales and other low-permeability formations solute transport is often dominated by diffusion.

The coefficient of free diffusion in water for most common ions lies in the range $1-2 \times 10^{-9} \text{ m}^2\text{s}^{-1}$. However, diffusion coefficients in porous media are smaller because diffusion takes place only in the pore spaces and follows a tortuous path. Coefficients of diffusion in fine-grained porous media generally fall in the range 10^{-10} to $10^{-11} \text{ m}^2\text{s}^{-1}$ while coefficients in coarse-grained media may be somewhat larger (Freeze and Cherry, 1979). Exact values vary by ion (because of different free-water coefficients; see Table 4.4) and change with temperature. There is also evidence suggesting that diffusion coefficients in low-porosity shales can be on the order of $10^{-12} \text{ m}^2\text{s}^{-1}$ because of ion exclusion effects. In relatively permeable formations where transport with flowing groundwater (advective transport) is significant, the values of dispersivity exert significant controls on solute spreading. It is now well established that the coefficients of longitudinal and transverse dispersivity have an apparent scale dependency (Fig. 4.6). This is thought to result from the incorporation of progressively greater lithologic heterogeneity (and thus more variation in flow velocities) as the scale increases. Fig. 4.6 suggests that at scales typical of basin simulations (on the order of 10^4 to 10^5 m), values of longitudinal dispersivity approximately 10^2 m or larger should be used. The transverse dispersivity is generally assumed to be about 10 times smaller than the longitudinal value. Note that RIFT2D uses the same longitudinal and transverse dispersivity coefficients to form the tensors in the heat and solute transport equations.

TABLE 4.4 Molecular Diffusivity of Chemical Components in Ground Water

Rock Type	D_d (m ² /yr)	Reference
NaCl	0.0511	1
Na ⁺ , Ca ²⁺ , Cl ⁻ , K ⁺ ,	0.0315 - 0.0631	2
Mg ²⁺ , HCO ₃ ⁻ , SO ₄ ²⁻		

References:

1 - Mercer et al. (1982) Table 8.1.2.1 after Camp (1963). D_d at 25° C.2 - Freeze and Cherry (1979; p. 103). D_d for major ions in ground water at 25° C.

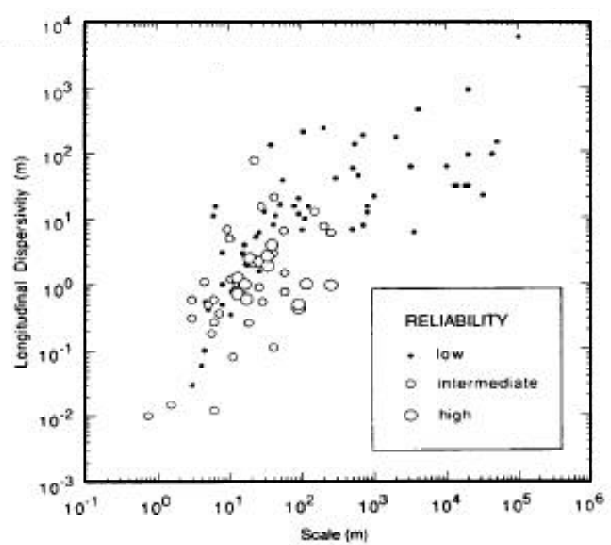


Figure 4.6. Effect of scale on longitudinal dispersion (from Gelhar, 1993).

Parameters for Petroleum Generation. In RIFT2D reaction rate constants reported by Ungerer and Pelet (1987) and shown in Table 4.5 are used to describe the degradation of types I and II kerogen into oil. These coefficients were determined from laboratory pyrolysis experiments but evidence indicates that they also describe petroleum formation within basins on geologic time scales. RIFT2D also uses the kinetic parameters of Burnham and Sweeney (1989) for Type III kerogen (Table 4.5). A large component of Type III kerogen is converted directly into gas whereas for Type I & II kerogen produces mostly oil.

The user specified parameters for petroleum generation are the concentration of kerogen in each unit (mass fraction; kg organic matter/kg sediment) and the fraction of types I, II, and III kerogen that compose it. In general, the fraction of kerogen should not exceed 0.1 and is generally between 0.03-0.5.

BOUNDARY AND INITIAL CONDITIONS

RIFT2D simulates fluid flow and heat and solute transport by solving equations that describe these processes over the simulation domain (see eqs. 2.1, 2.18, and 2.20 in Chap. 2). Basin simulation therefore requires that initial and boundary conditions be specified for the flow equation and, when heat and solute transport are simulated, for those transport equations as well. Choosing appropriate initial and boundary conditions is one of the more troublesome aspects of basin simulation because there are generally insufficient data to clearly define them. The difficulty is often exacerbated by the need to specify the boundary conditions through geologic time; typically conditions such as temperature, fluid heads or fluxes, and solute concentration at basin boundaries have evolved in complex ways and are poorly known. For example, we rarely know how water table elevation and basal heat flow in basins have evolved over millions of years. Because of the difficulties involved, uncertainty in initial and boundary conditions (particularly the latter) generally contributes significantly to uncertainty in simulation results.

Effects of errors in boundary and initial conditions are difficult to generalize; each case is different. Uncertainty in initial conditions may, for example, have little effect on results if one is interested only in later phases of a transient simulation. Simulations often quickly arrive at similar results despite significant differences the initial conditions specified. Similarly, one may be interested only in a subregion of the simulation domain that is relatively far from boundaries. In such cases boundary conditions may exert relatively little influence on the results. However, there are also

TABLE 4.5Kinetic Parameters for Types I, II and III Kerogen

Activation Energy (kcal/mole)	Genetic Potential (mg / g TOC)					
	Type I (oil)	Type II (oil)	Type III (H ₂ O)	Type III (CO ₂)	Type III (oil)	Type III (CH ₄)
38			4.4			
40		5	8.8			
42		3	13.2	14.5		
44			17.6	43.5		
46			17.6	72.5	0.35	
48	5	10	13.2	72.5	0.70	
50	10	30	8.8	43.5	1.40	7.56
52	15	150	4.4	29.0	0.70	12.96
54	20	325		14.5	1.40	15.12
56	800	60			0.70	14.04
58	10	20			0.35	12.96
60	15	10				11.88
62		5				9.72
64						7.56
66						5.40
68						4.32
70						3.24
72						2.16
74						1.08
Total Gen. Pot. (mg/gTOC)	875	618	88	290	7	108
Pre-Exponential Factor("A") (1/sec)	1E+14	1E+15	1E+13	1E+13	2E+13	1E+13

NOTE:

1. Kinetic parameters for Types I and II Kerogen taken from Tissot et al. (1987).
Pre-exponential factors from P.Eadington (pers. comm.)
2. Kinetic parameters for Type III Kerogen taken from Burnham and Sweeny (1989).

many instances where the boundary or initial conditions *do* make a significant difference to the results. In these cases one must pay particular attention to the boundary and initial conditions, assess the level of uncertainty associated with them, and factor this uncertainty into interpretations of the results. Often it is worthwhile to evaluate the sensitivity of simulation results to different initial and boundary conditions with multiple simulations. In any event, it is desirable choose boundary and initial conditions carefully and to recognize their effect on the results. Here we discuss tips on choosing initial and boundary conditions. Note that all boundary conditions in RIFT2D are specified by column. For example, head values along the upper boundary and heatflow values along the lower boundary can be specified and varied independently in each column.

Initial and boundary conditions for flow. The initial condition for flow is the pattern of fluid heads in the domain at the beginning of the simulation and is generally poorly known. Typically, however, this is not especially problematic because flow and head patterns adjust relatively quickly to reflect the processes simulated and the flow boundary conditions. The types of flow boundary conditions that can be used in RIFT2D simulations are somewhat restricted due to the nature of basin flow. Specifically, fixed heads must be specified along the upper boundary while the side and bottom boundaries are automatically treated as no-flow. While these boundary conditions would be rather restrictive for hydrogeological problems in general, they are well-suited to basins.

Specified heads have been shown to be a versatile and useful upper boundary condition for regional flow simulations. They are used to represent a water-table where the head is simply the water-table elevation. At basin scales, the water table can generally be considered a subdued replica of the land surface (Toth, 1962). Deep water tables are sufficiently rare that it is generally acceptable to approximate the water table elevations using topographic elevations. As such, the upper flow boundary condition in practice equates to specifying the land surface elevation through time. Anything that provides inferences about paleo-topography, such as apatite fission track studies, can be used as a guide for constraining elevations in basins during periods of tectonic uplift (Toupin et al., 1996). Modern measurements of depositional slopes within some sedimentary facies (such as alluvial fans) can help constrain the water table gradient in coarse clastic facies. It is a good bet to assume the water table is generally flat across playa/lacustrine paleoenvironments. Hydraulic head boundary conditions near coasts may need to account for temporal fluctuations in sea level.

As noted, RIFT2D treats side and lower boundaries as impermeable by requiring them them to be no-flow. Although this is generally quite sufficient for basin simulation, it does require that the simulation domain boundaries be chosen appropriately. The lower

boundary of the region to be simulated must be selected such that (1) it includes the entire permeable section or (2) it includes a portion of the section bounded below by a low-permeability stratum or other low-permeability feature. In simulating the Gulf Coast basin, for example, Bethke (1986a) chose the lower simulation boundary to coincide with the Louann Salt. Other workers have located the lower and side boundaries to coincide with the top of the underlying crystalline basement. With respect to the latter, it is well to keep in mind that crystalline rock, especially where it adjoins sedimentary units, is often fractured and weathered. Thus it may be desirable to include a "rind" of permeable crystalline rock in the domain. Side boundaries are often sloping portions of the lower boundary where the basin sediments thin and feather out. In other cases side boundaries can be chosen to correspond to an assumed plane of symmetry.

Initial and boundary conditions for temperature. Initial thermal conditions (temperatures at the beginning of a simulation), like initial flow conditions, are difficult to determine with any specificity but generally not critical to the simulation results. Boundary conditions for the heat flow equation in RIFT2D are specified temperatures along the upper boundary and a specified heat flux along the lower and side boundaries. Specified temperatures at the upper boundary represent long-term averages of climatic temperatures at the surface. Seasonal temperature signals and usually even longer-term variations have too high a frequency to be accounted for. However, it may sometimes be reasonable to account for shifts in surface temperatures due to processes such as surface glaciation and continental drift. Fortunately in the case of the latter, paleomagnetic reconstructions now provide reasonable information on the changes of latitude of continents through time. Other paleotemperature data, such as that provided by fossil assemblages, may also be of use.

Specifying heat fluxes through the bottom and sides of the domain is a more difficult problem. Many studies have presented evidence that basement heat flow is not constant through time, especially in extensional tectonic settings (McKenzie, 1978). This is thought to be due to crustal thinning and resultant shallowing of hot mantle rock. Igneous intrusions can also have a pronounced effect on basement heat flow. These tend to be extreme but short lived phenomena on the time scales of basin formation. Large

igneous intrusions can have high concentrations of radioactive elements that produce heat for long periods of time, resulting in the need to specify elevated heat flows where basins overly them. Note that where the domain boundary is slanted, the heat flux per horizontal area is maintained by correspondingly reducing the flux per area through the slanted boundary.

Initial and boundary conditions for concentration. Initial conditions for concentration of solutes, like initial distributions of head and temperature, typically are highly speculative. However, the effects of initial solute concentrations may persist well into a simulation. This is reason enough to pay particular attention to initial concentration conditions. However, it is also possible to specify an invariant concentration pattern in a RIFT2D simulation. An invariant salinity pattern is appropriate when it is thought that an approximate stasis or "steady state" exists with respect to the solute distribution whereby fluxes of solute have adjusted to a reasonably steady production of solute by various processes. It is also appropriate when a relatively small segment of time (compared to solute transport times) is to be considered. In either case the choice of solute distribution (and hence the density distribution) will affect the flow during the entire simulation. In these cases the specified solute distribution is especially important.

Clearly it is desirable to have basin-specific data to constrain salinity variation. Nevertheless, it is possible to draw some generalizations about salinity patterns. Significant salinity variations are the rule rather than the exception in large basins (Hanor, 1994). Generally, salinity increases with depth because meteoric recharge flushes solutes from shallow formations. Observed salinity gradients largely reflect the resulting upward transport of solutes by advection, dispersion and diffusion. Increases in salinity with depth can be seen in Fig. 4.7, a rendering of Hanor's (1987) plot of salinity-depth relations in several important basins. Fig. 4.7 also shows that complexities exist; salinities in the southern Gulf of Mexico *decrease* dramatically below about 3 km depth. Often, salinity gradients are relatively small; although concentrations typically range between nearly 0 and 0.2 to 0.4 kg/kg, the changes are spread over kilometers, as shown in Fig. 4.5. However, relatively sharp salinity gradients are also found. For example, Bachu (1995) indicates salinity differences exceeding 0.2 kg/kg exist across relatively thin shales in parts of the Alberta Basin. Salinity patterns are also affected by the

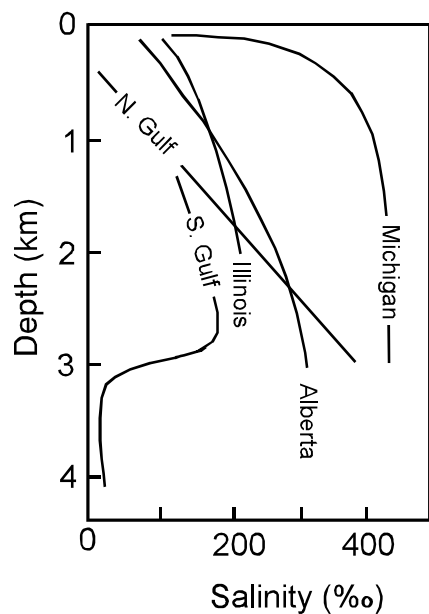


Figure 4.7. Variations in salinity with depth in select North American Basins (from Hanor, 1987).

presence of evaporites. Salt domes in the Gulf Coast, for example, are associated with zones of very high salinity water (at or approaching halite saturation of ~0.2 kg/kg) that may drive convective circulation (Hanor, 1987).

Concentration boundary conditions in RIFT2D are analogous to flow boundary conditions: specified concentrations are applied along the top boundary and no solute fluxes are permitted through the bottom and sides. Generally, recharge areas where meteoric water enters the system should be assigned low solute concentrations (~0.0 kg/kg) and fluxes into the system at marine coastlines should be assigned seawater concentrations (~0.03 kg/kg). In some cases, a knowledge of the geologic record and past environments provides necessary information. As already noted, evaporites within or bounding the system can be expected to dissolve and create brines. RIFT2D allows the user to specify solute concentrations in interior elements to mimic this process; these should be assigned a concentration representative of halite and other salt saturations (~0.2 kg/kg). Similarly, playa settings can generate brines by evaporation, and water-table recharge from them at the upper boundary should be assigned an elevated concentration based on the type of evaporite minerals thought to have formed. At best, this is crude approximation of the actual recharge concentrations from playas because their salinities evolve through evaporative pumping (salt concentration resulting from base soil evaporation) and solute losses caused by deflation.

CHAPTER 5 – RIFT2D DATA FILE DESCRIPTION

To help familiarize RIFT2D users with the variables used in a RIFT2D data file, the overall structure of the data file is presented here. It is recommended that one of the sample data files presented in Chapter 6 or 7 be used as a template by the RIFT2D user in building a basin simulation model. *We strongly recommend that new RIFT2D users start with relatively simple data decks that use relatively coarse discretization (less than 1000 nodes) and simple boundary conditions before trying to construct data sets with large numbers of nodes, complex geometries, and tectonic conditions (i.e. erosion, faulting, uplift, etc).* It is important to honor data-type convention in constructing a data file. These are specified in APPENDIX 2. All variables which utilize a decimal place and end with and exponent (e.g. "D+") indicate a REAL*8 variable. Any variables which have no decimal place are integers.

Assigning Input/Output file names and Dimensions

One input data file and a number of output files are used/created by RIFT2D (Table 5.1). Input and output data file names for RIFT2D are assigned in the file “RIFTFILES.TXT” (if you are running RIFT2D on Unix, remember that the operating system is case sensitive and the file name should be upper case). The names of the data files are arbitrary and up to the user. As an example, the contents of a sample “RIFTFILES.TXT” file is listed below along with its associated unit number:

jurassic3.dat	unit 7
rift.out	unit 8
rift_tec.dat	unit 11
sfc_tec.dat	unit 50
prf1_tec.dat	unit 55
prf2_tec.dat	unit 56
prf3_tec.dat	unit 57
prf4_tec.dat	unit 58
prf5_tec.dat	unit 59
prf6_tec.dat	uint 60
elem1_tec.dat	unit 65
elem2_tec.dat	unit 66
elem3_tec.dat	unit 67
elem4_tec.dat	unit 68
elem5_tec.dat	unit 69
elem6_tec.dat	unit 70

Table 5.1 Description of Input and Output Files

Unit Number	Description
7	Input data deck for RIFT2D. This data file is read in subroutines READIN and BCREAD. The later subroutine only reads in boundary condition data if more than one tectonic periods is required.
8	Contains nodal and elemental output for each time step specified. The relevant variables to control output file size are ISKIP, NTIME, and IPRINT. This output file is generated by subroutine OUTPUT.
11	Contains field variables from the model to construct contour maps of heads, temperatures, concentrations, velocity vectors (nodal weighted) as well as mesh and stratigraphy plots using TECPLOT. The relevant variables to control output file size are NTIME, IPRINT, and IPRSTR. This output file is generated in subroutine TECOUT.
50	Contains field variables for plotting surface flux data including ground water discharge/recharge and conductive heat flow. The relevant variables to control output file size are NTIME, IPRINT, PSFC, and NCOLS. Output variables include X, QX, QZ, and JZ. This output file is generated in subroutine SFCOUT.
55-60	Contains field variables from the model to construct scattergram profiles (e.g. depth versus temperature, head, pressure, lithostatic pressure, hydrostatic pressure, porosity, or vitrinite reflectance) within TECPLOT. The relevant variables to control output file size are NUMWEL, WELLID, IPRINT, and NTIME. This output file is generated by subroutine TECOUT. Up to 20 wells can be plotted using default dimensions set in program (MAXFLTS). Output variables include DEPTH, HEAD, PRES, PRESL, PRESH, VSM, PHI, SS, RHOF, TEMP, MASSOIL, MASGAS, RF, and TR. This output file is generated in subroutine TECOUT.
65-71	Contains field variables from the model to construct scattergram plots for up to six elements through time. The relevant variables that control output file size and number are NTIME and NRR. Variables plotted include HEAD, TEMP, QX, QZ, X, Z, and TIME for select elements. This output file is generated by subroutine PELEMOUT. Note that specified if an element doesn't exist at the start of the simulation, then fewer than NTIME "zones" will be created by RIFT2D. The user must then edit the output file to change the number associated the variable "I" at the top of each data set.

Once you have established the files names, simply type “RIFT2D” at the command line in UNIX or at the DOS prompt on your PC computer. The initial grid, tectonic, hydrologic, and thermal boundary conditions as well as simulation control parameters are read by RIFT2D in unit 7. Almost all of the input data is read in free format to reduce possible input errors. The dimensions of RIFT2D variables are specified in the file “RIFT2D_DIMENSIONS.TXT”. The program must be recompiled if these are changed. The variables assigned by this file are described in Table 5.2. With few exceptions, the array dimension should be large enough to accommodate most grids which can be solved efficiently using Gaussian elimination. Note that the RIFT2D_DIMENSIONS.TXT, RIFT2D, AND RIFTFILES.TXT must reside in the same directory.

Simulation Control Parameters

At the top of the data file, there are a number of variables which control the overall simulation (Table 5.3). Extra “descriptor” lines have been added to RIFT2D data files so that variables are easily associated to their numerical values. The descriptor labels are in bold in Table 5.3. Some of the more important of these include the number of nodal columns (NCOLS), the number of elemental columns (BEC) in each fault block, the number of elemental rows (BER) in each fault block, the number of time steps (NTIME), and the time step size (DT). A number of simulation control flags are provided to specify whether or not a particular transport/geochemical process is represented including ground water flow (IFLOW), heat transport (IHEAT), solute transport (IBRINE) as well as oil generation and migration (IOIL). These parameters should be set to 1 if the process is to be represented and 0 if the process is to be ignored in a given simulation. In addition it is possible to specify whether solutions to the groundwater flow equations are coupled to heat and/or solute transport (ICOUP). Because RIFT2D utilizes a particle tracking algorithm to represent solute transport a number of additional simulation control parameters are needed including: 1) the normalized distance (between 0-1) a particle may move across an element during a particle time step (GAMMA) 2) the maximum number of particle moves permitted in a particle time step (MAXIT), and 3) the time at which solute transport is “turned on” in the simulation (TBRSTR). The characteristic width and length of an element is used to

Table 5.2 RIFT2D Array Dimension Variables

Variable	Description
MAXNODES	Maximum number of nodes in finite element mesh. The default value is 20000.
MAXELEMS	Maximum number of triangular elements in finite element mesh. Generally, this should be set to twice the value of MAXNODES. The default value is 40000.
MAXWDT	Maximum bandwidth for Gaussian elimination matrix AA. This should be greater than the maximum difference in node numbers (MAXDIFF) in a triangular element. If only flow is simulated (IFLOW=1) then MAXWDT >MAXDIFF+1. If heat transport is specified (IHEAT=1), then MAXWDT >(MAXDIFF*2)+1. The default value is 200.
MAXBNDS	Maximum number out boundary nodes along top, bottom, and sides of solution domain. This number should be set larger than 2*(BEC+1) + 2*(BER+1). The default value is 2000.
MAXMATS	Maximum number of material tags. This is usually set to 9.
MAXFLTS	Maximum number of faults. The default value is 20.

Table 5.3 Simulation Control Parameters used in RIFT2D Data Files

```
Title Line
SIMULATION CONTROL PARAMETERS
  NCOLS   IOUT    IPRTNT  ISKIP   IPRFST   MAXIT   IPRSTR
  6       00      1800    1       1        500     0.0D+0
  IHEAT   IBRINE  ICOUP   IFLOW   IOIL
  0       0       0       1       0
  NTIME   DT      THETA   SGRAD   NFLT     GAMMA   TBRSTR  DELZMN
  1800   5.0D+04 1.d0    0.d0    1        0.5     6.0d+4  20.0d+0
  BEC    BER
  2       25
  2       25
```

control the particle time step size for solute transport (DTP). However, if a new elemental row has just been generated below the land surface (or sediment/water interface) then DTP can be set to such a small value that within one time step, thousands to millions of particle moves must be calculated within the larger flow and heat transport time step (DT). Thus, a cut-off criterion for particle time steps (MAXIT) and minimum cell width (DELZMN) are used to calculate the particle move time step size (DTP). The time step size for the flow and heat transport is defined by the user. RIFT2D determines DTP based on the velocity field and element dimensions. The value of DTP is calculated internally within the program. If solute concentrations are high (i.e. a solute mass fraction of 0.1-0.3), then care should be taken to set DT approximately equal to DTP in order to solve for fluid flow and solute transport sequentially.

If little is known about the time evolution of salinity, the user may wish to simply impose a salinity gradient using SGRAD, setting TBRSTR to be greater than the total simulation time (in years), and setting IBRINE to equal 1.

Printing & Graphical Output Parameters

While printed RIFT2D output is available in the file "rift.out", the most efficient way to interpret simulation results is by creating graphical output. Near the top of the data file, a number of print options are presented to control the frequency, amount, and format of printed and graphical output (Table 5.4). The time step interval for printed and graphical output is controlled by IPRINT. For example, if IPRINT is set to 5, then output is provided every five time steps. Graphical and printed output will only be generated after the time step number (IT; IT=1,NTIME) exceeds the value of IPRSTR. For printed output, the user may only wish to see a fraction of the calculated nodal and elemental variables. This can be done by setting the variable ISKIP to be greater than 1. For example, if output for every tenth node is desired, ISKIP should be set to 10.

In some instances, the user may wish to compare RIFT2D output to subsurface data (e.g. vitrinite reflectances or pressure profiles) from wells or monitor the temporal evolution of hydraulic heads, etc. within a given layer. Vertical profiles of hydraulic head, temperature, fluid pressure, porosity, and permeability as well as a number of organic maturation parameters can be generated using TECPLOT scattergram formats. These are listed in Table 5.4. If NUMWELS is greater than zero, then profiles of heads,

Table 5.4. Graphical output parameters specified in RIFT2D data files

OUTPUT CONTROL PARAMETERS(0=off, 1=on)						
ppec	pexp	psfc	pelem	NNR	NUMWEL	MSL
1	0	1	1	8	1	0000.0
NUMBER	ELEMENT					
1	1					
2	2					
3	3					
4	4					
5	5					
6	6					
7	7					
8	8					
NAME	COLUMN NUMBER					
WELL1	2					

temperatures, and vitrinite reflectance will be generated. The total number of columns (up to six) for which profile information is to be generated is specified using the variable NUMWEL. The nodal column number and associated "well id" is specified below this line in the data file. The output files which contain this data are in rift1.prf to rift6.prf (tab delimited format) and rift_tec_prf (TECPLOT format). Calculated surface heat flow and fluid flux across the land surface is often useful for model calibration and mass balance tests. This data is provided by setting the flag PSCF to be one (otherwise set to zero). Surface output data is generated in file sfc_rift.dat. The user may create contour maps of field variables such as hydraulic head, pressure, temperature in TECPLOT formats by setting the flag PTEC equal to 1 (otherwise set to zero). TECPLOT output is generated in the file rift_tec_dat. Output is sent to all of the above mentioned output files every IPRINT time steps. For TECPLOT plots, the calculated hydraulic heads may be adjusted to some reference datum using the MSL (mean sea level) variable.

The user may wish to also monitor the time evolution of elemental variables such as temperature, flow rates, and petroleum generation as the simulation progresses. This is particularly useful for modeling apatite ages for a given element. Monitoring the time evolution of elemental variables can be accomplished by setting the PELEM flag equal to 1 (otherwise set it to zero) and setting NNR equal to the number of elements for which temporal output is desired (up to 20). The element number for which temporal output is desired is specified using the variable NREL just below the line containing NNR.

Hydrostratigraphic Unit Parameters

The material properties assigned to a given hydrostratigraphic unit is listed in Table 5.5. In Table 5.5 two hydrostratigraphic units are specified. Determining the number of hydrostratigraphic units (NMAT) and their properties should be based on accurate geologic cross-sections or well log-in information. Adjacent rock units that have similar hydrologic properties (e.g., porosity and permeability) should be lumped into hydrostratigraphic units. Oil source rocks should be represented as separate hydrostratigraphic units. The boundaries of the hydrostratigraphic units is determined by the position and density of elemental rows. Thus, a relatively fine vertical discretization (30-50) is needed to approximate the location of sedimentary interfaces. The total number of hydrostratigraphic units is given by NMAT. The rock properties for each unit are input directly below beginning with hydrostratigraphic unit #1. This includes coefficients relating rock permeability to porosity (PM1, PM2, ANS), porosity/effective-

Table 5.5 Material Properties assigned to a hydrostratigraphic Unit in RIFT2D Data File

stress coefficients (PHI_o, BETA, PHI_IR, BETA_UL, RHOS), thermal properties (TKF, TKS, LDIS, TDIS, CVF, CVS, ALPHA), and source rock data (PERCT1 to PERCT3, TOC). These are described in more detail in APPENDIX 2. Rock properties are assigned to triangular elements by assigning an integer material tag (MAT) to each element. For example, if element 1 has a MAT tag of 3, then it is assigned the hydrologic and source rock coefficients corresponding to hydrostratigraphic unit #3. Assigning material tags to elements is done by creating an integer material tag matrix for each fault block. Each integer material tag corresponds to two triangular elements within an elemental row. Material tags matrices are read in a column/row format for each fault block moving from left to right across the basin and from bottom to top. In Table 5.5, a basal aquifer is specified comprised of three elemental layers. The aquifer is overlain by a source rock comprised of three elemental layers. It is important to note that the material tags read into RIFT2D here represent the basin at its maximum thickness. In general, at the start of the simulation, only a bottom most material tag data is used. As subsidence and sedimentation occurs, additional elemental columns are generated. The variables BEC and BER specify the total number of elemental columns and rows in each fault block, respectively. In Table 5.5, BEC is 44 and BER is 6.

Fault Block Rotation Parameters & Setting Tectonic Time Periods

A number of parameters must be specified to control the style of subsidence within the basin and the initial basin configuration (Table 5.6). Most important of these is ROTFLAG (Fig. 2.5) which determines whether subsidence occurs without faulting (ROTFLAG=0, NFLT=0), with vertical fault block motion (ROTFLAG=1; NFLT>0), or with domino-style fault block rotation (ROTFLAG=2; NFLT>0). The program can be dimensioned to accommodate any number of faults (and NFLT+1 fault blocks). If fault block rotation is specified, then the initial tilt of the fault block (ALPHA) and change in angle per times step (OMEGA) must be specified. If the user doesn't wish to represent domino-style fault block rotation, set OMEGA=0.0 and ALPHA=0. In order to represent domino-style fault block rotation, the user must also specify the depth of the centroid of each fault block (CENTZ). Setting the centroid depth influences which portion subsides and which is uplifted. In general, setting the centroid depth deeper causes more of the fault block to subside. Setting the centroid depth equal to the fault width causes fifty percent of the fault block to rise and fifty percent to subside.

Table 5.6 Fault Block Rotation and Tectonic Time Period Data used by RIFT2D

```
Structural imformation on faults, if no faults then ignore
rotation flag    omega      alphas     DELZ      init_rows
0                0.0        -90.0      55        17
Fault block Centz
1    1.0
TECTONIC TIME PERIODS:
TZTIM2      TZTIM3      TZTIM4      TZTIM5      TZTIM6      TZTIM7
9.50D+07    6.00D+09    12.00D+09   15.0D+09   19.1D+09   25.00D+09
TZTIM8      TZTIM9      TZTIM10     TZTIM11     TZTIM12     TZTIM13
1.00D+09    6.00D+09    12.00D+09   22.0D+09   19.1D+09   25.00D+09
```

When ROTFLAG>1, the number of nodes within a column is determined by DELZ, ZMAX, and ZMIN such that NROWS = (ZMAX-ZMIN)/DELZ. DELZ is the specified width of the elements, ZMAX is the initial position of the water table along a column and ZMIN is the initial position of the base of the sedimentary basin at IT=0 along a column. When ROTFLAG=0, then the initial number of nodes in a column is determined by Dividing ZMAX-ZMIN by INIT_ROWS.

As basin evolution occurs, the user may wish to change the subsidence or rotation rate or any of the transport boundary condition data. Currently, the user may specify up to 12 new tectonic time periods (TZT1M2 to TZT1M13). New tectonic time periods are specified in years. When the basin simulation time (TIME) equals one of the tectonic time periods, the new tectonic and boundary condition information is read in (see Table 5.6). The user must include, in chronological order, this information at the bottom of the data set. If the RIFT2D user does not want to read in additional tectonic or transport boundary condition data, then TZT1M2-TZT1M13 should be set to very large numbers (e.g. 1.0E+09 if it is not going to be used).

Setting Boundary Conditions for Mesh Evolution Along Nodal Columns

The initial position of each nodal column (X), initial subsidence rate applied to the bottom node of each column (VBASE), linear time step multiplier to change subsidence rate (VINC), erosion rate applied to the top node (VER), initial top (land surface or sediment/water interface) of the basin (ZMAX), initial base (sediment/crystalline rock contact) of the basin (ZMIN), style of subsidence/uplift (ICASE), and scaling parameter controlling the width of new elements generated due to subsidence (GRDFAC) must be specified for each nodal column (Table 5.7). Column spacing should be sufficiently refined to capture stratigraphic variations across the basin. Between 30-50 nodal columns is a good number to start with. However, if significant amounts of erosion occur in one portion of the basin, significant mesh refinement (in terms of adding additional nodal columns) must be added to insure the change in the number of nodes per column does not exceed 2. If basin evolution begins with subsidence along a particular column, set ICASE=1 (Fig. 2.6). If uplift with no erosion occurs along a column, set ICASE=2. If erosion occurs at the top of a nodal column, set ICASE=3. It is possible to specify uplift along some nodal columns and subsidence along other nodal columns within a given

Table 5.7 Subsidence Boundary Condition information for RIFT2D

Fault Block #1								
COL #	X	VBASE	VINC	VER	ZMAX	ZMIN	ICASE	GRDFAC
1	0.0	-1.0E-4	0.00	0.00	10000.	9000.	1	100.
2	2500.	-1.0E-4	0.00	0.00	10000.	9000.	1	100.
3	5000.	-1.0E-4	0.00	0.00	10000.	9000.	1	100.

FAULT BLOCK #2								
COL#	X	VBASE	VINC	VER	ZMAX	ZMIN	ICASE	GRDFAC
4	5000.	-1.0E-4	0.00	0.00	10000.	8900.	1	100.
5	7500.	-1.0E-4	0.00	0.00	10000.	8900.	1	100.
6	10000.	-1.0E-4	0.00	0.00	10000.	8900.	1	100.

tectonic time period. In the example shown in Table 5.6, column information has been specified for a two fault block (NFLT=1) data file comprised of three nodal columns each. It is important to point out that along each fault surface the X position of columns on either side of the fault must share the same location (in this case 5000m). This is required so that individual fault blocks can move independently of one another. The initial thickness of the fault blocks differs because ZMIN is 9000 meters in fault block 1 and 8900 meters in fault block 2.

Setting Hydrologic, Thermal, and Solute Mass Transport Boundary Conditions

Throughout the simulation, hydrologic, thermal, and chemical boundary conditions must be specified at the top and base of each nodal column (Table 5.8). These are read in once at the start of the simulation and once for each new tectonic time period. Currently, only specified value boundary conditions can be imposed at the land surface for the ground water flow (water table position; HDBASE, HDINC), heat transport (water table temperature at the water table; TPBASE, TPINC), and solute transport (water table concentration; CNBASE, CBASE) equations. The suffix “BASE” refers to the value assigned regardless of simulation time. The suffix “INC” refers to the desired incremental change that the user may wish to specify to allow the heads, temperatures, and/or concentrations to increase/decrease through time. For example, the specified head or temperature at the water table (or sediment/water interface) can be increased linearly during a tectonic time period. For example, to allow the water table head to increase during the tectonic time period in a linear fashion (IHCHK=2), equation (5.1) is used:

$$\text{HEAD}(NBN(n)) = \text{HDBASE}(n) + \text{HDINC}(n) * (\text{TIME} - \text{THA}) \quad (5.1)$$

Similar expressions are available for the heat (ITCHK=1) equation substituting TPBASE and TPINC for HDBASE and HDINC. The position of the water table can also be set equal the position of the land surface (top most node elevation in each column; IHCHK=1). The RIFT2D user can also allow the specified head boundary condition at the top of each column to vary as a sine function during a tectonic time period (IHCHK=3):

$$\text{HEAD}(NH(n)) = \text{MSL} + \text{HDINC}(n) \left[1 + \sin \left(\frac{2\pi(\text{TIME} - \text{THA})}{\text{THB}} \right) \right] \quad (5.2)$$

Table 5.8 Hydrologic, Thermal, and Solute Boundary Condition Information for First Tectonic Time Periods used by RIFT2D

SPECIFIED HEAD BOUNDARY CONDITION DATA				
COL#	ITCHK	THA	THB	
1	2	0.00D+00	5.00D+07	
2				
3				
4				
5				
SPECIFIED HEAT FLUX BOUNDARY CONDITION DATA:				
COL#	IJCHK	TJA	TJB	
1	1	0.00D+00	5.00D+07	
2				
3				
4				
5				
6				
SPECIFIED TEMPERATURE BOUNDARY CONDITION:				
COL#	ITCHK	TTA	TTB	
1	0	0.00D+00	1.00D+4	
2				
3				
4				
5				
SPECIFIED CONCENTRATION BOUNDARY CONDITION:				
COL#	CNBASE	NEVAP	CEVAP	
1	0.0D-02	0	1.00D-01	
2	0.0D-02	0	1.00D-01	
3	0.0D-02	0	1.00D-01	
4	0.0D-02	0	1.00D-01	
5	0.0D-02	0	1.00D-01	

The sine function boundary condition can also be specified for the heat equation for the top of the solution domain (ITCHK=2):

$$\text{TEMP}(\text{NT}(n)) = \text{TPBASE}(n) + \text{TPINC}(n) \left[1 + \sin \left(\frac{2\pi \text{TIME} - \text{TTA}}{\text{TTB}} \right) \right] \quad (5.3)$$

For the groundwater flow equation, the sine function boundary condition is intended to represent sea level fluctuation conditions in evolving marine basins. As such, head of the top node falls below the elevation of the top node, then if solute transport is also specified, then the

No flow boundary conditions are applied along the sides and base of the solution domain

$$J1(n) = J1\text{BASE}(n) + J1\text{INC2}(n) \left[\exp \left(\frac{J1\text{INC1}(n)(\text{TIME} - \text{TJA})}{TJB} \right) \right] \quad (5.4a)$$

$$J2(n) = J2\text{BASE}(n) + J2\text{INC2}(n) \left[\exp \left(\frac{J2\text{INC1}(n)(\text{TIME} - \text{TJA})}{TJB} \right) \right] \quad (5.4b)$$

for the ground water flow and solute transport equations. For heat transfer, insulated side wall boundary conditions are assigned to the sides of basins when no rotation is occurring (ROTFLAG<2). Under these conditions, a specified heat flux (J1BASE, J2BASE) and incremental change in heat flux (J1INC, J2INC) are assigned to all nodes along the base at the bottom node of each column. The magnitude of the flux boundary condition assigned to each node depends on the heat flux crossing the left (J1BASE) and right (J2BASE) adjoining line segments. As with specified value boundaries, the heat flux may be increased/decreased using J1INC and J2INC. The RIFT2D user can specify changes in basal heat flow (Figure 2.7) using a sine function (IJCHK=2) or exponential boundary condition (IJCHK=3):

A portion of the specified heat flux is automatically assigned to the sides of the solution domain for ROTFLAG=2. Internal specified concentration boundary conditions can be applied to certain sedimentary layers (e.g. evaporite beds) by specifying the material tag (NCLAY) of that bed. The associated concentration of the layer is given by CLAY. In hydrologically closed basins, significant salt accumulations can occur at the land surface when playas are being deposited. The user can specify a concentration at the land surface when the playa is being deposited by identifying what material tag is a playa

(NEVAP) and what the concentration of the playa should be (CEVAP) at that column. For the example data file listed in Table 5.7, two fault blocks each containing 3 nodal columns is specified (ROTFLAG>0). Because of the overlapping column along the fault surface at X=5000, the RIFT2D data file only requires 5 (rather than 6) surface boundary conditions are required for hydraulic head, temperatures, and solutes. Note that 6 are required for assigning basal heat flux. However, if ROTFLAG=0, then all 6 columns of boundary condition data would be needed in the data file.

Initial Conditions

For groundwater flow, hydrostatic initial conditions are assigned to RIFT2D by setting the head of every node in each column equal to the value of HDBASE for that column. It is recommended that HDBASE be assigned the value of the initial elevation of the top node or the height of the water column above the top node. Temperatures are assigned conductive geothermal gradient consistent with the surface temperature (TPBASE) and the heat flow (J1BASE) boundary conditions assigned to that column. The initial porosity at the land surface (PHI_O) and the thermal conductivity of hydrostratigraphic unit 1 are used in the calculating the initial conductive temperatures in RIFT2D. For solute transport, the initial concentrations are assigned consistent with the concentration of the top node (CNBASE) and the salinity gradient (SGRAD).

Resetting Tectonic, Hydrologic, Thermal, and Solute Mass Transport Boundary Conditions for New Tectonic Time Periods

As stated above, every new tectonic time period requires that a new set of column-wise tectonic and boundary condition information must be specified; one for each new time period specified using TZTIM2 to TZTIM13. The only difference between the format of this data and that for specifying this information initially is that a few parameters (e.g. ZMAX, ZMIN, X, TPBASE, TPINC) are not read in again because they don't need to be changed or are irrelevant. If no changes in boundary conditions or subsidence rates are requested, then the user should set TZTIM2 to TZTIM13 to be greater than the total simulation time (DT*NTIME). The surface hydrologic, thermal, and solute mass transport boundary conditions must be read in at each new tectonic time period using the same format described above.

Reading-in Information for Fault Block Rotation and Elemental Material Tags for New Tectonic Time Periods.

For each tectonic time period (TZTIM2-TZTIM12) the tectonic and transport boundary conditions data as well as the fault block rotation parameters are reset. When the simulation time TIME is equal to TZTIM2, TZTIM3, etc, the additional boundary condition data is read in at the end of the file. In addition, because eroded elements can be redeposited with new material properties, the elemental material tags are also re-assigned each new tectonic time period (Table 5.9). Note that the x position of the columns nor the temperature boundary conditions are specified at subsequent tectonic time periods.

Table 5.9 New boundary condition information for Subsequent Tectonic Time Periods

```

TECTONIC TIME PERIOD 2
X-, Z-COORDINATE DATA
COL # VZTBASE VZTINC1 VER ICASE GRDFAC
1 -5.00E-04 0 0.00E+00 1 10.0
2 -5.00E-04 0 0.00E+00 1 10.0
3 -5.00E-04 0 0.00E+00 1 10.0
4 -7.00E-04 0 0.00E+00 1 10.0
5 -7.00E-04 0 0.00E+00 1 10.0
6 -7.00E-04 0 0.00E+00 1 10.0
SPECIFIED HEAD BOUNDARY CONDITION DATA
IHCHK THA THB
1 0.00D+00 0.00D+00
COL# HDBASE HDINC
1 0000.00 0.00E+00
2 0000.00 0.00E+00
3 0000.00 0.00E+00
4 0000.00 0.00E+00
5 0000.00 0.00E+00
SPECIFIED CONCENTRATION BOUNDARY CONDITION:
COL# CNBASE NEVAP CEVAP NCLAY CLAY
1 0.000D-01 0 0.000D-01 0 0.000D-01
2 0.000D-01 0 0.000D-01 0 0.000D-01
3 0.000D-01 0 0.000D-01 0 0.000D-01
4 0.000D-01 0 0.000D-01 0 0.000D-01
5 0.000D-01 0 0.000D-01 0 0.000D-01
Structural information on faults; no faults then ignore
omega rotflag
0.0 0
block# centz rotation case
1 0.0 0
REASSIGNED MATERIAL TAG DATA: (FAULT BLOCK #1)
11
11
22
22
REASSIGNED MATERIAL TAG DATA: (FAULT BLOCK #2)
11
11
22
22

```

CHAPTER 6 - SAMPLE RIFT2D DATA FILES

In this chapter, three example data deck are presented to provide illustrated examples of the types of problems which can be addressed using RIFT2D. The examples differ primarily in the degree and style of fault block motion represented. In the first example, no faults are present (ROTFLAG=0; jurassic3.dat). In the second example, one fault is represented but with vertical tectonic movement (ROTFLAG=1; fault3.dat). In this example, the two fault blocks move past one another at different rates. In the final example, domino-style rotation is represented using two fault blocks (ROTFLAG=2; rotate3.dat). These files are included on the compact disk accompanying this documentation.

Example 1: Sedimentary Basin Evolution with Heterogeneous Sand/Shale Facies

In our first example data file (jurassic3.dat) we will consider the rather complex stratigraphic column shown in Figure 6.1. This experimental sedimentary profile was generated in the three-dimensional experimental basin facility of the Saint Anthony Falls Laboratory at the University of Minnesota (Jurassic Tank). The dark material in Figure 6.1A is coal and is meant to represent the deposits of fine grained facies such as clay or shale. The lighter colored material in Figure 6.1A is 1.5 mm diameter sand. The deposits were generated by maintaining a constant rate of sediment supply, constant (but spatially varying) subside rate, and temporally varying base level (sea level) in a sinusoidal manner first slowly (over most of the basins depositional history) and then much more rapidly. The dimensions of this experimental cross section are 1.2x0.8meters. While this basin was generated in the laboratory in a matter of days, the cross-sectional image display many of the basin-scale natural complexities of shoreline and transgressive/regressive facies at an unprecedented level of detail. For the first RIFT2D simulation example, we will up-scaled this cross section to natural dimensions of about 400x4 km (Figure 6.1B). We will assume that the deposits were generated over a period of 17 million years.

In this example, we will represent groundwater flow, thermal history, and oil generation during the basins development. This is specified by setting the following flags in the top of the RIFT2D data file: IFLOW=1, IHEAT=1, IBRINE, IOIL=1, ICOUP=1. Thus flow, heat, and brine transport are all specified. We will start with a

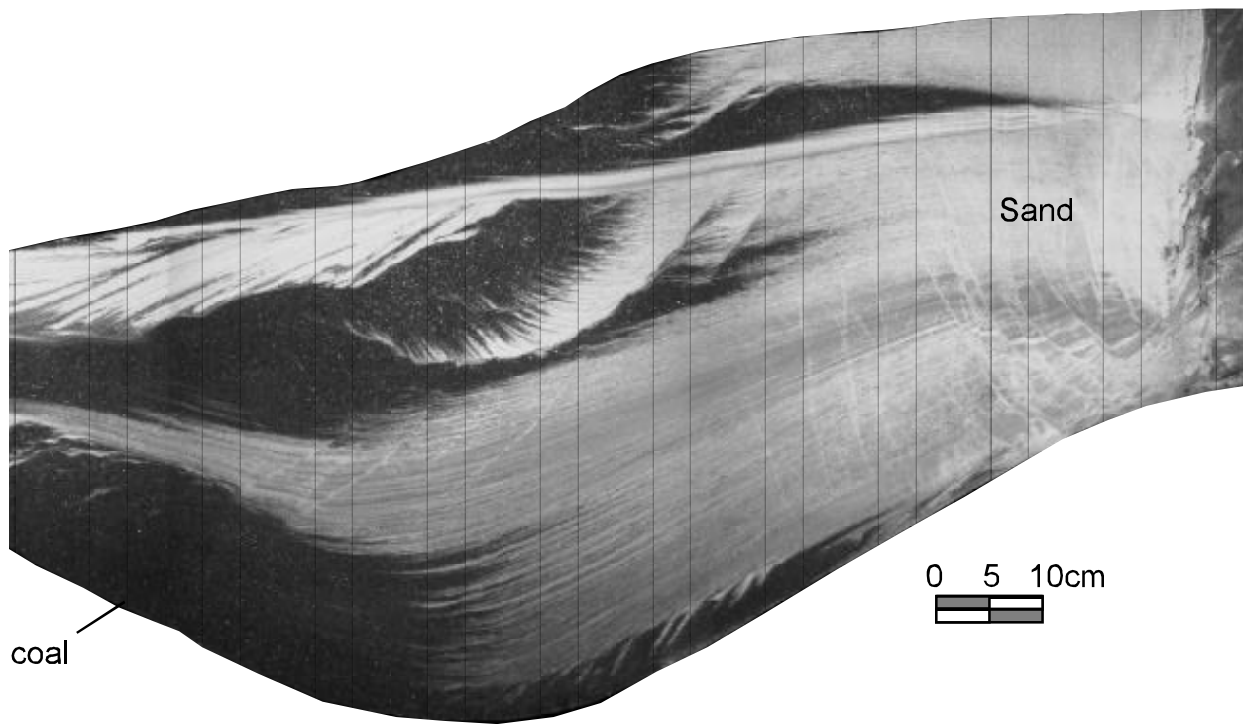


Figure 6.1. Jurassic tank experimental sediment distribution used to guide the assignment of hydrostratigraphic facies in the first example RIFT2D simulation in chapter 6. The light and dark sediments are sand and coal, respectively and are assigned hydrologic properties in the simulation of sand and shale, respectively. The figure illustrates the heterogeneous nature of sediments and the difficulty in assigning effective properties to hydrostratigraphic units. The sedimentary basin experiments were carried out at Saint Anthony Falls Hydraulics Lab at the University of Minnesota and are provided courtesy of Dr. Chris Paola.

uniform grid 200 m thick ($ZMAX(n)-ZMIN(n)=200m$) and slowly deposit the remaining portion of the basin (about 3000m) using a time step size of 17000 years (Figure 6.2). Additional elemental thicknesses depend on the product of the subsidence rate (VZT), the time step size (DT), and the parameter GRDFAC. The initial thickness and the number of time steps is somewhat arbitrary. However, care should be taken to ensure that a layer of elements is deposited over at least 20-30 time steps. For this example, we will use a time step size of 17,000 years. The basin formed over a period of 1000 time steps (NTIME=1000). The first step in spatially discretizing the sedimentary basin into a series of nodal columns along the horizontal axis. In this case a lateral discretization of 50 elemental columns (NEC=50; NCOLS=51) adequately captures the lateral variations in lithofacies (Figure 6.1B). Because no faults are represented, NFLT=0, ROTFLAG=0. We will not allow the grid to deform with porosity changes (ICASE=0). Along each column, the subsidence/sedimentation rates must be assigned. This involves dividing the basin thickness (i.e. the difference between the elevation of the sediment-water interface and base of the sedimentary pile) by the time required to deposit the sediments along each column. For the first column, we find a subsidence rate of:

$$VBASE(1) = - (2823 \text{ m} - 538\text{m}) / 17,000,000 \text{ years} = - 6.96d-05 \text{ m/yr}$$

This procedure can be easily carried out on a spreadsheet program. Subsidence is assigned a negative value for VBASE. For uplift VBASE is positive. For this example, we will assume that there is no uplift/erosion and that sedimentation occurs in a time invariant manner. We will further assume that sedimentation keeps pace with subsidence using a non deforming grid so that the elevation of the sediment/water interface is fixed (ICASE=0). If one wished to represent the subsidence history of a basin as a sequence of different time periods (i.e. tectonic time periods) for each individual lithologic units or groups of units, then the above procedure must be broken down into a series of steps where the thickness of individual layers or groups of layers is considered. Because individual layers compact as they are buried depth, some type of backstripping procedure should be implemented to obtain accurate estimates of subsidence and sedimentation rates (Slater and Christie, 1980). To ensure that the basin is properly discretized, we must assign a value of GRDFAC which is consistent with the assigned subsidence/sedimentation rates and time step size. This can either be done by trial and error or by making some simple calculations. Our goal is to have a final discretization of approximately 40 elemental rows. This discretization is only approximate since we can't easily account for sediment

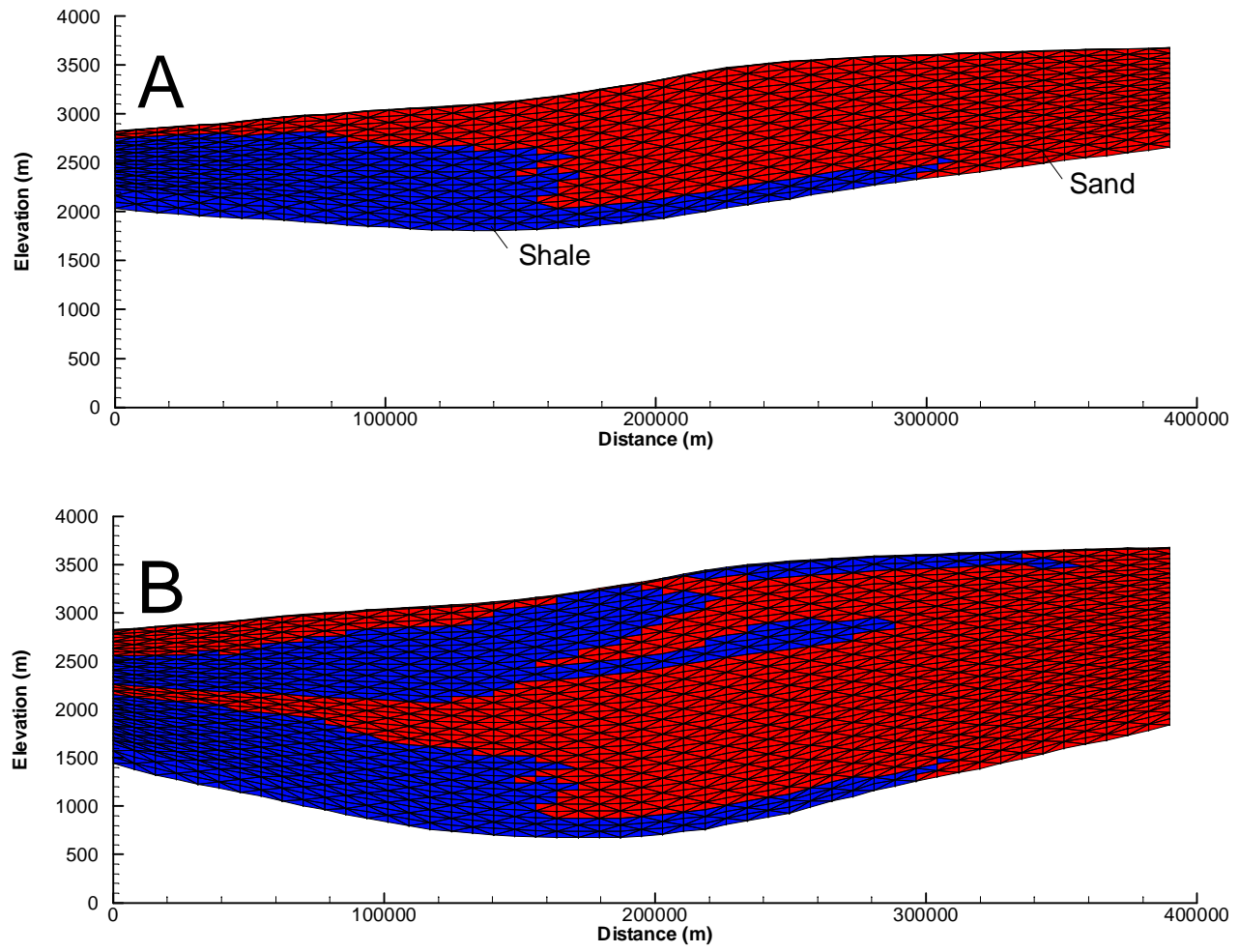


Figure 6.2. Finite element mesh and hydrostratigraphy after 8.5 (A) and 17 (B) million years of basin evolution for Jurassic Tank simulation.

compaction effects on element row thickness. We estimate DELZ and GRDFAC as follows:

$$\text{DELZ}(1) = \frac{\text{ZMAX}(1) - \text{ZMIN}(1)}{41} = 100\text{m}$$

$$\text{GRDFAC} = \frac{\text{DELZ}(1)}{\text{DT} * \text{VBASE}} = \frac{100\text{m}}{1700 * 6.96\text{e}-4} = 30$$

GRDFAC is held constant across the domain to try to maintain the same number of nodes in each column. This is critical! *The mesh generation algorithm employed by RIFT2D requires that the maximum difference in the number of nodes in adjacent nodal columns be less than or equal to 2.* If the number of nodes being generated in adjacent cells is greater than 2 during the simulation, then the triangular grid will not generate a regular grid and the code will either stop automatically, crash, or generate spurious results (physically unreasonable values of hydraulic head and temperature). Inspection of the file ‘rift.out’ will generally identify this problem. In addition to print outs of computed dependent variables, a list of the number of nodes per column is given:

COL #	NO. OF NODES	GRDFAC
1	5	30
2	5	30
3	5	30
.	.	.
.	.	.
.	.	.
50	5	30
51	5	30

If the difference in the number of nodes in adjacent columns is greater than 2, then additional nodal columns must be added or GRDFAC needs to be. The final set of subsidence rates are shown in Table 6.1. The entire data file is listed in Appendix 6.

For the basin cross-section represented in Figure 6.2A, we must decide two important questions. How many hydrostratigraphic facies show we use to represent the shale and sand facies within the basin? What level of discretization is needed to represent basin-scale transport through these facies? There are clearly a number of different depositional environments represented in Figure 6.1A. One approach might be to break the facies down based on the percent of coal and sand; say into five units. Another

Table 6.1. RIFT2D subsidence data along select columns

count	x	vbase	vinc	ver	zmax	zmin	icase	grdfac
1	0.0d+1	-6.96E-05	0	0	2823.926	2623.926	1	30
2	780.d+01	-7.44E-05	0	0	2841.443	2641.443	1	30
3	1560.d+01	-7.85E-05	0	0	2858.842	2658.842	1	30
4	2340.d+01	-8.24E-05	0	0	2876.175	2676.175	1	30
5	3120.d+01	-8.59E-05	0	0	2889.395	2689.395	1	30
.
.
48	36660.d+01	-1.05E-04	0	0	3664.699	3464.699	1	30
49	37440.d+01	-1.02E-04	0	0	3668.413	3468.413	1	30
50	38220.d+01	-9.95E-05	0	0	3672.909	3472.909	1	30
51	39000.d+01	-9.65E-05	0	0	3678.223	3478.223	1	30

approach could be to simply use two units (sand and shale) assigning a cut off criteria (e.g. the sand facies is any deposit with 80% sand or greater). Since oil generation is being represented, an additional consideration is its organic content and characteristics (Type I, II, or III kerogen) of the fine grained facies (i.e. the coal). For this example, we will keep it simple and only choose two hydrostratigraphic units (NMAT=2; Figure 6.1B) to represent the sand (Hydrostratigraphic Unit #1) and shale (coal; Hydrostratigraphic Unit #2) facies. In order to represent these two facies, we will use 40 elemental rows (BER=40). The material tags (MAT) of 1 or 2 are read into RIFT2D for every element to represent sand and shale facies respectively.). These must be ‘painted’ into the RIFT2D data file by trial and error or using the graphical preprocessor RIFT2D_INTERACTIVE (Table 6.2).

The petrophysical and geochemical properties for the two hydrostratigraphic used in example 1 are listed below (Table 6.3). Since the sand and shale (coal) hydrostratigraphic units do not represent actual lithologic units, there is no available permeability data. Arbitrary values of permeability of 10^{-16} and 10^{-18} m^2 were assigned to the sand and shale facies (PM1=-16 for sand; PM1=-18 for shale). The logarithmic porosity-permeability model (IPERM=1) was used in this example. Permeability was not allowed to change due to porosity reduction (PM2=0 for both hydrostratigraphic units). Typical consolidation parameters were assigned for the sand and shale hydrostratigraphic units (BETA, BETA_UL, PHI_O, PHI_IR) in Table 6.3. Representative properties for thermal conductivity, heat capacity, and dispersivities were assigned to these units for the fluid and solid phases. The shale unit (#2) was assigned a TOC content of 3% with 50% of the organic matter being composed of type I kerogen and 50% of the kerogen being type III. Because some of the organic matter is type III kerogen (derived from woody plant precursors), vitrinite reflectance levels calculated by RIFT2D will provide useful information about the thermal maturity of the source rocks in this basin. Because no organic matter is present in hydrostratigraphic unit #1, vitrinite reflectance levels will be zero for this unit. Even though the fine grained deposits may have identical petrophysical characteristics, in some cases different deposits may need to be represented as different hydrostratigraphic units to accurately represent their petroleum generation potential.

Table 6.2. Material tags used to represent sand and shale hydro-stratigraphic units in first example.

MATERIAL TAG DATA:

Table 6.3 Petrophysical and Geochemical Properties used to Represent Sand and Shale Hydrostratigraphic Units in Example 1.

Hydrostratigraphic Unit#1 (Sand)						
pm1	pm2	ans	gdiam			
-14.0	0.0	10.0	1.0E-5			
tkf	tks	alpha				
0.58	2.5	0.0				
cvf	cvs	ldis	tdis			
1000.0	200.0	1000.0	100.0			
phi_o	beta	phi_ir	beta_ul	diff		rhos
0.5	5.0E-4	0.1	5.0E-6	1.0E-12		2500.0
perct1	perct2	perct3	toc			
0.0	0.0	0.0	0.0			
Hydrostratigraphic Unit#2 (Shale)						
pm1	pm2	ans	gdiam			
-17.0	0.0	100.0	1.0E-6			
tkf	tks	alpha				
0.58	2.5	0.0				
cvf	cvs	ldis	tdis			
1000.0	200.0	1000.0	100.0			
phi_o	beta	phi_ir	beta_ul	diff		rhos
0.6	6.0E-4	0.05	6.0E-6	1.0E-12		2500.0
perct1	perct2	perct3	toc			
0.5	0.0	0.5	0.03			

For our first example, the position of the water table in the lower portion of the basin was allowed to vary through time to account for sea level fluctuations. This was implemented in the RIFT2D data file using 5 tectonic time periods (Figure 6.3):

```
Vztim2 = 2.992E6  
Vztim3 = 1.2988E7  
Vztim4 = 1.4994E7  
Vztim5 = 1.5963E7  
Vztim6 to Vztim13 = 4.0E9
```

During the 2nd and 4th tectonic time periods, sea level was allowed to decline using the sine function feature (IHCHK=3). The parameters MSL and HDINC were adjusted to allow the upper head condition to change across the basin as shown in Figure 6.3. If sea level was higher than the base water table elevation (HDBASE) assigned for a particular column, then the sea level boundary condition was assigned to the top node in that column. If the base head was higher than the sea level boundary condition for that time step, then the base condition was implemented instead. All other boundary condition parameters, such as the rate of tectonic subsidence, were held constant. The boundary condition information for tectonic time periods 2-5 are read in at the end of the RIFT2D data set. Note that by setting IHCHK=3 and IBRINE=1, the upper solute concentration applied to nodal columns was consistent with sea level elevation (i.e. if sea level was greater than the elevation of the top node, then sea water salinity was assigned to that node, otherwise, the solute concentration was set to 0.0).

The model was run for 1000 time steps (17 million years). The saucer shaped subsidence pattern produced a sedimentary basin fill geometry similar to many deltaic environments. Deposition of relatively fine grained facies resulted in the formation of an over-pressured cell (Figure 6.4) on the left side of the basin during basin evolution. Temporal variations in sea level can be seen by changes in the position of the 3200m head contour in Figure 6.4A-B during basin evolution.

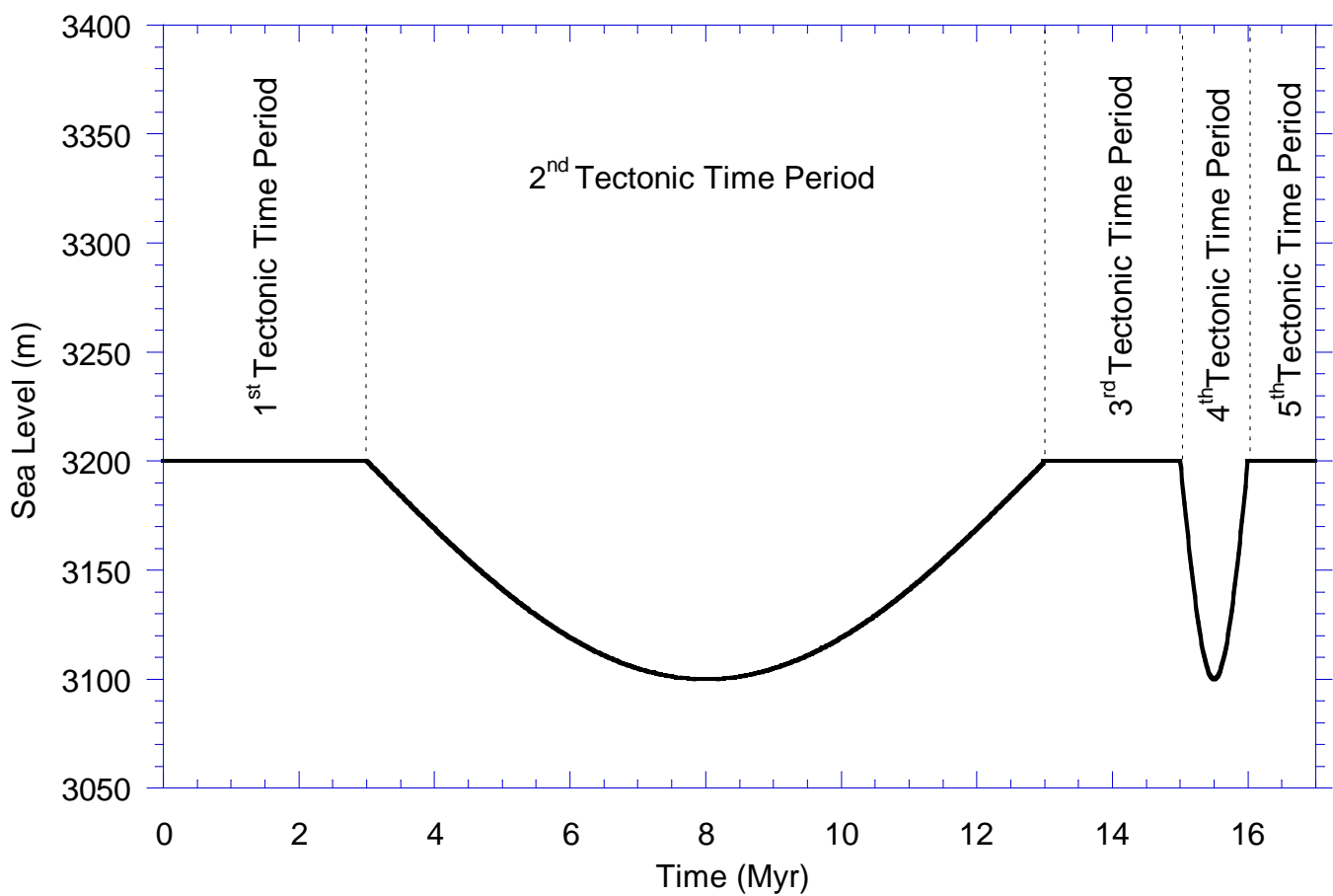


Figure 6.3 Sea level fluctuations used in example simulation 1 to illustrate implementation of tectonic time periods in RIFT2D.

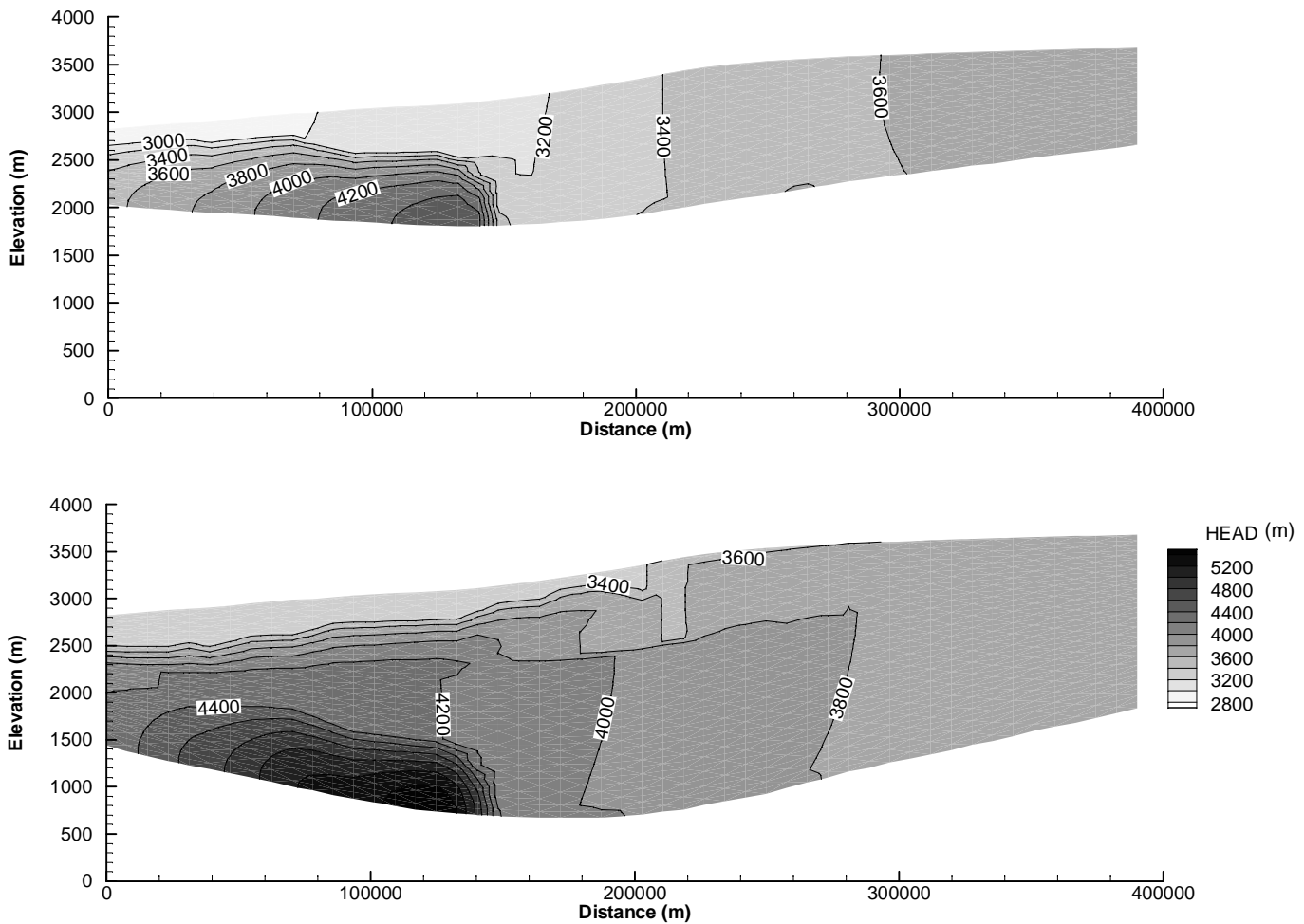


Figure 6.4. Computed hydraulic heads (m) from RIFT2D at 8.5 (A) and 17 (B) million years since start of simulation using Jurassic Tank data file.

Computed temperatures increase in a linear fashion with depth (Figure 6.5). Groundwater flow rates are too slow ($\sim 10^{-4}$ to 10^{-5} m/yr) to disturb the conductive thermal regime. Source rock maturation in the shale unit approached 0.9 % R_v at the base of the sedimentary pile (Figure 6.6). Flow vectors presented in Figure 6.6 illustrate the interaction between a topographic- and compaction-driven flow system. During the deposition of fine grained shale facies during marine transgression, a low permeability “lid” is placed on top of much of the basin. Velocity vectors are highest in the sandstone facies. Calculated solute concentrations reflect changes in the sea level near the surface (Fig. 6.7). The low permeability shale layer which is deposited results in a saltwater/freshwater transition zone which is far out of equilibrium with the compaction dominated flow field.

Example 2: Fault Block Motion Using “Piano Key” Tectonics

This example (fault3.dat) is intended to familiarize the RIFT2D user with how to construct input data files which accommodate vertical fault block motion (piano key tectonics) in evolving basins. This is typical of some extensional and strike-slip basins in which subsidence is accommodated along relatively high angle fault surfaces. There is no limit to the number of faults or fault blocks that can be represented as long as the user follows a few simple rules which guide data file construction. The main rule being that input of material tags and subsidence rates is specified on a “fault block” by “fault block” basis. Another important difference is that the vertical dimensions each triangular element is fixed in a given data file by the parameter DELZ (rather than by GRDFAC*VZT*DT as in example 1) which is found immediately following the material tag data in the data input file. This must be done in order to prevent the creation of triangular elements with more than four nodes along fault surfaces. In this example, the element height is fixed at 200 meters. On the same line where DELZ appears, the ROTFLAG variable must also be set

to 1 (its default value is 0). There are some other important differences between representing

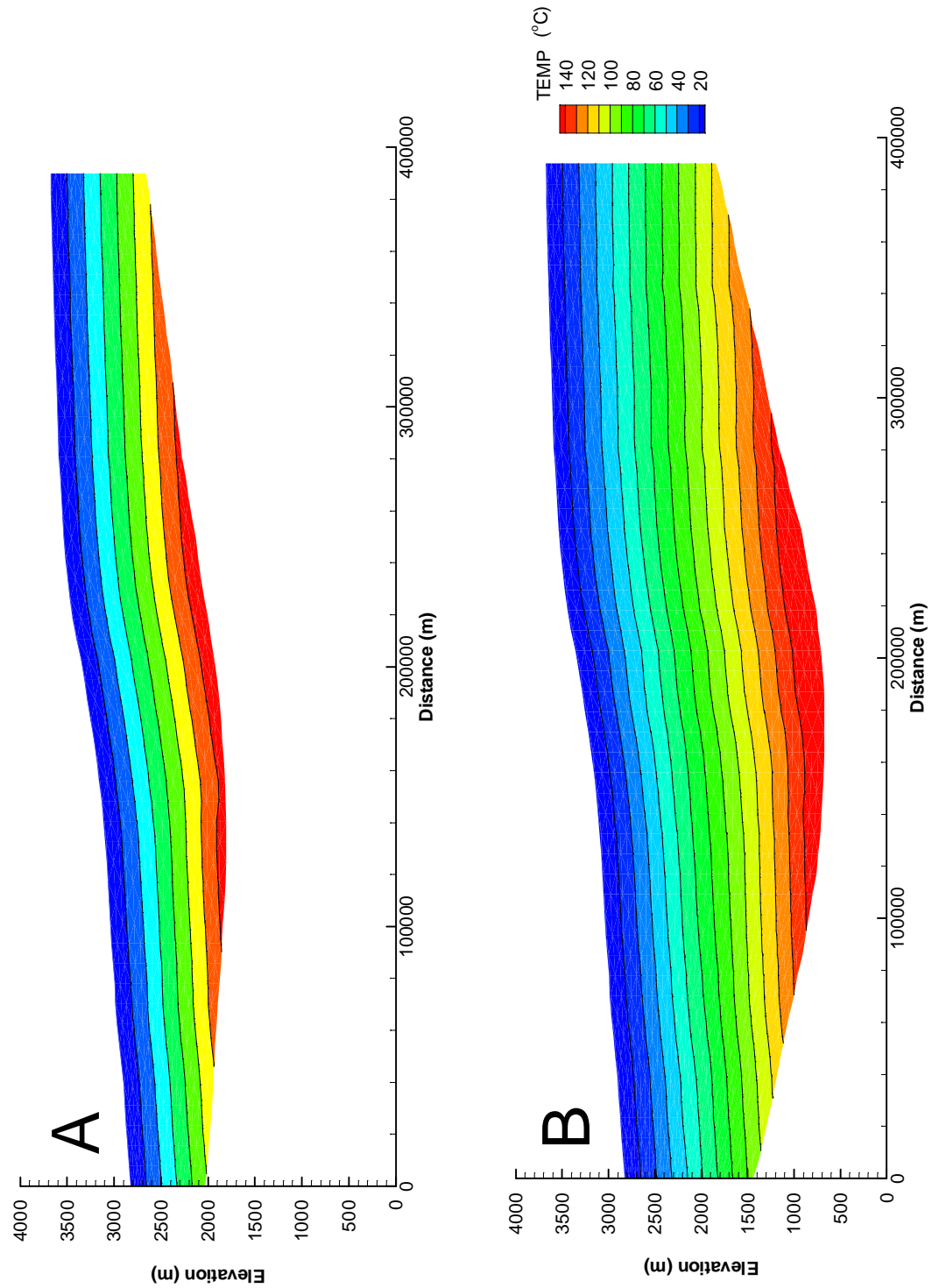


Figure 6.5 Computed temperatures from Jurassic Tank model runat 8.5 (A) and 17 (B) after million years.

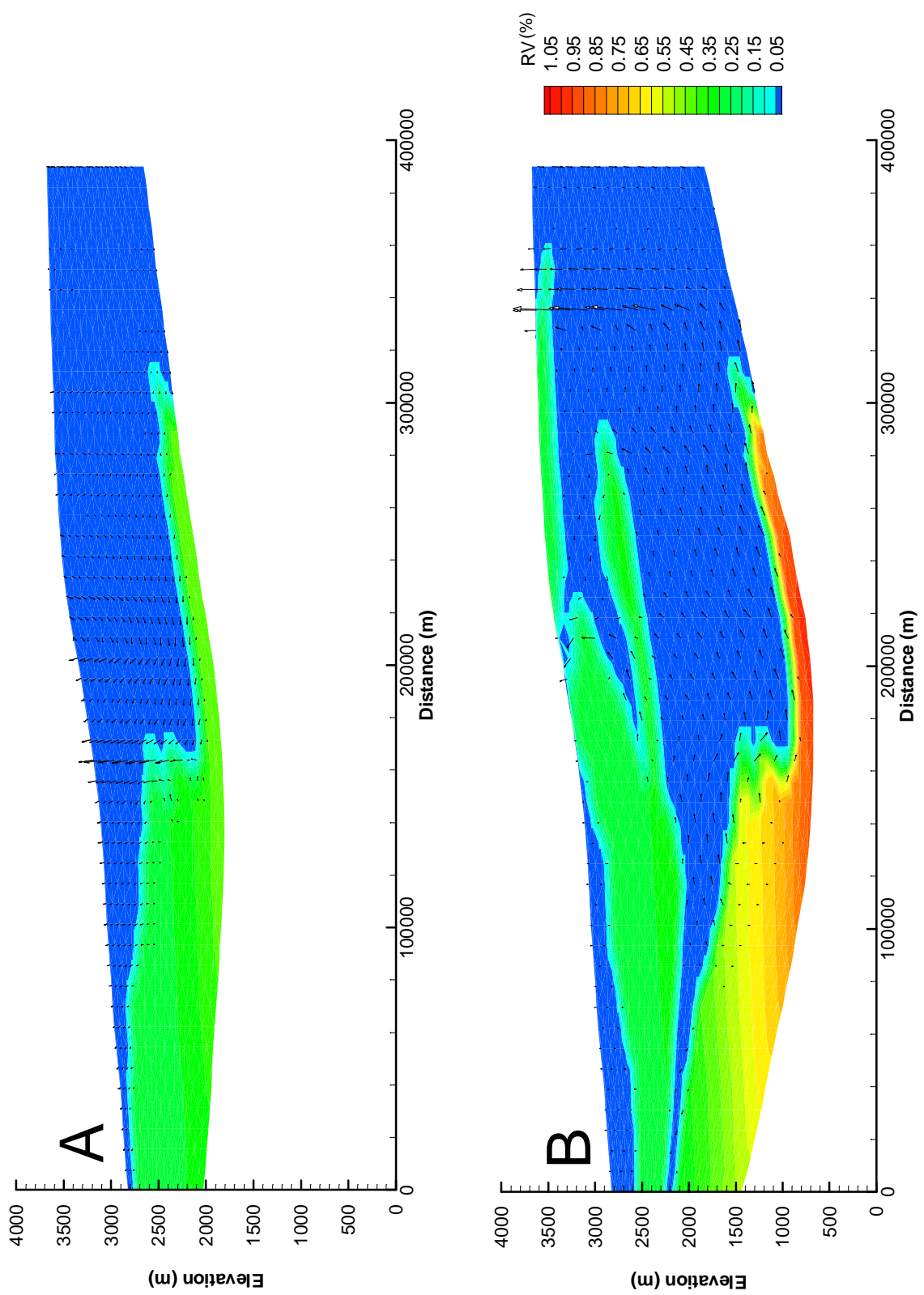


Figure 6.6. Computed maturation levels (% RV) of kerogen after 8.5 (A) and 17 (B) million years of basin evolution using Jurassic Tank data file.

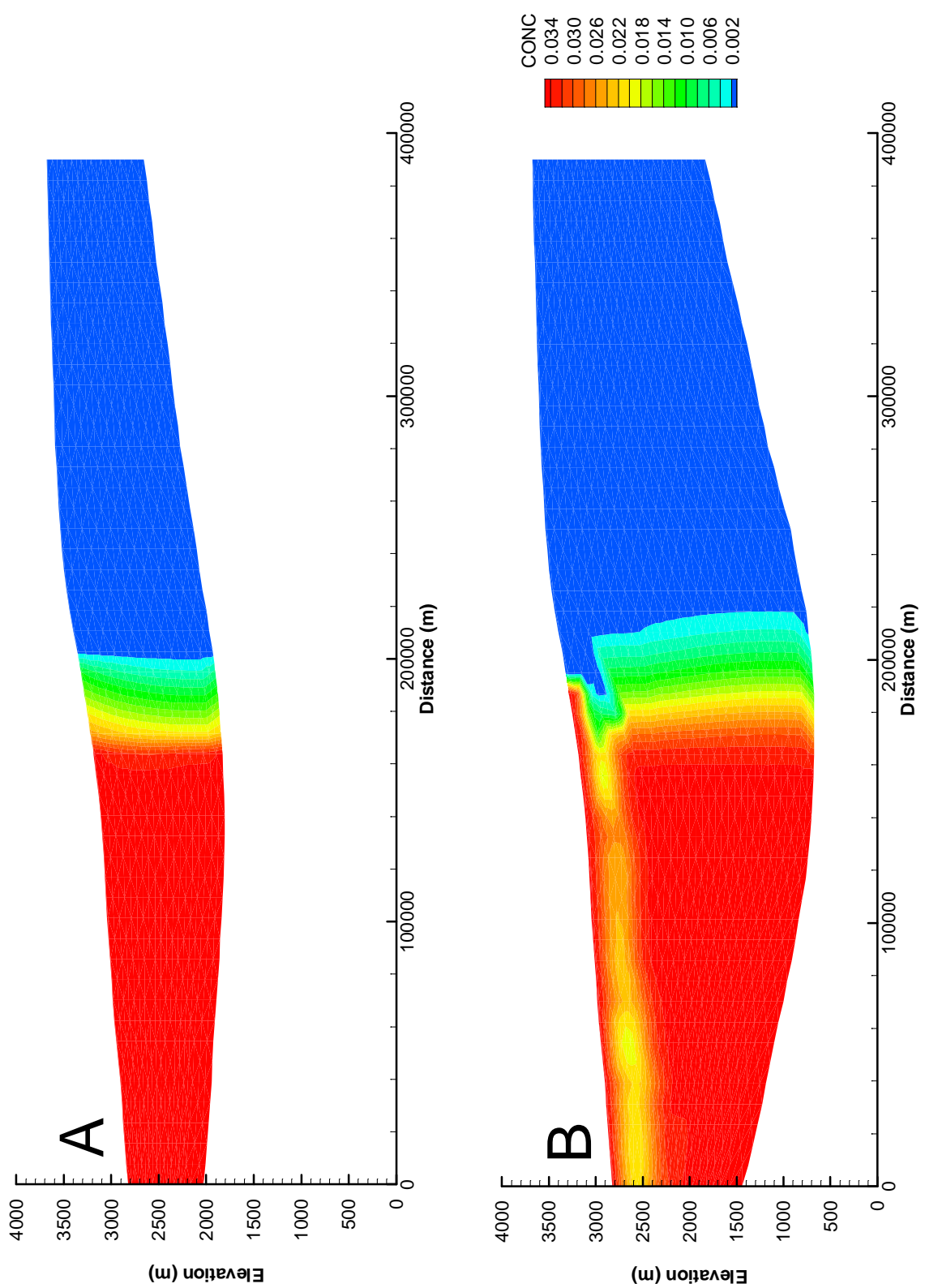


Figure 6.7. Computed solute concentration (mass fraction) after 8.5 (A) and 17 (B) million year of basin evolution using Jurassic Tank data file.

“flexural” and “fault block” subsidence using RIFT2D but these are the most important ones.

The user needs to first determine how many faults to include. This is done using the variable NFLT. In this example, only three fault blocks are represented so NFLT is set to 2 (see data input line 8 in Table 6.4). There are always NFLT+1 fault blocks in a RIFT2D data file. The user must first specify the total number of elemental columns (BEC) and rows (BER) for each fault block (Table 6.4). In our example, each fault block will be composed of 3 elemental columns (and thus 4 nodal columns; Fig. 6.8). Note that BEC is specified twice, one for each fault block. The RIFT2D fault block algorithm requires that two nodal columns be specified along a fault surface (on top of one another) so that the two blocks can move past each other at different rates. Thus, the total number of nodal columns (NCOLS) is 12. The basin is 18 km wide. The column of elements along the fault zone can be assigned distinctive properties (not done here) to represent fault zone properties. The maximum thickness the three fault blocks varies between is about 5 and 8 km (Figure 6.8). To accommodate this thickness, the maximum number of elemental rows (BER) is set to 30 for each fault block in Table 6.4. Because the first fault block is thinner, we could have specified fewer elemental rows for the first fault block (Table 6.4).

In this example, we will represent groundwater flow, heat, and solute transport across the basin from left to right. The subsidence rates (VBASE) assigned to each fault block differ by a factor of over 2.5. In this example, no lateral variation in subsidence rate within the fault blocks has been represented. This could be done provided that the subsidence rates do not vary so much as to allow for the creation of more than two extra nodes in an adjacent nodal columns within a given fault block. Smoothly varying changes in subsidence rates along nodal columns is recommended. Thus, if large variations in subsidence occur within a block over a short distance, then the user should

Table 6.4. Simulation Control Parameters from Second RIFT2D Example Data File

fault3.dat Piano key tectonics with three fault blocks
SIMULATION CONTROL PARAMETERS

NCOLS	IOUT	IPRINT	ISKIP	IPRFST	MAXIT		
12	1	10	10	1	500		
IHEAT	IBRINE	ICOUP	IFLOW	IOIL IPERM IMTAG IFLTAG			
1		0	1	0 1	2 99		
NTIME	DT	THETA	SGRAD	NFLT	GAMMA	TBRSTR	DELZMN
700	5.0D+03	1.d0	0.0d	2	0.5	0.0d+4	20.0d+0
BEC	BER						
3	30						
3	30						
3	30						

Table 6.5. RIFT2D subsidence data along select columns for Example 2.

X-, Z-COORDINATE DATA:

Fault Block #1

COL #	X	VBASE	VINC1	VER	ZMAX	ZMIN	ICASE	GRDFAC
1	0.0d0	-3.0E-04	0.00	0.00	10000.d0	6000.d0	1	100.00
2	2000.0d0	-3.0E-04	0.00	0.00	10000.d0	6000.d0	1	100.00
3	4000.0d0	-3.0E-04	0.00	0.00	10000.d0	6000.d0	1	100.00
4	6000.0d0	-3.0E-04	0.00	0.00	10000.d0	6000.d0	1	100.00

FAULT BLOCK #2

COL#	X	VBASE	VINC1	VER	ZMAX	ZMIN	ICASE	GRDFAC
5	6000.0d0	-5.0E-04	0.00	0.00	10000.d0	5500.d0	1	100.00
6	8000.0d0	-5.0E-04	0.00	0.00	10000.d0	5500.d0	1	100.00
7	10000.0d0	-5.0E-04	0.00	0.00	10000.d0	5500.d0	1	100.00
8	12000.0d0	-5.0E-04	0.00	0.00	10000.d0	5500.d0	1	100.00

FAULT BLOCK #3

COL#	X	VBASE	VINC1	VER	ZMAX	ZMIN	ICASE	GRDFAC
9	12000.0	-8.0E-04	0.00	0.00	10000.d0	5000.d0	1	100.00
10	14000.0	-8.0E-04	0.00	0.00	10000.d0	5000.d0	1	100.00
11	16000.0	-8.0E-04	0.00	0.00	10000.d0	5000.d0	1	100.00
12	18000.0	-8.0E-04	0.00	0.00	10000.d0	5000.d0	1	100.00

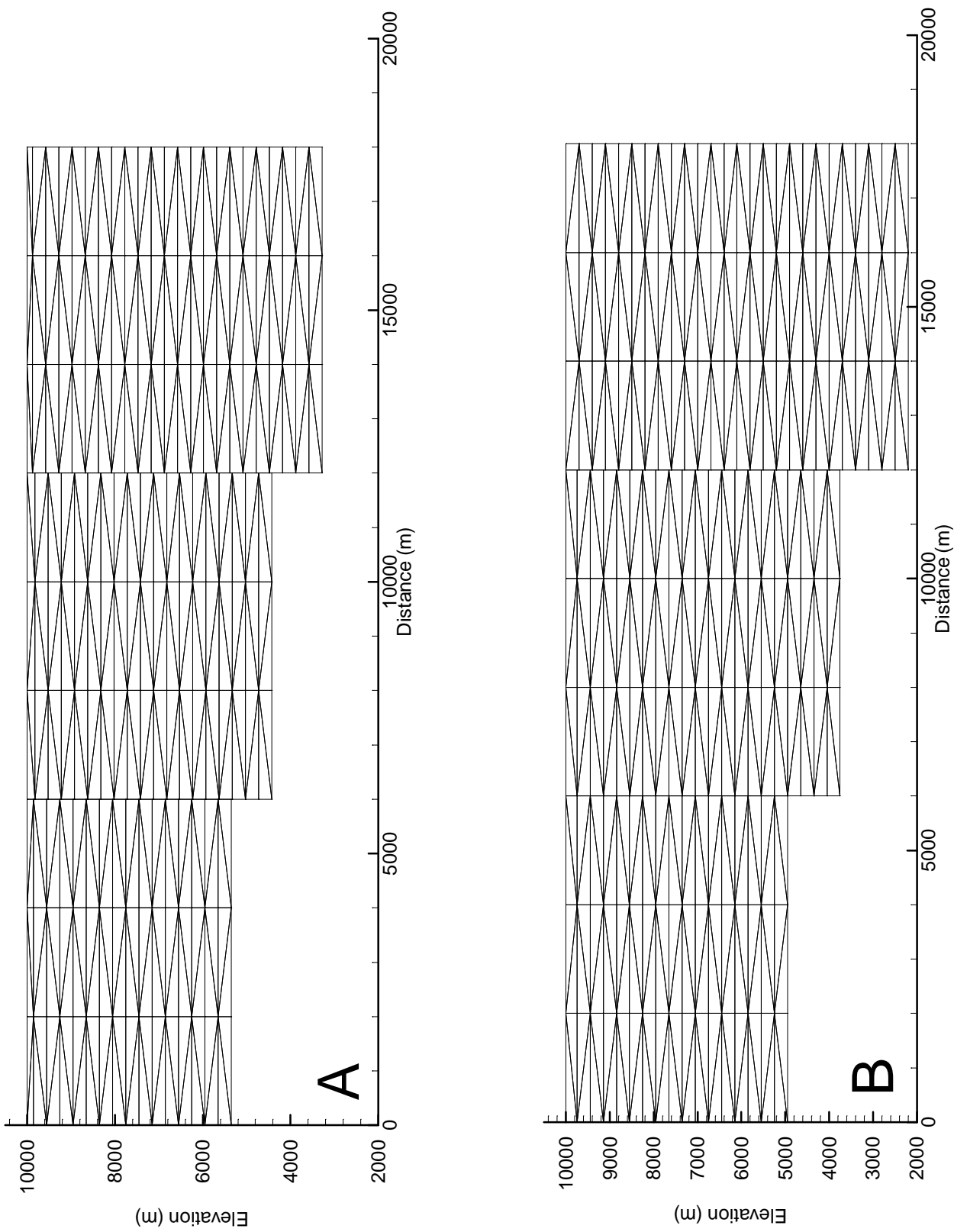


Figure 6.8. Finite element mesh for example 2 after 0.5 (A) and 3.5 (B) million years.

increase the density of nodal columns to accommodate this. Note that in the output (rift.out), the program “lumps” the number of nodes listed for the columns containing the fault surface so that a difference of more than two nodes will appear to be accommodated along the fault zone surface. The initial dimensions of the basin are determined using ZMAX and ZMIN variables in Table 6.5. The number of nodes per column in the first fault block at the beginning of the simulation are:

$$\frac{ZMAX - ZMIN}{DELZ} + 1 = \frac{10000 - 6000}{300} + 1 = 14$$

Material tag 1 is assigned to the fault blocks while material tag two is reserved to denote a specified concentration node at depth (Table 6.6-6.7). Material tags for each fault block are assigned individually beginning in the lower left hand corner of the first fault block and moving across the fault block to the upper right hand corner. Note that tag 2 is assigned along the left edge of fault block one. While it has the same petrophysical properties as tag 1, tag 2 is used to represent a specified concentration element (e.g. salt bed). The permeability of the both hydrostratigraphic units is $10^{-13.5}$ m² and are ten times lower in the vertical direction (see PM1 and ANS for hydrostratigraphic units in Table 6.7). In this example, the basin was allowed to evolve over a 3.5 million year period using a time step size of 5000 years (DT in Table 6.4) and 700 time steps (NTIME in Table 6.4). This is done by assigning 2 to NCLAY and CLAY=0.01 (10,000 mg/l) for columns 1 and 2 in the specified concentration boundary condition data.

A head boundary condition, which varied laterally by 28 meters across the basin, was specified along the top edge of the basin by setting the HDBASE variable to vary between 10030 meters on the right side of the basin (nodal column 11) to 10012 meters on the left side of the domain (nodal column 1). Note that the elevation of the top node is not equal to the height of the water table. Note that only one specified head, concentration, and temperature boundary condition is required along the fault surface

Table 6.6. Material tags used to represent sand and shale hydrostratigraphic units in second example.

MATERIAL TAG DATA: (FAULT BLOCK #1)

111	PM1	PM2	ANS	DGRN		
111	-1.35D+01	0.00D+00	10.0	1.00D-06		
111	TKF	TKS	ALPH			
111	5.80D-01	2.50D+00	0.00D-01			
221	CVF	CVS	LDIS	TDIS		
221	1000.D+00	200.D+00	500.D+00	50.D+00		
221	PHI_o	BETA	PHI_IR	BETA_UL	DIF	RHOS
111	0.50D+00	3.0D-04	0.00D+0	5.0D-06	3.0D-03	2.5D+03
111	PERCT1	PERCT2	PERCT3	TOC		
.	0.0	0.0	0.0	0.000		
111	UNIT #2					
111	PM1	PM2	ANS	DGRN		
111	-1.35D+01	0.00D+00	10.0	1.00D-06		
111	TKF	TKS	ALPH			
111	5.80D-01	2.50D+00	0.00D-01			
111	CVF	CVS	LDIS	TDIS		
111	1000.D+00	200.D+00	500.D+00	50.D+00		
111	PHI_o	BETA	PHI_IR	BETA_UL	DIF	RHOS
111	0.50D+00	3.0D-04	0.00D+0	5.0D-06	3.0D-03	2.5D+03
.	PERCT1	PERCT2	PERCT3	TOC		
.	0.0	0.0	0.0	0.000		
111						
111						
111	MATERIAL TAG DATA: (FAULT BLOCK #3)					
111						
111						
111						
.						
.						
111						
111						

Table 6.7 Petrophysical and Geochemical Properties used to Basin Properties in Example 2.

NMAT

2

UNIT #1

PM1	PM2	ANS	DGRN		
-1.35D+01	0.00D+00	10.0	1.00D-06		
TKF	TKS	ALPH			
5.80D-01	2.50D+00	0.00D-01			
CVF	CVS	LDIS	TDIS		
1000.D+00	200.D+00	500.D+00	50.D+00		
PHI_o	BETA	PHI_IR	BETA_UL	DIF	RHOS
0.50D+00	3.0D-04	0.00D+0	5.0D-06	3.0D-03	2.5D+03
PERCT1	PERCT2	PERCT3	TOC		
0.0	0.0	0.0	0.000		

UNIT #2

PM1	PM2	ANS	DGRN		
-1.35D+01	0.00D+00	10.0	1.00D-06		
TKF	TKS	ALPH			
5.80D-01	2.50D+00	0.00D-01			
CVF	CVS	LDIS	TDIS		
1000.D+00	200.D+00	500.D+00	50.D+00		
PHI_o	BETA	PHI_IR	BETA_UL	DIF	RHOS
0.50D+00	3.0D-04	0.00D+0	5.0D-06	3.0D-03	2.5D+03
PERCT1	PERCT2	PERCT3	TOC		
0.0	0.0	0.0	0.000		

UNIT #2

PM1	PM2	ANS	DGRN		
-1.35D+01	0.00D+00	10.0	1.00D-06		
TKF	TKS	ALPH			
5.80D-01	2.50D+00	0.00D-01			
CVF	CVS	LDIS	TDIS		
1000.D+00	200.D+00	500.D+00	50.D+00		
PHI_o	BETA	PHI_IR	BETA_UL	DIF	RHOS
0.50D+00	3.0D-04	0.00D+0	5.0D-06	3.0D-03	2.5D+03
PERCT1	PERCT2	PERCT3	TOC		
0.0	0.0	0.0	0.000		

(hence only 11 columns are used for the condition data). However, for basement heat flow, all twelve columns are required. A sinusoidal upper temperature boundary Specified land surface temperatures were allowed to sinusoidal varying (ITCHK=2) while basal heat flow was permitted to decay exponentially (IJCHK=3) from 70 mW/m² (Fig. 6.9).

Calculated heads and temperatures 3.5 million years after the onset of subsidence are shown in Figure 6.10. Flow occurs from level to right across the basin (Fig. 6.10A). Flow rates were high enough to disturb the conductive thermal regime (Fig. 6.10B). Computed isotherms and heads vary smoothly across the fault zone as do computed concentrations during basin evolution (Fig. 6.11)

Example 3: Fault Block Motion Using the domino model

In our final example (rotate3.dat), a RIFT2D simulation is presented which represents three fault blocks which are actively rotated using the domino-model (see equations 2.25-2.27). This is done by setting the ROTFLAG= 2 in the data file. All of the data file modifications described in example 2 apply here. The main difference between representing fault block motion using “piano key” tectonics (example 2) and the domino model is that the geometric evolution of the basin is controlled by several rotation parameters (OMEGA, ALPHAS, CENTZ; Table 6.8) which are specified for each fault block rather than by subsidence rate data specified along each column (e.g. VBASE, VINC1, etc). The variable OMEGA controls the total amount of rotation that occurs in the simulation regardless of the time step size or the number of time steps.

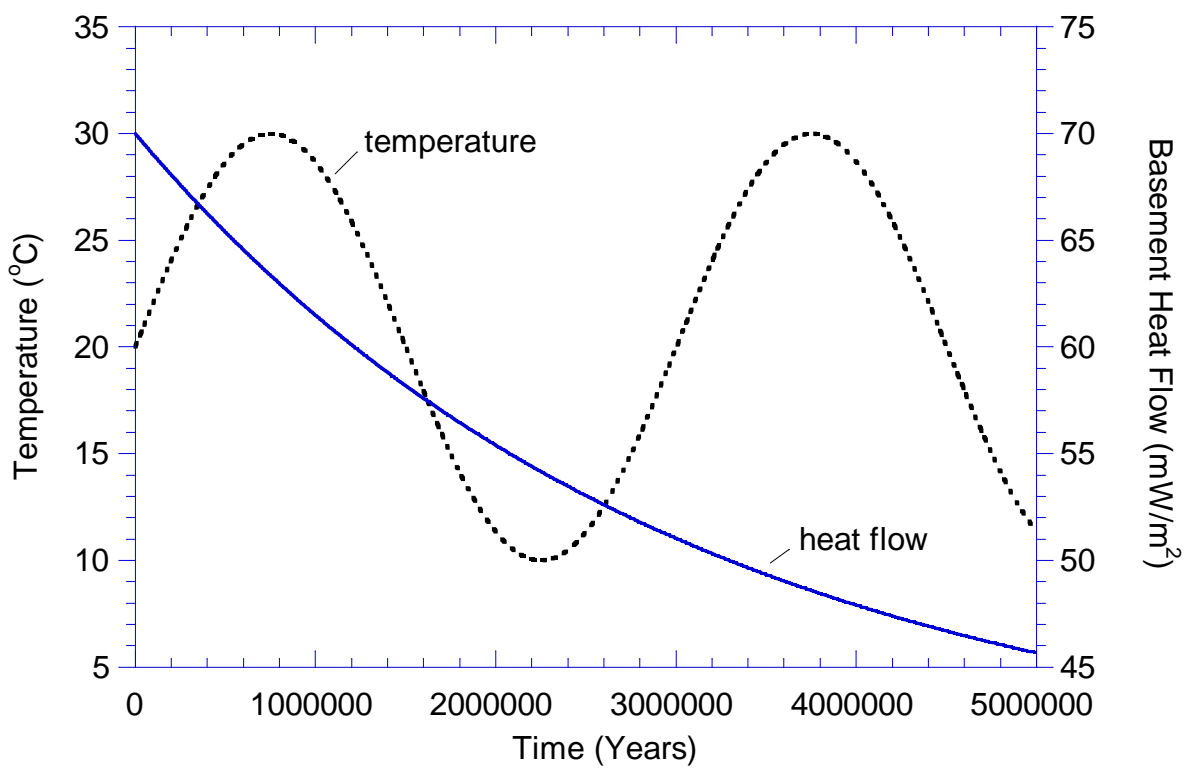


Figure 6.9. Hydrologic and thermal boundary conditions used in example 2.

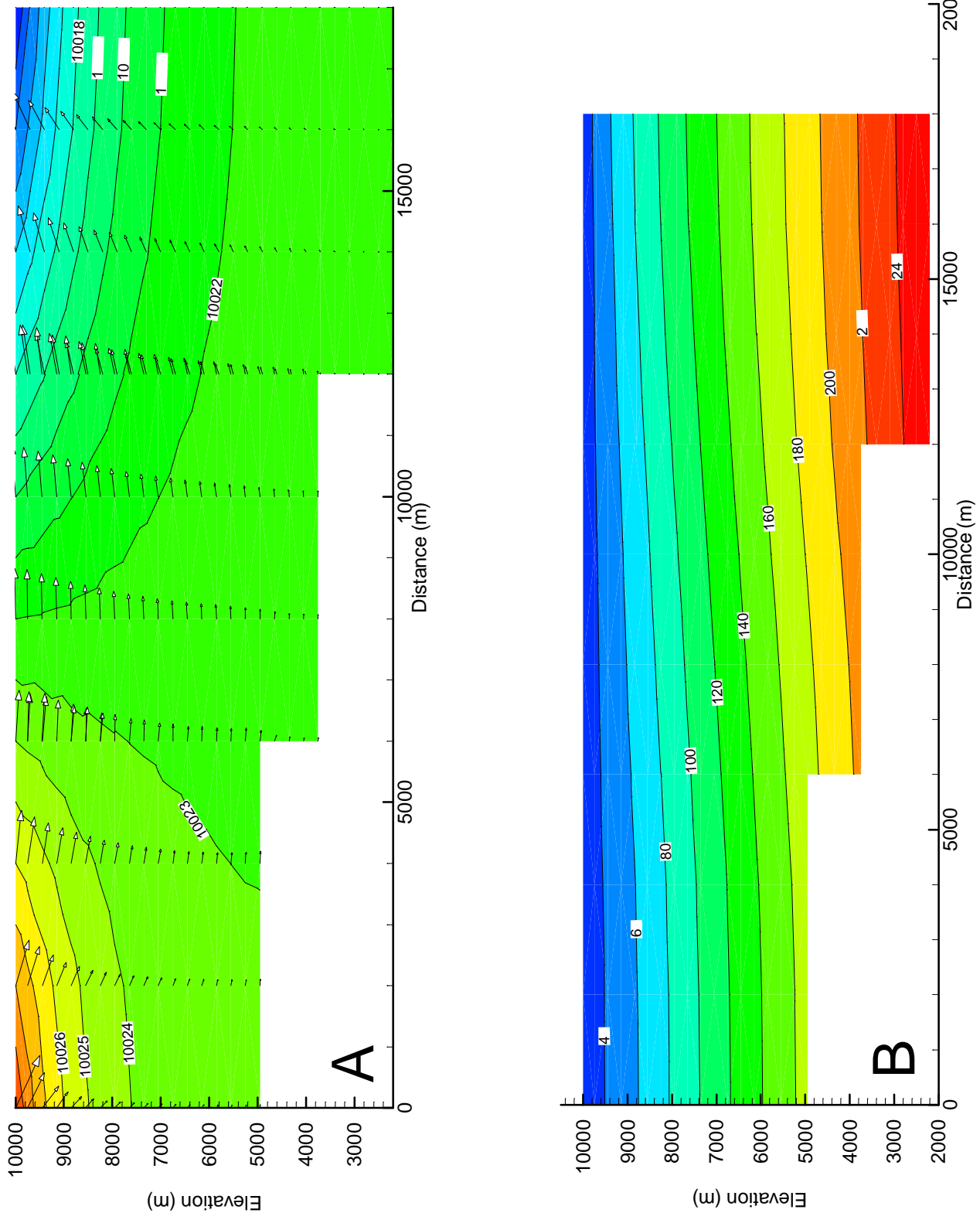


Figure 6.10. Calculated head and velocity vectors (m/yr; A) and temperatures ($^{\circ}\text{C}$; B) after 3.5 million years for example 2.

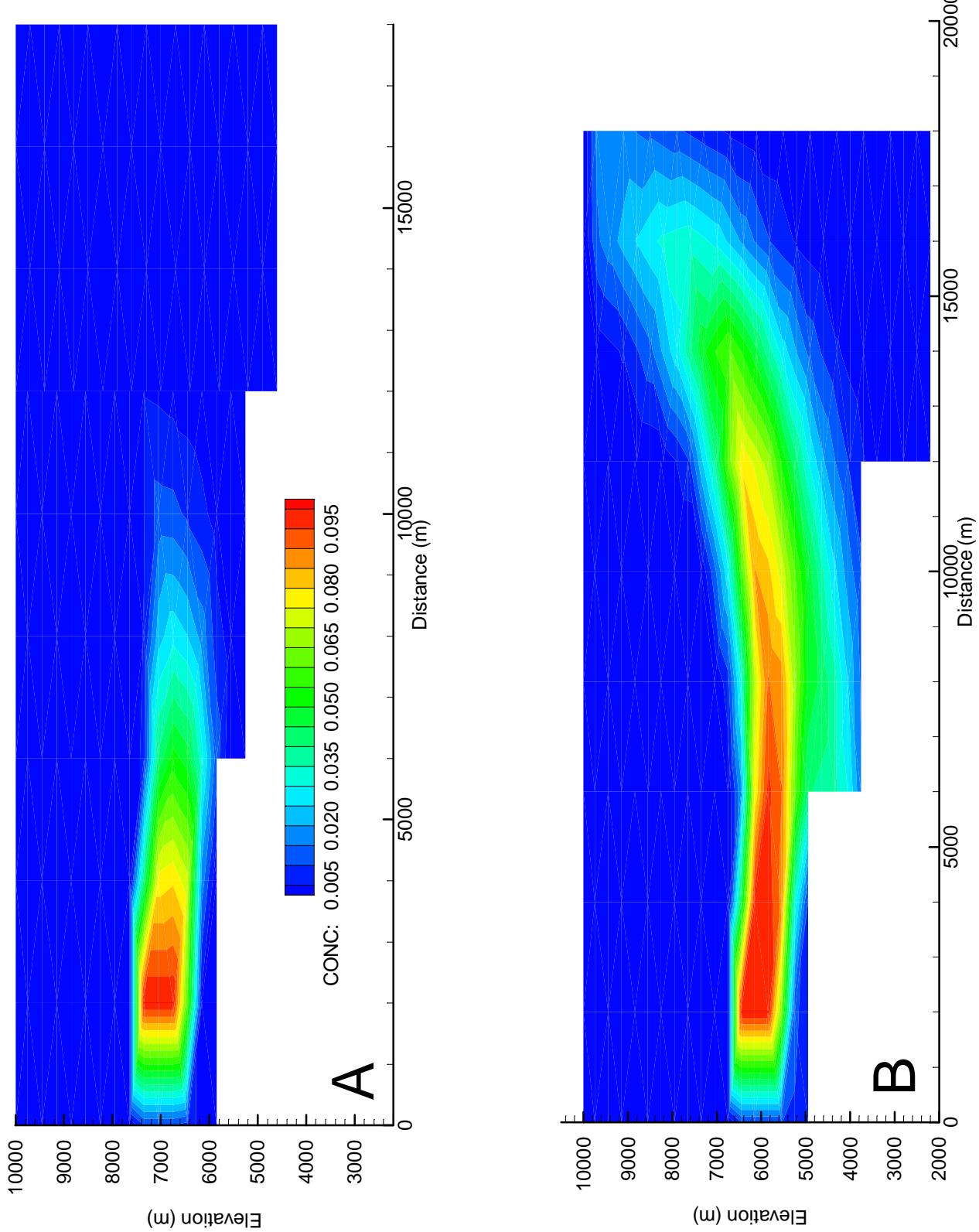


Figure 6.11. Calculated solute mass fraction (mass fraction) after 0.5 (A) and 3.5 (B) million years for example 2.

Table 6.8. Rotation Information used in Domino-Model

STRUCTURAL INFORMATION on FAULTS and ROW THICKNES

rotation flag	omega	alphas	delz	init_rows
1	10.0d0	-65.d0	200.d0	2

BLOCK# centz

1	10000.d00
2	10000.d00
3	10000.d00

TECTONIC TIME PERIODS:

TZTIM2	TZTIM3	TZTIM4	TZTIM5	TZTIM6	TZTIM7
5.10D+09	6.00D+09	12.00D+09	22.0D+09	19.1D+09	25.00D+09

TZTIM8	TZTIM9	TZTIM10	TZTIM11	TZTIM12	TZTIM13
1.00D+09	6.00D+09	12.00D+09	22.0D+09	19.1D+09	25.00D+09

Table 6.9. Simulation Control Parameters used in Domino-Model

Rotate3.dat: Groundwater Flow with Domino-style rotation

SIMULATION CONTROL PARAMETERS

NCOLS	IOUT	IPRINT	ISKIP	IPRFST	MAXIT
15	0	10	1	1	500

IHEAT	IBRINE	ICOUP	IFLOW	IOIL	IPERM	IMTAG	IFLTAG
0	0	0	1 0	1	2	99	

NTIME	DT	THETA	SGRAD	NFLT	GAMMA	TBRSTR	DELZMN
600	5.0D+0	1.d0	0.d0	2	0.5	0.0d+4	20.0d+0

BEC	BER
4	40
4	40
4	50

In this example, two fault surfaces are represented so NFLT is set to 2. The user must specify the total number of elemental columns (BEC) and rows (BER) for each fault block (Table 6.9). In our third example, there are four elemental rows in each fault block (Table 6.9). Note that the maximum number of elemental rows differs among the fault blocks to accommodate different amounts of space created by rotation. The user may either specify that the fault surfaces are initially vertical (ALPHAS= -90) or dip at some initial dip angle. In our case, we wish to set the initial angle of the two faults to dip $^{\circ}64$ to the east from the horizontal axis (ALPHAS = -65). The basin rotates by 10 degrees (OMEGA=10) during the simulation. The RIFT2D user must also select the initial position of the centroid location for each fault block. The position of the centroid should be set well below the land surface (ZMAX; 10000 m) and probably well below the initial base elevation of the sedimentary pile (ZMIN; 6000 m). In general, the greater the centroid depth, the more subsidence and extension will occur relative to uplift. Also, wider fault blocks tend to produce more subsidence and less uplift relative to thin ones (Fig. 2.7). In this example, the initial centroid depth is at an elevation of 10000 m for all three fault blocks. The centroid elevations can be set at different elevations to produce different amounts of uplift and erosion. In this example, the total number of nodal columns (NCOLS) is 15. The basin has an initial width of 17 km but extends itself by rotation to 22 km by domino rotation at the end of the 30 million year simulation period (Fig. 6.12). The basin has an initial thickness of 4000 m. Between 28-32 elemental rows (Table 6.10) comprised, two pre-rift (units 1 and 2), and one sin-rift hydrostratigraphic units (3; Table 6.10; Fig. 6.12). The pre-rift units have a two order of magnitude permeability contrast between them (Table 6.11). As in example 2, the width of the elements is fixed by DELZ (200 m; Table 6.8). Computed heads from this run are shown in Figure 6.13.

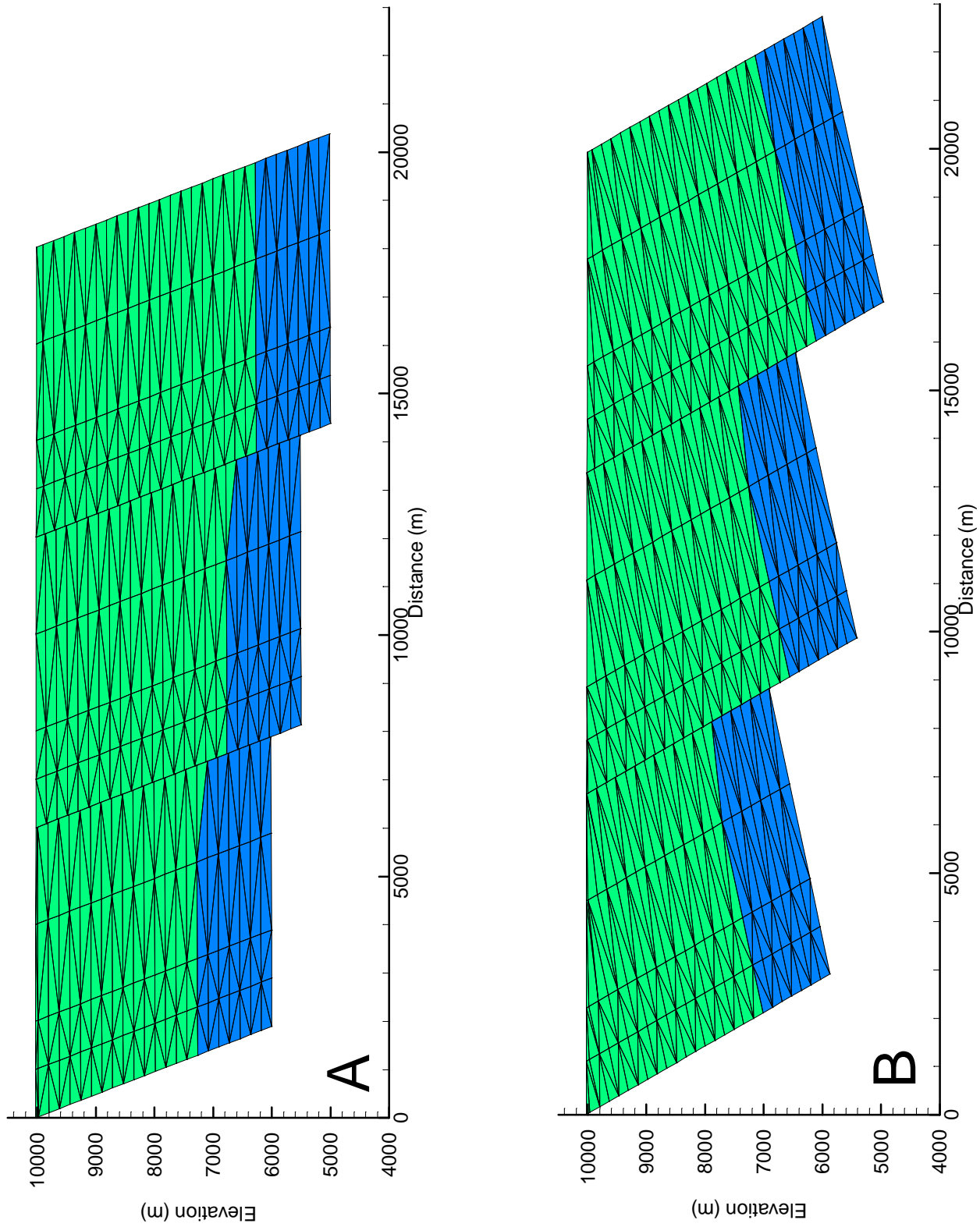


Figure 6.12. Finite element mesh and hydrostratigraphy after 0. (A) and 30 (B) million years of basin evolution.

Table 6.10. Material tags used to Represent Pre- and Syn-rift hydro-stratigraphic units in example 3.

```
INITIAL MATERIAL TAG DATA: (FAULT BLOCK #1)
11111
11111
11111
11111
11111
11111
11111
22222
22222
.

MATERIAL TAG DATA: FAULT BLOCK #2
11111
11111
11111
11111
11111
11111
11111
11111
22222
22222
.

MATERIAL TAG DATA: FAULT BLOCK #3
11111
11111
11111
11111
11111
11111
11111
11111
22222
22222
.
```

Table 6.11 Petrophysical and Geochemical Properties used to Represent Fault Block and Fault Zone Units in Example 3.

PM1	PM2	ANS	DGRN
-1.30D+01	0.00D+00	10.0	1.00D-06
TKF	TKS	ALPH	
5.80D-01	2.50D+00	0.00D-01	
CVF	CVS	LDIS	TDIS
1000.D+00	200.D+00	100.D+00	10.D+00
PHI_o	BETA	PHI_IR	BETA_UL DIF RHOS
0.50D+00	0.0D-04	0.00D+0	0.0D-06 3.0D-03 2.5D+03
PERCT1	PERCT2	PERCT3	TOC
0.0	0.0	0.0	0.000
UNIT #2 Pre-Rift Confining Unit			
PM1	PM2	ANS	DGRN
-1.50D+01	0.00D+00	10.0	1.00D-06
TKF	TKS	ALPH	
5.80D-01	2.50D+00	0.00D-01	
CVF	CVS	LDIS	TDIS
1000.D+00	200.D+00	100.D+00	10.D+00
PHI_o	BETA	PHI_IR	BETA_UL DIF RHOS
0.50D+00	0.0D-04	0.00D+0	0.0D-06 3.0D-03 2.5D+03
PERCT1	PERCT2	PERCT3	TOC
0.0	0.0	0.0	0.000
UNIT #2 Sin-Rift Sediments			
PM1	PM2	ANS	DGRN
-1.50D+01	0.00D+00	10.0	1.00D-06
TKF	TKS	ALPH	
5.80D-01	2.50D+00	0.00D-01	
CVF	CVS	LDIS	TDIS
1000.D+00	200.D+00	100.D+00	10.D+00
PHI_o	BETA	PHI_IR	BETA_UL DIF RHOS
0.50D+00	0.0D-04	0.00D+0	0.0D-06 3.0D-03 2.5D+03
PERCT1	PERCT2	PERCT3	TOC
0.0	0.0	0.0	0.000

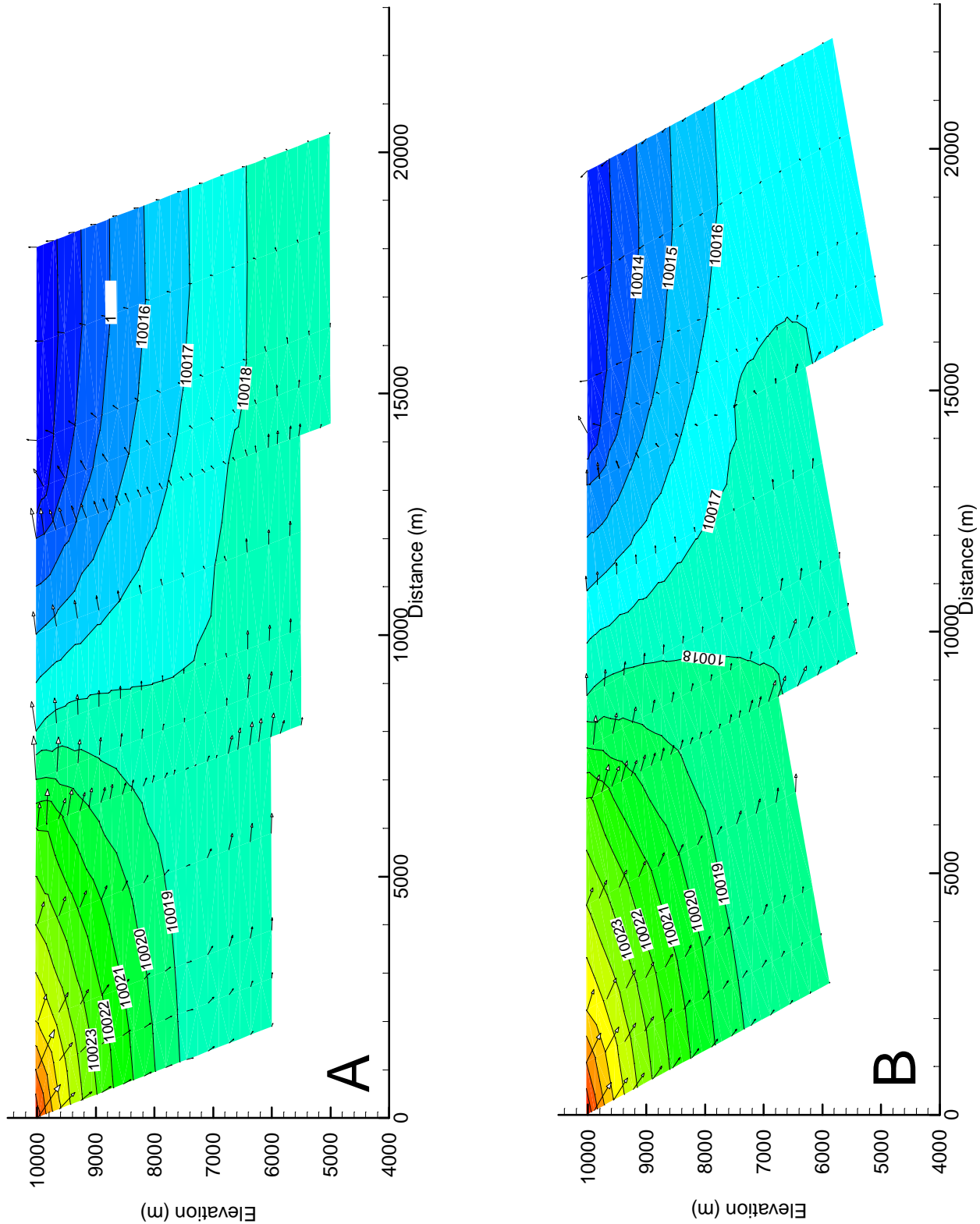


Figure 6.13. Computed heads (m) and velocity vectors after 0 (A) and 25 (B) million years of basin evolution for example 3.

CHAPTER 7: RIFT2D MODEL VALIDATION

In this chapter, four simulations are presented to provide the user with a set of template data sets which can be used to generate their own data files. These simulation examples are taken from the hydrologic and petroleum literature (Table 7.1) and thus also serve to partially validate RIFT2D's solution of the governing transport equations. A complete description of these data files is on the compact disk, which accompanies this document.

These simulation examples also help to establish the numerical accuracy of RIFT2D in simulating ground water flow, heat and solute transport, and basin subsidence. While it is impossible to fully verify the numerical model, individual components of the program could be isolated and compared to published numerical solutions.

Example 1: Excess Fluid Pressure Generation

To demonstrate the ability of RIFT2D to represent ground water flow and excess pressure generation within sedimentary basins, two quasi-one-dimensional simulations are presented which represent vertical subsidence, sedimentation, mechanical loading, and excess fluid pressure generation along two nodal columns. In the first example (overpres_1d.dat), calculated excess pore pressures, which incorporate some of the non-linear features RIFT2D, are compare to Bethke and Corbets (1988) numerical model BASIN2. The fluid and rock properties, sediment loading rates are taken from Bethke and Corbet (1988). The variables chosen are meant to reproduce conditions presented in Figure 3C of Bethke and Corbet (1988). These are listed below:

sedimentation rate	5×10^{-4} m/year
total simulation time	20 million years
fluid density	1000 kg/m^3
sediment density	2300 kg/m^3
sediment permeability	$3 \times 10^{-19} \text{ m}^2$
sediment compressibility	$3 \times 10^{-4} \text{ m}^{-1}$
porosity at sediment/water interface	0.5

Table 7.1. Validation Simulation Descriptions

Validation Simulation	Processes Represented	Reference
1	Compaction-driven Groundwater Flow	Gibson (1958); Bethke and Corbet (1988)
2	Conductive/ Convective Heat Transfer	Smith and Chapman (1983)
3	Petroleum Generation Variable-Density Flow	Tissot et al. (1987) Konikow et al. (1994)
4	Solute Transport	

A specified hydraulic head of 10,000 m was specified at the sediment water interface. No flow boundaries were assigned to the base and sides of the basin. After 20 million years, a total of 21 element rows were generated. Vertical profiles of excess head and porosity are presented in Figure 7.1. Output used to construct this figure was extracted “prf1_tec.dat” using TECPLOT. Because rock permeabilities are relatively low and sedimentation rates relatively high, fluid pressures approach lithostatic levels in the upper portion of the basin. In the upper 4000 meters, porosity does not decrease in an exponential manner at these depths (Fig. 7.1B). The calculated excess heads and porosity values are consistent (although not identical) to published results of Bethke and Corbet (1988; Fig. 3C). The variations in the two model results are probably due to differences in the way total stress is calculated between the two codes.

A second comparison was made between RIFT2D and the analytic solution of Gibson (1958). This solution assumes that excess pressure generation can be represented using a linearized source term. The solution is given by the following integral expression:

$$h(z,t) = \frac{L(\rho_f - \rho_s)}{\rho_f} \left[1 - \frac{1}{\sqrt{\frac{\pi Kt}{L^2 S_s}}} \right] \exp \left[\left(-\frac{z}{l} \right)^2 \frac{L^2 S_s}{\pi Kt} \right] \\ \bullet \int_0^\alpha \zeta \tanh \left(\frac{\zeta L^2 S_s}{2\pi Kt} \right) \cosh \left(\left(\frac{z}{l} \right) \frac{L^2 S_s}{\pi Kt} \right) \exp \left(-\frac{\zeta L^2 S_s}{4\pi Kt} \right) d\zeta \quad (7.1)$$

Where L is the thickness of the basin. This solution is subject to the following boundary

$$\frac{\partial h(z=0,t)}{\partial z} = 0 \\ h(L,t) = 0 \quad (7.2) \\ L = 0, t = 0$$

and initial conditions:

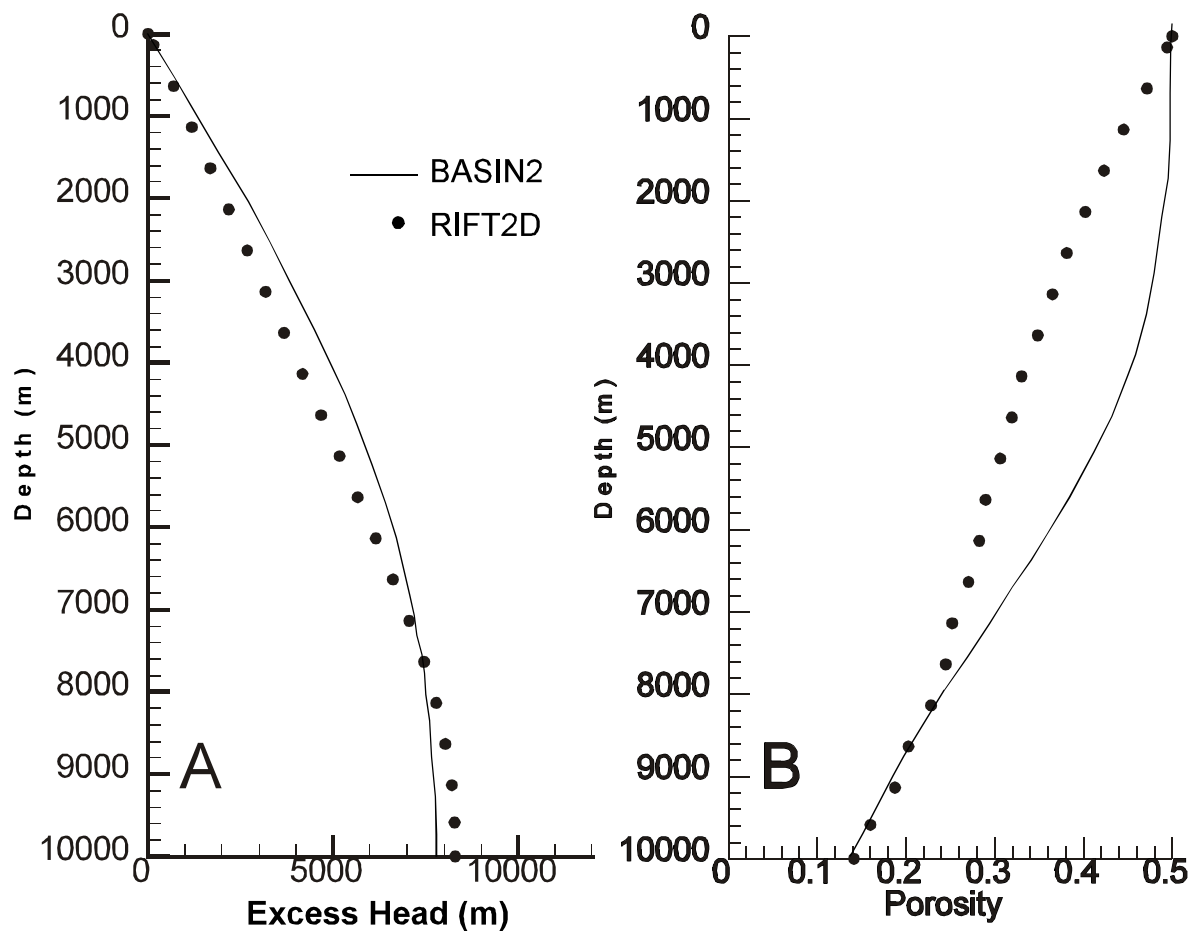


Figure 7.1 Comparison of excess head generation (m) and porosity using RIFT2D and BASIN2 (Bethke and Corbet, 1988, Fig. 3C). Differences in calculated heads are probably due to differences in the way total stress is calculated between the two codes.

The solution expressed in equation (70) was compared to a "linearized" form of RIFT2D. The linearization of RIFT2D was achieved by: fixing ϕ , S_s , and K in subroutines PORPERM; recasting the load term as a constant value using sedimentation rate (rather than total stress changes) in subroutine FLOW; and fixing ρ_f and μ in subroutine DENSITY and VISCOS at their standard state values (1000 kg/m^3 and 0.001 Pa-s). The numerical and analytical values of excess head are nearly identical (Figure 7.2). Thus, it appears that the compaction algorithm in RIFT2D works "well".

Example 2. Topography-Driven Flow with Heat Transport

To illustrate the ability of RIFT2D to represent coupled ground water flow and heat transport, a data file was constructed to represent the hypothetical example of topography driven flow presented by Smith and Chapman (1983; their Figure 4). Smith and Chapman used steady-state finite element analysis to investigate the controls of permeability and water table configuration on subsurface thermal patterns in idealized sedimentary basins. The RIFT2D grid used in this simulation was comprised of 45 nodal columns and 17 nodal rows (Fig. 7.3A). The mesh was refined in the discharge area to accommodate relatively large temperature gradients. The basin was 40 km long and up to 5 km thick.

The following parameter values were used in the simulation:

Number of Time Steps	200
Basal Heat Flux	60 W/m^2
Land Surface Temperature	20°C
Sedimentation Rate	0.0 m/yr
Longitudinal Dispersivity	100 m
Transverse Dispersivity	10 m
Rock thermal Conductivity	$2.51 \text{ W/m}\cdot^\circ\text{C}$
Fluid thermal Conductivity	$0.58 \text{ W/m}\cdot^\circ\text{C}$
Porosity	0.07
Porous Media Compressibility	10^{-5} m^{-1}

The water table varied across the top of the solution by 500 m from the left to right edge of the basin. No flow boundaries were assigned along the base and sides of the solution domain. For heat transfer, a specified temperature of 20°C was assigned at the water table. The specified heat flux was 60 mW/m^2 along the base of the solution domain. The

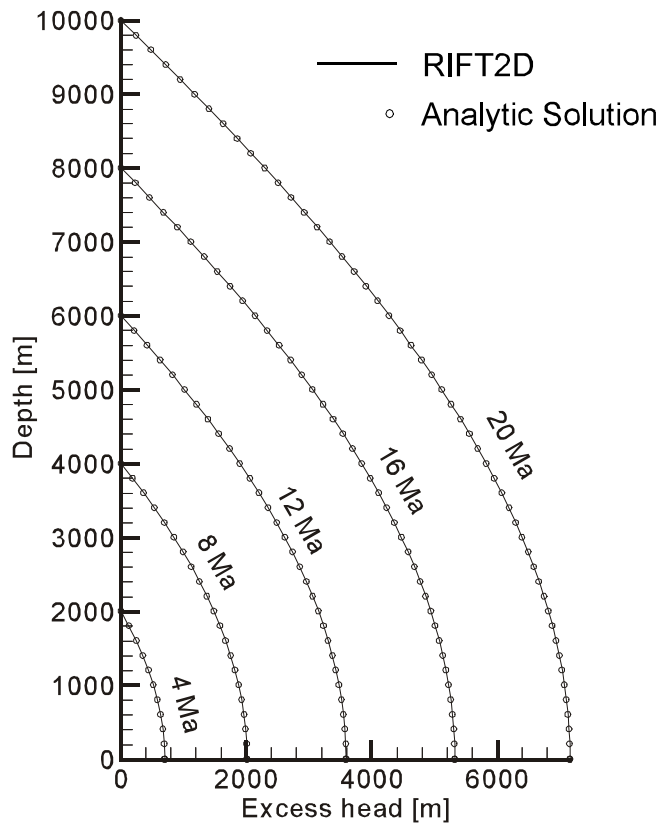


Figure 7.2. Comparison of RIFT2D and analytic solution of Gibson (1958) using a hydraulic conductivity of 10^{-10} m/s, a specific storage of 0.0021 m^{-1} , and a sedimentation rate of 0.0005 m/yr .

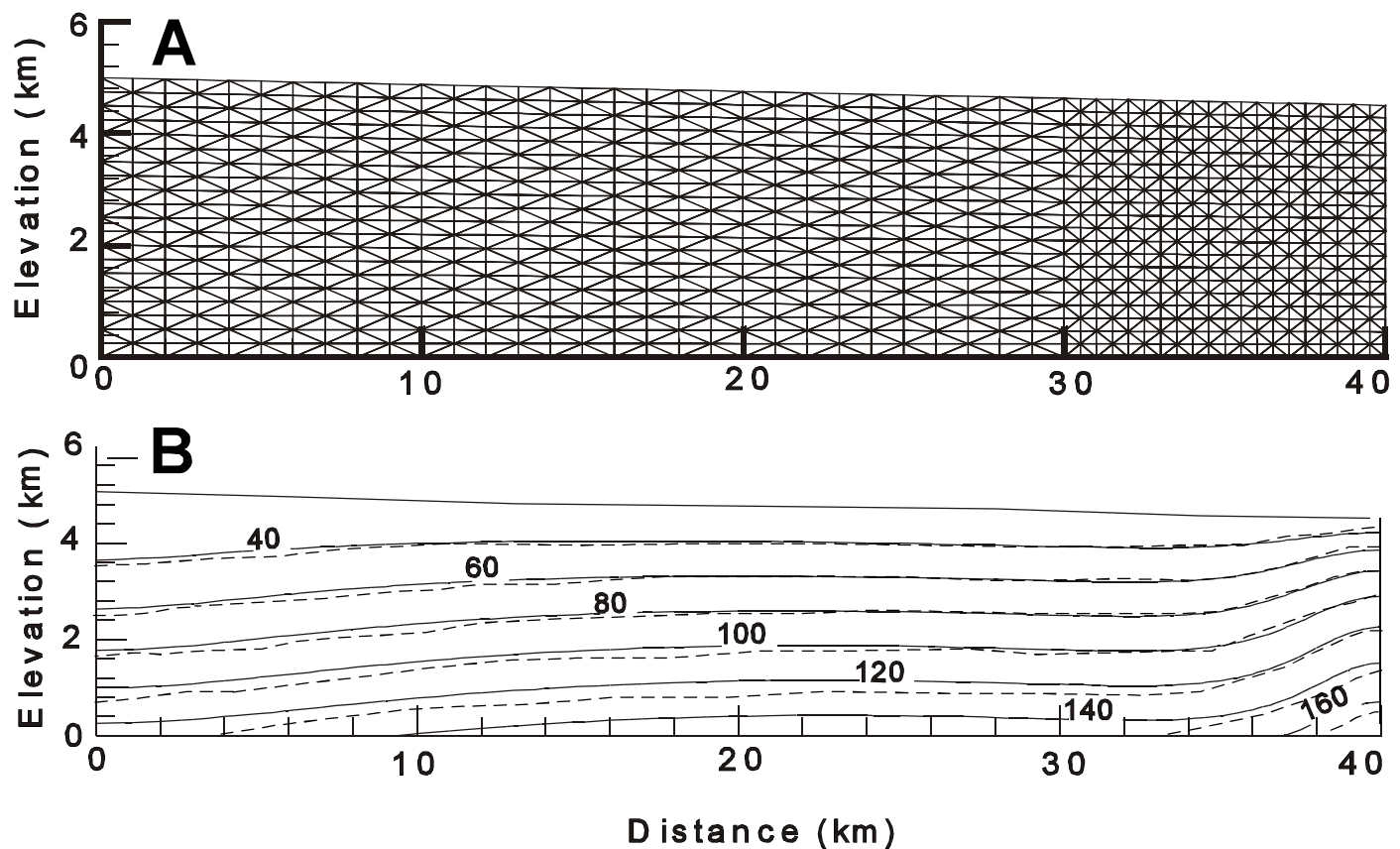


Figure 7.3. (A) Finite element mesh and (B) comparison of computed temperatures ($^{\circ}\text{C}$) using RIFT2D (solid lines) to published hydrothermal model results from Smith and Chapman (1983, Fig4C; dashed lines).

sidewalls were treated as no flux boundaries. Two hundred time steps were required before computed temperatures changed less than 0.1 °C. Smith and Chapman (1983) varied basin permeability between 10^{-18} and $10^{-15.3} \text{ m}^2$ to illustrate the critical range over which variations in this parameter could affect subsurface temperatures. We reproduce their to the high permeability case ($10^{-15.3} \text{ m}^2$) in Figure 7.3B. The differences in RIFT2D (solid lines in Fig. 7.3B) and Smith and Chapman's (dashed lines in Fig. 7.3B) computed temperatures are small (about 5°) and probably result from differences in the equation of state used in the two models. The porosity used in RIFT2D was estimated by model calibration because this parameter was not discussed by Smith and Chapman (1983). The porosity affected the bulk thermal conductivity of the porous medium and ground water flow velocities.

Example 3. Petroleum Generation

A quasi-one-dimensional RIFT2D data file was constructed to demonstrate the ability of the code to accurately calculate petroleum generation for type I, II and III kerogen as the source rock. Simulation was run for type I, II, and III kerogen. These simulations are intended to reproduce kinetic model results presented in Figure 26A of Tissot et al. (1987). The RIFT2D simulations utilized a three nodal column grid, with an initial thickness of 100 m, was allowed to grow to 6000 m at a rate of 0.0001 m/yr over 600 time steps (DT=10⁵ years; 50 Myr). The entire column was assumed to be composed of source rock with the exception of the initial sediments. A basal heat flux of 70 W/m² was imposed at the base of the column. The temperature at the land surface was fixed at 15 °C. The simulation parameters used in all three simulations are:

Number of Time Steps	600
Sedimentation Rate	0.0001 m/yr
Basal Heat Flux	70 W/m ²
Land Surface Temperature	15 °C
Time Step Size	1.0x10 ⁵ yr
Longitudinal Dispersivity	100 m
Transverse Dispersivity	10 m
Rock thermal Conductivity	2.51 W/m·°C
Fluid thermal Conductivity	0.58 W/m·°C
Porosity	0.05-0.2
Porous Media Compressibility	3.0x10 ⁻⁵ m ⁻¹
Rock Permeability	10^{-17} m^2

The transformation ratio using RIFT2D assuming type I, II, and III kerogen (PERCT1=1.0, PERCT2=PERCT2=0.0; TOC=0.08) is presented in Figure 7.4 along with computed temperatures. The kerogen transformation ratio ($0 < Tr < 1$), which tracks the proportion of the kerogen that has been converted to petroleum and its byproducts. Calculated oil generation parameters are in good agreement with those of Tissot et al. (1987). The discrepancies between the transformation rate for Type III kerogen is probably due to differences in the kinetic parameters used by RIFT2D (based on Burnham and Sweeney, 1989) and those used by Tissot et al. (1987). Simulations run with smaller time steps yielded almost identical results.

Example 4. Variable-Density Ground water flow and Brine Transport

To illustrate the ability of RIFT2D to represent variable-density ground water flow and brine migration, a data file was constructed in an attempt to reproduce the Hydrologic Intercomparision (HYDROCOIN) project case 5 described in Konikow et al. (1997). In this example, a topography-driven flow system was imposed across a rectangular solution domain with a basal specified brine concentration of 0.3 weight % NaCl ($\rho_f = 1200 \text{ kg/m}^3$) which was imposed in the center of the domain (between 300 and 600 meters; Fig. 7.5). Note that because of the linear equation of state used by Konikow et al. (1997), this density corresponds to a solute mass fraction of 0.8 in their MOCDENSE model. The rectangular solution domain was 900 m long and 300 m deep. A specified fluid pressure of 10^5 Pa (10 m of head) was imposed in the upper left hand corner of the solution domain and decreased linearly across the top of the solution domain to 0 Pa (0 m of head) at the far right boundary. No flow boundaries were imposed along the sides and base of the solution domain. For solute transport, a specified concentration of 0.0 mg/l was imposed uniformly across the top of the solution domain. No flux boundaries were imposed everywhere except at along the base of the solution domain between 300-600 m as described above. A list of the rock and fluid properties used in this simulation are presented below:

Number of Time Steps	400
Sedimentation Rate	0.0 m/yr
Land Surface Concentration	0.0 weight % NaCl
Longitudinal Dispersivity	20 m
Transverse Dispersivity	2 m
Porosity	0.2
Molecular Diffusivity	$0 \text{ m}^2/\text{yr}$
Porous Media Compressibility	$0.0 \times 10^{-5} \text{ m}^{-1}$
Rock Permeability	10^{-12} m^2

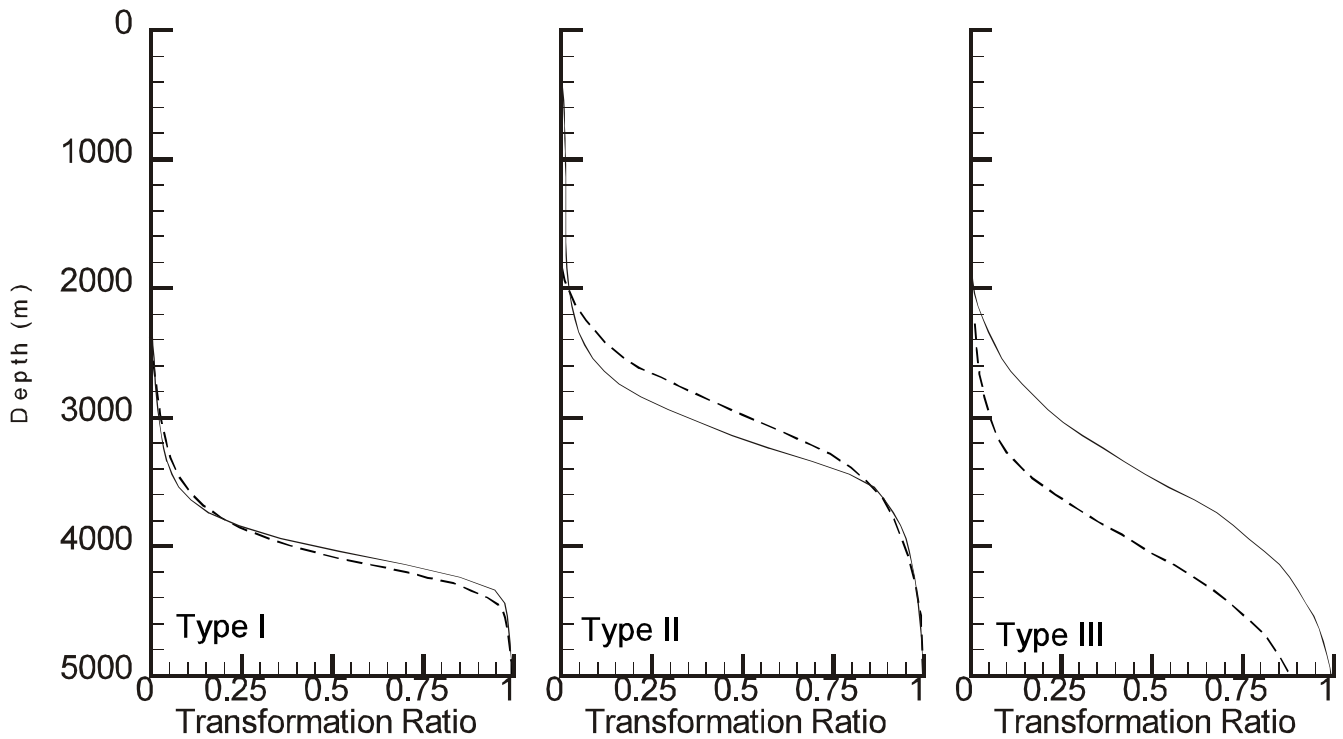


Figure 7.4. Comparison of simulated transformation ratio of Types I, II, and III kerogen using RIFT2D with published model results presented in Tissot et al. (1987; Fig 26A).

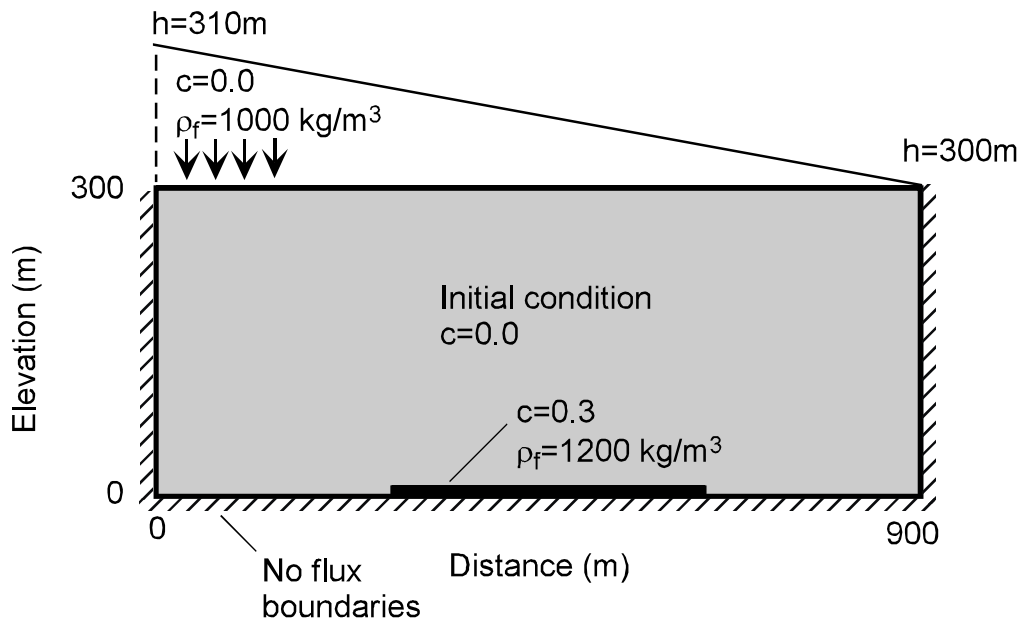


Figure 7.5 Geometry and boundary conditions used in HYDROCOIN case 5 (after Konikow et al. 1997)

The RIFT2D data file was composed of 76 nodal columns and 40 nodal rows. To account for the lower specified concentration boundary condition, we specified a second rock type for which the concentration was always specified at 0.3 weight % NaCl by specifying NCLAY=2 and CLAY=0.2 under the specified concentration boundary condition. Thus, for any nodal column in the center of the solution domain which contained a material property tag (MAT) of 2, the concentration was fixed at 0.3. Note that Konikow et al. (1997) used a linear equation of state in MOCDENSE relating mass fraction to density. Their range of solute mass fraction was 0.0-0.8 mass fraction verses 0.0-0.3 used by RIFT2D. Three rock types were included in this simulation, 1 for the solution domain and 2 for the base of the solution domain. The basal units were assigned low permeability (10^{-16} m²). One of these was assigned a solute mass fraction of 0.3 in the center of the domain. RIFT2D results (Figure 7.6) compares favorably with calculated normalized brine concentration based on the US Geological Survey simulation model MOCDENS (Konikow et al., 1997; Fig. 4). It is difficult to directly compare these model results because of differences in the range of solute concentrations used (MOCDENSE 0.0-0.8 mass fraction verses 0.0-0.3 used in RIFT2D). However, the shape and general range of the solute concentrations are very similar.

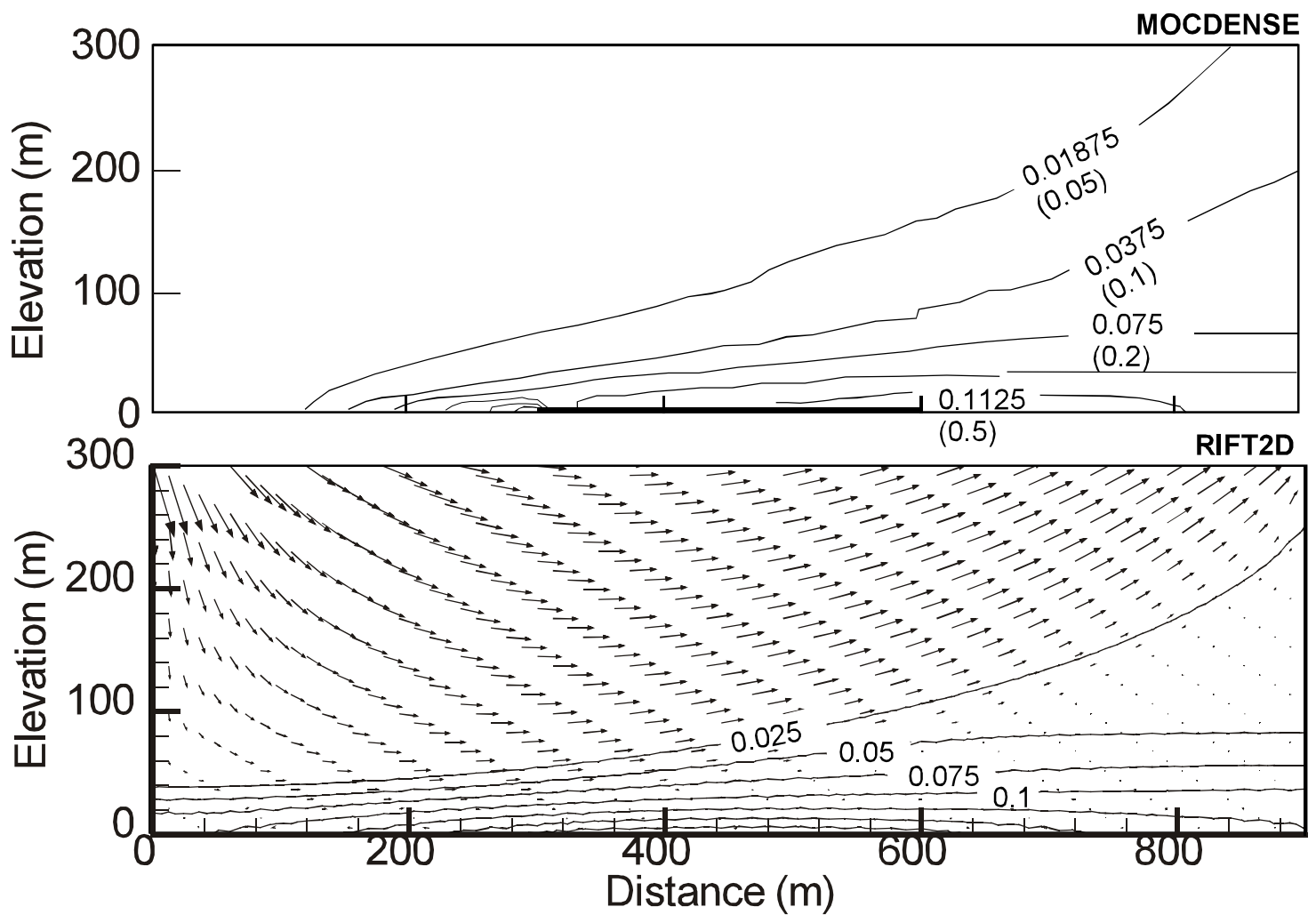


Figure 7.6, Comparison of simulated solute concentration (mass fraction) using MOCdense and RIFT2D. The simulations are intended to reproduce the HYDROCOIN Case 5 example reported in Konikow et al. (1997; Fig. 4). The groundwater velocity vectors (arrows) shown in the RIFT2D output ranged between about 20 - 0.1 m/yr. The solute mass fraction values reported by Konikow et al. (1997) have been re-scaled (original values in brackets) to conform with those used by RIFT2D.

CHAPTER 8 – RIFT2D PREPROCESSOR AND POST PROCESSORS

CREATING RIFT2D DATA DECKS USING RIFT2D_INTERACTIVE

Before you launch the preprocessor application, you'll need to create a GIF image of your basin and decide on the basin parameter information you want to use in your RIFT2D application. The GIF image of your basin must display the boundaries of your stratigraphic units. This image should represent the basin at its maximum thickness. If erosion hasn't removed significant amounts of material, then this would simply be an image of the present day cross section. However, if you wish to represent erosion, then you'll need to create a GIF image, which represents the basin geometry prior to erosion. You'll also need to know the material properties you wish to assign to various hydrostratigraphic units (e.g. thermal conductivity, permeability, porosity at land surface, compressibility, etc.) and boundary conditions parameters (e.g. basal heat flow, surface temperature, water table heads, etc.) information. Below we describe the steps required to generate a RIFT2D data set using the preprocessor. Note that these data sets can be run within the preprocessor using RIFT2DI or saved as ASCII files for later use in RIFT2D.

Step 1: Start up the Pre Processor

Double Click on “**rift2di.exe**” within the rift2di_8d folder on your hard drive or from Start>Programs>RIFT2DI. This will launch the pre-processor application program. A window containing five menus (**File, Edit, Options, Show, Help**), an *Active Data Box*, and a ruled Drawing Area will appear on your screen (Figure 8.1).

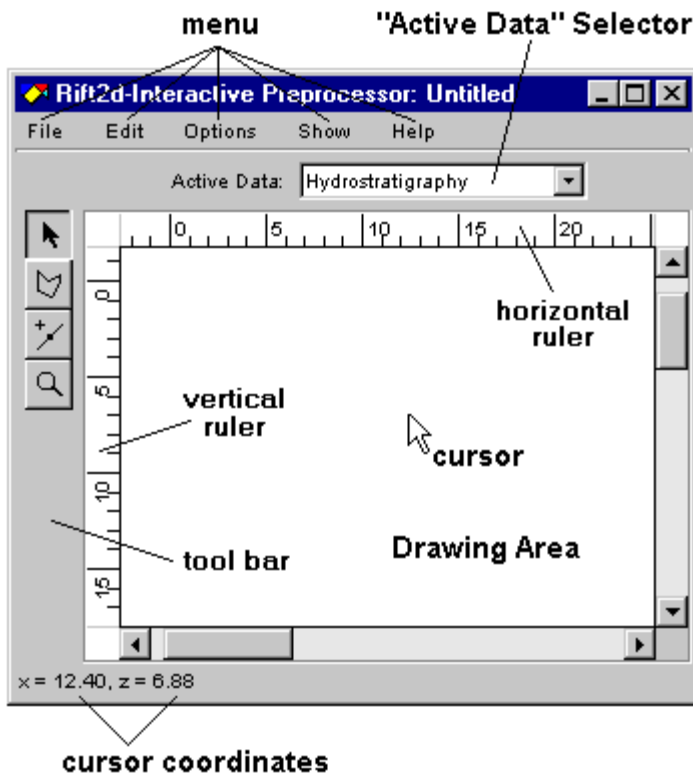


Figure 8.1. Window which appears upon launching preprocessor for RIFT2D.

The “Active Data” box will appear on the center top portion of the application. This box allows the user to select different parts of the input (such as basin geometry, material properties, or boundary conditions) to work on. The contents of each menu are listed in an online help resource which can be accessed at any time by selecting the **Contents** Option under the **Help Menu** (**Help>Contents**).

Several icons will appear on the left column of the application window which will assist you in generating a RIFT2D data deck. The particular suite of icons changes depending on what is selected within the *Active Data* box. When you launch the preprocessor, the following icons will appear under the *Active Data>Basin Outline*:

Icons which appear when the*Active Data> Basin Outline* is Selected

Icon Symbol	Description
	Arrow icon: Allows user to select various objects
	Top Boundary Icon: Allows user to draw in position of top boundary
	Bottom Boundary Icon: Allows user to draw in position of bottom boundary
	Add Vertex Icon: Adds a vertex handles to top or bottom boundary.
	Zoom Icon: Click this and click on image to zoom in. Hold shift key and click on image to zoom out.

Step 2. Set-up Spatial Coordinates of Basin & Simulation Control Parameters

Now select **Options>Drawing** menu. This will open a window containing the set up parameters for basin dimensions you desire. Under the **Scale** Parameters, define the physical dimensions of the model domain (e.g. 1 inch = 10,000 meters). You might want to set your scales a bit larger than the basin's size so that there is a small margin around the basin. Now select **Options>Model** to define the simulation control parameters (e.g. IFLOW, IHEAT, Data Deck Title, etc.) at this time. Also, select **Edit>Horizontal Limits** to select horizontal extent of your numerical grid. Once this is selected, vertical lines will appear at the left and right edges of your domain.

Step 3. Import GIF Image of Basin into RIFT2DI

Select the “Basin Diagram” option under the “Active Data “ box (*Active Data>Basin Diagram*).

Now open a GIF image of your basin which you have scanned into the computer. Do this by clicking on the *Load Site Map Icon* on the left boarder of the application. A dialog box will appear. Double click on the name of the GIF image you wish to import. Your GIF image should now appear in the drawing area. You can stretch your image by selecting (clicking on) it and grabbing the handles with your mouse. You may want to pin your image first. Do this by selecting the *Resize Icon* (resembling an earthquake first motion symbol) on the left edge of the application window. A red circle should appear in the drawing area where the image has been pinned. Move the circle to the desired location you wish to pin (usually the lower left hand corner of your image) using your left mouse button. Return to the Arrow Icon to select and stretch your image by grabbing the handles of the image. The dimensions of your basin image are determined by Step 2.

Icons which appear when *Active Data> Basin Diagram* is Selected

Icon	Description
	Arrow Icon: Allows user to select various objects
	Resize with Fix Point Icon: Allows user to fix a point to on the drawing page.
	Zoom Icon: Click this and click on image to zoom in. Hold shift key and click to zoom out.
	Load Site Map Icon: Opens dialog box to import GIF image of basin.
	XOR Icon: Makes top image translucent.

Step 4. Define the Top and Bottom Dimensions of the Basin

For this step, make sure you have selected *Active Data>Basin Outline*. To define the top boundary of your basin, select the *Create Top Boundary Icon* on the left edge of the application window. Position the mouse along the left edge of the basin diagram. Cross hairs should appear when you approach the left edge. Hold the right mouse bottom down while dragging the mouse to the right along the top boundary. A line should appear tracking the trajectory of your mouse. You may click the left hand mouse button at any point to change in shape of the top boundary. Each time you click on the left mouse, new handle points will be created which will be important later for defining spatial changes in boundary conditions. So, if you wish to have heads, temperatures, or solute concentrations vary along the top boundary, you should establish a number of these handle points by clicking your left mouse button often. To complete the process, “left click” your mouse on the right side of the right (vertical line) boundary of your basin. Repeat this procedure for the bottom boundary using the *Create Bottom Boundary Icon*.

Icons which appear when *Active Data> Basin Outline* is Selected

Icon	Description
	Arrow Icon: Allows user to select various objects
	Discretize Icon: Interpolates mesh to basin boundary and assigns hydrostratigraphic units to individual element columns
	Zoom Icon: Click this and click on image to zoom in. Hold shift key and click to zoom out.
	Create Top Boundary Icon: Allows user to draw in position of top boundary.
	Create Bottom Boundary Icon: Allows user to draw in position of bottom boundary.
	XOR Icon: Makes top image translucent.

Step 5. Define Hydrostratigraphic Units

For this step, select the *Active Data>Hydrostratigraphy*. A material property window will appear. You'll now need to define one or more hydrostratigraphic units including rock, thermal, and hydrogeologic information for each unit you wish to create. To do this, click on the "ADD" button on the bottom of the hydrostratigraphic unit data window. A new window will appear. First select a color that you want to use to represent that hydrostratigraphic unit in the preprocessor. Another window will appear with Red-Green-Blue color slider bars. Adjust the slide bars until you get the desired color. For example, if you want your hydrostratigraphic unit to be colored Red, move the Green and Blue slider bars to zero. Once you've picked a color, click on the "Okay" button. Now specify the material property information. You must completely fill this information in. If you don't know the value of a given parameter, refer to tables 3-6 and Chapter 6-7 for representative values. Repeat the above steps until you've added the desired number of hydrostratigraphic units.

Icons which appear when *Active Data> Hydrostratigraphic Units* is Selected

Icon	Description
	Arrow Icon: Allows user to select various objects
	Polygon Icon: Allows user to draw in hydrostratigraphic units by clicking repeatedly with the left mouse button. To terminate the unit outline, the user clicks on the right mouse button.
	Add Vertex Icon: Adds a vertex handles to top or bottom boundary.
	Discretize Icon: Interpolates mesh to basin boundary and assigns hydrostratigraphic units to individual element columns
	Zoom Icon: Click this and click on image to zoom in. Hold shift key and click to zoom out.
	XOR Icon: Makes top image translucent.

Once you've completed this, it is time to specify the configuration of the hydrostratigraphic units using the *Polygon* icon on the left margin of the application window just below the *Arrow* icon. In some instances, the order you draw in the layers is important. The first unit you select should be the material, which appears most frequently. The first step is to click on the material

property dialog box and then select (highlight) the hydrostratigraphic unit which you want to draw in first by clicking on its color. Then, select the polygon icon and begin to draw a polygon around the outside of the entire solution domain. Every time you click with the left-hand mouse button, you specify a handle position. Don't worry if your polyline extends beyond the boundaries of the domain. It will be trimmed by the preprocessor. Double click using the right mouse button to end the poly zone. If you have layer cake geology or no formations repeat themselves, then the order you draw in your hydrostratigraphic units is not important. It is possible that in some instances, you're polylines will block the GIF image. To bring the GIF image forward (by making the polygons translucent) simply click on the XOR icon (bottom icon on left margin pallet). If you want to change the shape of an existing polyzone, select the Arrow Icon. Then click on a polyzone. The handles of the zone will appear. You can click on these and move them.

Note that if you want to display (or hide) additional parts of your data set (e.g. mesh, hydrostratigraphy, basin diagram) either select or de select these using the *Show* menu.

Step 6. Define Finite Element Mesh

For this step, select the *Active Data>Mesh*. Several new icons will appear on the left hand of the preprocessor window. These provide you with several different options for discretizing your solution domain. You may add nodal columns individually (Add Vertical Lines Icon), using a spreadsheet (Mesh Icon), or uniformly distributed. To add columns individually, select the Add Vertical Lines Icon and click on your basin where you wish to add nodal columns. The easiest thing to do, however, is to generate columns uniformly across the domain. To do this, select *Edit>Uniform Columns* menu. Specify the number of evenly spaced columns you wish to generate. For the spreadsheet option, click on the Mesh Icon. Then select two columns (typically the first and last) that appear in the spreadsheet. Highlight these by holding down your mouse and dragging it downward. You can then subdivided two selected columns using the subdivide features of the spreadsheet. You can allow the mesh to telescope in a particular direction by selecting the subdivide option and specifying multiplication factor (usually between 1.01 and 1.1). To view the stratigraphy and grid, click on the "Discretize Icon". You can add an individual column(s) by selecting the "Add Vertical Lines Icon" and then clicking on the position where you wish do add a column. To vertically discritize your domain, you'll also need to select *Edit>Rows*

and specify the number of element rows you wish to have. The current version of the preprocessor does not allow you to vary element thickness with depth.

Icons which appear when *Active Data> Mesh* is Selected

Icon	Description
	Allows user to select various objects.
	Add Vertical Lines Icon: Adds nodal columns individually.
	Zoom Icon: Click this and click on image to zoom in. Hold shift key and click to zoom out.
	Mesh Spreadsheet Icon: Opens spreadsheet window for generating nodal columns with telescoping features.
	Discretize Icon: Interpolates mesh to basin boundary and assigns hydrostratigraphic units to individual element columns.
	XOR Icon: Makes top image translucent.

Step 7. Define Boundary Conditions

For this step, first select **Show>Tectonic Period Window**. A data window will appear with a number of columns. Make sure the arrow icon is specified and click on the ADD button in the data window. You must specify at least one tectonic time period to cover the beginning of the simulation. If you wish to modify boundary conditions during the simulations, then ADD additional tectonic time periods. The following data items must be specified along the top boundary:

Length – length of a time period for which boundary conditions are held constrained

Water Table – specify either having the water table equal the elevation of the top node (LS) or specifying a value for that node.

ICASE – specifies the style of subsidence, uplift, erosion (ICASE 0-3; see Appendix 3).

GRDFAC – Multiplier variable which specifies the width of newly generated elements if subsidence occurs (see Appendix 3).

Icons which appear when the *Active Data> Boundary Conditions* is Selected

Icon Symbol	Description
	Arrow Icon: Allows user to select various objects
	Top Boundary Icon: Allows user to specify input for top head, temperature, and concentration boundary conditions.
	Bottom Boundary Icon: Allows user to specify input for bottom head, temperature, and concentration boundary conditions.
	Add Vertex Icon: Adds a vertex handles to top or bottom boundary.
	Zoom feature
	Discretize Icon: Interpolates mesh to basin boundary and assigns hydrostratigraphic units to individual element columns
	XOR Icon: Makes top image translucent.

Now select the *Active Data>Boundary Condition* menu. Several new icons will appear on the left hand menu. These provide you with different options for assigning boundary conditions at the top and base of the solution domain. Click on the top boundary icon. You'll see the handles appear (the number of these depends on how many "left clicks" you made when you were defining the top and bottom boundaries of the solution domain). A spreadsheet window will also appear. If you wish to set all of the boundary conditions at the surface to the same values, highlight all of the rows in the spreadsheet. If you wish to vary these individually, then only select the individual row(s) you wish to assign. You'll see which handles have been selected in the background. Now, select the Edit button at the bottom of the dialog box. You'll have to enter the following information for each nodal column of the top boundary:

HDBASE	HDINC
TPBASE	TPINC
NEVAP	CNBASE
NCLAY	CEVAP

CLAY

Refer to Appendix 3 for the definition of these variables. If you set unique variables for each handle, the preprocessor will interpolate the boundary condition information onto nodal columns between the handles. You need to repeat the process for the bottom boundary condition data by selecting the bottom boundary icon. The data you'll need to add for the bottom boundary relates to heat flow:

JBASE

JINC

Step 8. Define Observation Points inside Mesh.

If you want to monitor time dependent output at specific locations within the basin, select *Active Data>Observation Points* window. A dialog box will appear. Select the diamond icon and then click on the location(s) where you wish to monitor output. You can select up to six points. These will be written to the last six files in riftfiles.txt (e.g. elem1_tec.dat: elem1_tec.dat, elem2_tec.dat, elem3_tec.dat elem4_tec.dat, elem5_tec.dat, elem6_tec.dat).

Icons which appear when *Active Data>Observation Points* is Selected

Icon	Description
	Arrow Icon: Allows user to select various objects in picture.
	Diamond Icon: Creates observation points. Select this to locate which element(s) you wish time-dependent output.
	Discretize Icon: Interpolates mesh to basin boundary and assigns hydrostratigraphic units to individual element columns
	Zoom Icon: Click this and click on image to zoom in. Hold shift key and click to zoom out.

Step 9. Run Model and View Results

To run your data set and view the model results, select *Show>Postprocessor*. Before you do this, however, double check that you've selected the desired model options under *Options>Model*. If you want an ASCII file saved of your session, this would be a good time to do this by selecting "File>Export data". The data set you've just created will begin to run using RIFT2D. The simulation time is listed in the center, bottom portion of the window frame which appears. The variables which can be displayed as contour maps using the post processor include:

1. Stratigraphy
2. Heads
3. Temperatures

4. Solute Concentrations
5. Porosity
6. Vitrinite Reflectance
7. Darcy Flux (magnitude)

You can also (simultaneously) display the mesh and the velocity vectors along with a contour variable. Choose which variable you wish to look at using the display dialog box. To display the triangular mesh and velocity vectors selected click on their respective icons (see table below).

Note that only the variables which pertain to the simulation you've set up under the *Options>Model* menu will appear. For example, if you don't activate the IHEAT and IOIL options, then the Temperature and Vitrinite Reflectance variable will not appear in the dialog box. You will also need to choose whether you want to look at the average value of the triangular elements (Cell option) or a smoothed contour map (Contours option) using nodal contoured values of the variable selected. These options are listed in the dialog box to the right of the variable box.

To change the maximum, minimum, and contour interval value to be displayed, select *Options>Color Scale*. If you want to display the velocity vectors (as ball and stick figures), click on the Arrow Icon. You can select the length of the vector shaft and opt to display a circle at the origin of the vector shaft by selecting *Options>Velocity*. Note that the smaller you make the scale, the larger the shaft becomes.

To run the data set to the end of the simulation (NTIME), you simply need to click on the Run Icon in the upper left hand corner of the post processor window. You can also step through the simulation, one time step at a time, go back to the beginning of the simulation, or stop the simulation using these buttons. If you decide you wish to change some aspect of the data set, you can return to the preprocessor by selecting *Action>Done*.

Icons which appear when *Show>Postprocessor* is Selected

Icon	Description
	Run Icon: Runs simulation to end (NTIME).
	Stop Icon: Stops simulation.

	Step Icon: Run simulation one time step at a time
	Reset Icon: Rest model to beginning of simulation
	Zoom Icon: Click this and click on image to zoom in. Hold shift key and click to zoom out.
	Vector Display Icon: Click on this to display velocity vectors as ball and stick figures.
	Mesh Display Icon: Click on this to display triangular finite element mesh

The *Action* menu also allows you to print out time steps or export bit map images of specific time steps to files. Additional help is available by selecting the help menu.

VIEWING RIFT2D OUTPUT USING TECPLOT

RIFT2D output can be graphically displayed using the commercially available plotting software Tecplot. Information regarding Tecplot can be obtained by contacting AMTEC Engineering at the following web site: www.amtec.com. Tecplot is a powerful visualization tool capable of representing output from irregularly gridded data such as triangular finite element grids. By specifying PTEC=1 in the RIFT2D input data file, a Tecplot formatted output file (rift_tec.dat) is created. This file can be rendered using Tecplot. The number of variables (up to 28) which can be rendered using Tecplot will vary depending on what simulation options are specified (i.e. whether IFLOW, IHEAT, IBRINE, and IOIL are set to 1 or 0). A listing of the RIFT2D variable names that may be plotted using Tecplot are listed in Table 8.1 below. The size of the tecplot output file will vary depending on the number of time steps that the user wishes to be displayed. This is controlled using the variable IPRINT and NTIME. The number of time steps represented is given by NTIME/IPRINT + 1. Each time step that is included in a tecplot output file is referred to as a “zone”. Instructions on how to utilize Tecplot are found in the Tecplot users guide.

As of the publishing of this manual, the package sells for \$700 dollars for private companies and about \$700 for Universities. This graphics package is especially suited for display and animation of finite element model output. In addition, TECPLOT can generate graphical output in many formats including postscript, TIFF, GIF, and EMF. The package is menu driven and fairly easy to use. Several TECPLOT output files can be generated by RIFT2D by specifying PTEC = 1 on line 13 of the input data files. See Table 5.1 for a more complete description of these files (rift_tec.dat, sfc_tec.dat, prf1_tec.dat to prf6_tec.dat, and elem1_tec.dat to elem6_tec.dat).

Details of using TECPLOT to display RIFT2D model results can be found in the TECPLOT Users guide. Below we provide a brief primer on how to display model results. Once TECPLOT is installed and launched on your pc or Unix workstation, go to the file menu and select the load option. Before displaying your data, TECPLOT will convert RIFT2D data to binary format (Note that this can be done in advance of implementing TECPLOT by typing “PREPLOT filename”). A list of variables and units in the output files is provided in Table 8.1. The binary file will appear with a '.plt' suffix.

Displaying contour maps and Velocity Vectors

The following steps will allow you to view RIFT2D mesh and select field variables:

1. Select the file “rift_tec.dat” (or whatever name you have selected for Unit #11; if you have created a binary file, select it). Each time step output will be read into TECPLOT as a separate “zone”. Recall that the total number of zones is NTIME/IPRINT. Initially only the finite element mesh will be graphically displayed (each zone in a different color).
2. To display the mesh and stratigraphy together, click on the “Contour” box in the upper left hand corner of the TECPLOT window. The contour variable selection window will appear. Select the “STRAT” variable (MTAG).
3. Select “Plot Attributes” at the bottom left part the TECPLOT window (just above the “snap to grid button”). Click on “Zone Num” button and select “select all”. All zones should be highlighted now.

TABLE 8.1 RIFT2D Variables used by TECPLOT

Variable Name	Variable Description (units)
X	Node x coordinate (m)
Z	Node z coordinate (m)
STRAT	Hydrostratigraphic unit number (MAT)
NODE_ANGL	Local angle of mesh (degrees)
E	
KX	Hydraulic conductivity tensor component K_{xx} (m/yr)
KZ	Hydraulic conductivity tensor component K_{zz} (m/yr)
KXZ	Hydraulic conductivity tensor component K_{xz} (m/yr)
VX	Darcy velocity in x-direction (m/yr)
VZ	Darcy velocity in z-direction (m/yr)
HEAD	Head (m)
PRES	Fluid pressure (Pa)
PRESH	Hydrostatic fluid pressure (Pa)
PRESL	Lithostatic fluid pressure
PHI	Porosity (dimensionless)
RHOF	Groundwater density (kg/m ³)
RHOO	Oil density (kg/m ³)
RHOG	Gas Density (kg/m ³)
VSM	Sediment velocity (m/yr)
SS	Specific Storage (m ⁻¹)
TEMP	Temperature (°C)
CONC	Concentration (mass fraction)
MASSOIL	Mass oil generated (mg oil/gram total organic carbon)
MASGAS	Mass gas generated (mg oil/gram total organic carbon)
RV	Vitrinite reflectance (%)
HEADOIL	Oil head (m)
VOX	Oil velocity in x-direction (m/yr)
VOG	Oil velocity in z-direction (m/yr)
Ss	Specific storage coefficient (m ⁻¹)
PRESH	Hydrostatic Pressure (Pa)
PRES	Pressure (Pa)
PRESL	Lithostatic Pressure (Pa)
VSM	Sediment velocity (m/yr)
Jz	Surface conductive heat flux (m/yr)
Qx	Darcy flux at top boundary in x-direction (m/yr)
Qz	Darcy flux at top boundary in z-direction (m/yr)
XP	Particle position in x direction (m)
ZP	Particle position in z direction (m)
CONCP	Particle concentration (mass fraction)
ELHOM	Element number particle resides in. Use d for debugging purposes
IPFLAG	Integer array associated with particles. Identify whether particle was found: in neighboring elements (IPFLAG=1); by a wider search involving the entire finite element mesh (IPFLAG=2); by looking along the boundaries of the solution domain and reflecting the particle back inside (IPFLAG=3); by moving the particle back towards its original node by increments of 0.1 until it is located in neighboring elements (IPFLAG=4). If the particle is never found, IPFLAG=0.

4. Click on the “Cont Plotype” button. Select the “Corner” option. This contour style is ideal for stratigraphy while for other field variables such as HEAD or TEMP, we recommend selecting “Flood” or “Both Flood and Line”. Next, select the “Mesh” option at the top left part of the “Contour Attributes” window. Click on “Mesh Color” button and choose a color for your mesh (we recommend black).
5. To view an individual zone, select that “Zone Show” in the Plot Attributes menu and activate that zone (select “activate”). All other zones should be deselected (highlight these and select “deactivate”). Then click on “Redraw” button on the left side of the TECPLOT window. To animate all of the zones select “Tools>Animate>Zones”. animation window will appear. Click on “Animate”.
6. To view heads and velocity vectors, go the “Field” menu and select “Field>Contour Variable”. Choose “HEAD”. Next Click on the “Vector” button on the left edge of the TECPLOT window. A “Select Variables” window will appear. Enter “VX” for “U” and VZ for “V” (the x and z components of the velocity vector). Click on “Redraw”.
7. Select “Plot Attributes” and choose “Vector”. Select “Zone Num” and choose “Select All”. Now select “Vect Color” and choose a color (we recommend black). If the velocity vectors are too small. Go to the “Field” menu and select “Field>Vector Length”. To increase the size of the vector shaft, make the number larger in the “Relative (grid units/cm) Field”. To make all vectors the same size, select the “Uniform” option.

You can save a file graphics options you have selected by choosing “File>Save Layout”.

Time Dependent Scattergrams for an Element

In some instances, the RIFT2D user may wish to display temporal output at a given location (PELM=1). RIFT2D allows the user to generate up to six output files (elem1-6_tec.dat; units 66-71). In addition, the user may wish to view surface conductive heat flow and/or recharge/discharge across the top boundary (unit 50, scf_tec.dat). Finally, profiles of head may be viewed along a well(s) using TECPLOT (unit 55-60; prf1_tec.dat to prf6_tec.dat). These scattergram plots can be displayed in TECPLOT by reading one or more of these files. The instructions for viewing elemental output are as follows:

1. Select the file “elem1_tec.dat” (or whatever name you have selected for Unit #65). Each time step will be read into TECPLOT. The total number of records is NTIME. Do this by going to the File>Load Data menu option.
2. Initially, temperature (TEMP) verse time will be plotted as a scattergram. Other variables that may be displayed include head (HEAD), the horizontal component of velocity (QX), the vertical component of velocity (QZ), and the spatial coordinates (X,Z). These are represented as different “maps”.
3. To display different variables, select “Plot Attributes” button. Then simply select (highlight) a given map number and click on “map show”. Activate that scattergram (e.g. map 7; time verses head). Be sure to deselect all other variables.
4. Select the menu option “View>Fit to Full size” to resize the scattergram.
5. To print output, select “File>Print”. To export in various formats, select “File>Export”.

Displaying Profile Scattergrams Using Tecplot

RIFT2D permits the generation of time dependent output files which display vertical profiles of select output variables (e.g. depth verse pressure, temperature, head, vitrinite reflectance). These plots can be used to calibrate RIFT2D model against observed data fields. The number of times this data is printed to the files prf1_tec.dat to prf6_tec.dat is determined by NTIME/IPRINT. The following steps allow you to view transient results.

1. Select the file “prf1_tec.dat” (or whatever name you have selected for Unit #55). Each zone will be read into TECPLOT. The total number of records is NTIME/IPRINT. Data is loaded by selecting the File>Load Data menu option.
2. Initially, head (HEAD) verse depth will be plotted as a scattergram. Other variables that may be displayed include fluid pressure (PRES: as well as hydrostatic, PRESH and lithostatic pressures, PRESL), porosity (PHI), specific storage (SS), and fluid density (RHOF). These are represented as different “maps”.
3. To display time dependent evolution of heads, select the "Plot Attributes" menu. Select are "Maps" in the Window. Next Click on the "Create Map" button. Select the Option "X Axis Var verse Y Axis Var for all zones". Before closing the window, select " X Var verses Y Var for All Zones". Tecplot will generate a separate Map (time slice) for each time step written the file.

4. Select all Maps using the "Map Num" option.
5. Select the Line option. Select the "Line Color" option and make all lines the same color.
6. Select Fit to Full size to resize the scattergram.
7. Select "Tools>Animate>XY Mapping" to display a time dependent results.

REFERENCES

- Allen, A. A. and J. R. Allen, 1990, Basin analysis, principles and applications, Blackwell Scientific Publications, 451 p.
- Arne, D., P. F. Green, and I. R. Duddy, 1990, Themochronologic constraints on the timing of Mississippi Valley-Type ore formation from apatite fission track analysis, *Nucl. Tracks Radia. Meas.*, 17, 319-323.
- Athy, L. F., 1930, Density, porosity, and compaction of sedimentary rocks, *American Association of Petroleum Geologists Bulletin*, v. 14, p. 1-23.
- Belitz, K., and Bredehoeft, J. D., 1989, The role of confining layers in controlling large-scale regional flow, in *Hydrology of Low Permeability Environments*, Vol. 2, ed. by S. P. Neuman and I. Neretnieks, Verlag Heinz Heise, p. 7-17.
- Bethke, C. M., 1985, A numerical model of compaction-driven ground water flow and heat transfer and its application to the paleohydrology of intracratonic sedimentary basins, *Jour. Geophys. Res.*, 90(B8), 6817-6828.
- Bethke, C. M., 1986a, Inverse hydrologic analysis of the distribution and origin of Gulf Coast-type geopressured zones, *Jour. Geophys. Res.*, 91, 6535-6545.
- Bethke, C. M., 1986b, Hydrologic constraints on the genesis of the Upper Mississippi Valley mineral district from Illinois Basin brines, *Econ. Geol.*, 81(2), 233-249.
- Bethke, C. M., 1989, Modeling subsurface flow in sedimentary basins, *Geologische Rundschau*, 78(1), 129-154.
- Bethke, C. M., and T. F. Corbet, 1988, Linear and nonlinear solutions for one-dimensional compaction flow in sedimentary basins, *Water Resources Res.*, 24, 461-467.
- Bethke, C. M., and S. Marshak, 1990, Brine migrations across North America—the plate tectonics of groundwater, *Annual Rev. Earth Planet. Sci.*, 18, 287-315.
- Bethke, C. M., W. J. Harrison, C. Upson, and S. P. Altaner, 1988, Supercomputer analysis of sedimentary basins, *Science*, 239, 261-267.
- Bethke, C. M., J. D. Reed, and D. F. Oltz, 1991, Long-range petroleum migration in the Illinois Basin, *American Assoc. Petroleum Geologists Bulletin*, 75, 925-945.
- Bethke, C. M., M.-K. Lee, H. A. M. Quinodoz, and W. N. Kreling, 1993, Basin Modeling with Basin2, A guide to Using Basin2, B2plot, B2video, and B2view, 225 pp., University of Illinois.
- Biot, M.A., 1941, General theory of three-dimensional consolidation, *Jour. Appl. Phys.*, 12, 155-164.

- Brace, W.F., Permeability of crystalline and argillaceous rocks, *Int. J. Rock Mech. and Min. Sci.*, 17(5), 241-245, 1980.
- Brace, W.F., 1984, Permeability of crystalline rocks: New insitu measurements, *Jour. Geophys. Res.*, v. 89(B6), p. 4327-4330.
- Bredehoeft, J. D., and B. Hanshaw, On the maintenance of anomalous fluid pressures: I. Thick sedimentary sequences, *Geol .Soc.Amer. Bull.*, 79, 1097-1106, 1968a.
- Bredehoeft, J. D., Neuzil, C. E., and Milly, P. C. D., 1983, Regional flow in the Dakota Aquifer: A study of the role of confining layers, *U. S. Geol. Sur. Water-Sup. Pap.* 2237, 45p.
- Burrus, J., and F. Audebert, Thermal and compaction processes in young rifted basins in the presence of evaporites; consequences for petroleum potential; the Gulf of Lions case study, submitted, *Jour. of Geophys. Res.*, 1988.
- Burnham, A. K. and J. J. Sweeney, 1989, A chemical kinetic model of vitrinite maturation and reflectance, *Geochimica et Cosmochimica Acta*, v. 53, p. 2649–2657.
- Clauser, C. 1992, Permeability of crystalline rocks, *EOS, Trans. Amer. Geophys. Union.*, v. 73(21), p. 233-240.
- Corbet T. and C. M. Bethke, 1992, Disequilibrium fluid pressures and groundwater flow in the Western Canada sedimentary basins, *Jour. Geophys. Res.*, 97, 7203-7217.
- Domenico, P. A., and V. V. Palciauskas, 1979, Thermal expansion of fluids and fracture initiation in compacting sediments, *G.S.A. Bull.*, 90, 953-979.
- England, W. A., A. S. Mackenzie, D. M. Mann, and T. M. Quigley, 1987, The movement and entrapment of petroleum fluids in the subsurface. *Jour. Geol. Soc. London*, v. 144, p. 327–347.
- Elliott, W. C., and J. L. Aronson, 1993, The timing and extent of illite formation in Ordovician K-bentonites at the Cincinnati Arch, the Nashville Dome and north-eastern Illinois Basin, *Basin Res.*, 5, 125-135.
- Evans, D. and J. Nunn, J., 1993, Free thermohaline convection in sediments surrounding a salt column, *Jour. Geophys. Res.*, v. 94, p. 413-422.
- Freeze, R.A., and J.A. Cherry, 1985, *Groundwater*, 604 pp., Prentice-Hall, New Jersey, 1979
- Garven, G., 1985, The role of regional fluid flow in the genesis of the Pine Point deposit, western Canada sedimentary basin, *Econ. Geol.*, 80, 307-324.
- Garven, G., 1986, The role of regional fluid flow in the genesis of the Pine Point deposit, western Canada sedimentary basin—a reply, *Econ. Geol.*, 81(4), 1015-1020.

- Garven, G., 1989, A hydrogeologic model for the formation of the giant oil sands deposits of the Western Canada Sedimentary Basin, Amer. J. Sci., 289(2), 105-166.
- Garven, G., 1994, Coupled hydrogeologic models for MVT ore genesis (abstract), G.S.A. Abstracts with Programs, 26, A107.
- Garven, G., 1995, Continental-scale ground water flow and geologic processes, Ann. Rev. Earth Planet. Sci., 24, 89-117.
- Garven, G., and R. A. Freeze, 1984a, Theoretical analysis of the role of ground water flow in the genesis of stratabound ore deposits 1. Mathematical and numerical model, Amer. J. Sci., 284, 1085-1124.
- Garven, G., and R. A. Freeze, Theoretical analysis of the role of ground water flow in the genesis of stratabound ore deposits 2. Quantitative results, Amer. J. Sci., 284, 1125-1174, 1984b.
- Garven, G., and J. P. Raffensperger, Hydrogeology and geochemistry of ore genesis in sedimentary basins, in Geochemistry of Hydrothermal Ore Deposits, 3rd ed., edited by Barnes, H. L., John Wiley & Sons, New York, in press.
- Garven, G., S. Ge, M. A. Person, and D. A. Sverjensky, Genesis of stratabound ore deposits in the Midcontinent basins of North America. 1. The role of regional ground water flow, Amer. J. Sci., 293, 497-568, 1993.
- Ge, S., and G. Garven, Hydromechanical modeling of tectonically driven ground water flow with application to the Arkoma foreland basin, J. Geophys. Res., 97(B6), 9119-9144, 1992.
- Gelhar, L., 1993, Stochastic Subsurface Hydrology, Prentice -Hall, Inc. Englewood Cliffs, NJ, 390 p.
- Gibson, R. E., The progress of consolidation in a clay layer increasing in thickness with time, Geotechnique, 8, 171-182, 1958
- Gibbs, A. D., 1983, Balanced cross-section construction from seismic sections in areas of extensional tectonics, Journal of Structural Geology, v. 5, p. 153-160.
- Giles, M. R., 1997, Diagenesis: A quantitative perspective, Boston, Kluwer Academic Publishers, 526p.
- Gordon, D. S., 1996, One- and two-dimensional modelling of groundwater flow in rapidly subsiding sedimentary basins, M.S. Thesis, Pennsylvania State University, State College, PA, 123 p.
- Gregg, J. M., P. R. Laudon, R. E. Woody, and K. L. Shelton, Porosity evolution of the Cambrian Bonneterre Dolomite, south-eastern Missouri, USA, Sedimentology, 40, 1153-1169, 1993.

- Haneberg, W., C., Steady state ground water flow across idealized faults, *Water Resour. Res.*, 317, 1815-1820, 1995b.
- Hanor, J. S., Origin and Migration of Subsurface Sedimentary Brines, SEPM Short Course No. 21, 247 pp., Society of Economic Paleontologists and Mineralogists, Tulsa, OK, 1987.
- Harrison, W. J., and L. L. Summa, Paleohydrology of the Gulf of Mexico Basin, *Amer. J. Sci.*, 291, 109-176, 1991.
- Hart, B. S., Flemings, P. B., and A. Deshpande, 1995, Porosity and pressure: Role of compaction disequilibrium in the development of geopressures in a Gulf Coast Pleistocene basin, *Geology*, v. 23, p. 45-48.
- Hay, R. L., M. Lee, D. R. Kolata, J. C. Mathews, and J. P. Morton, Episodic potassic diagenesis of Ordovician tuffs in the Mississippi Valley area, *Geol.*, 16, 743-747, 1988. Hay et al., 1988.
- Hayba, D., and S. E. Ingebritsen, The computer model HYDROTHERM, a three-dimensional finite-difference model to simulate ground-water flow and heat transport in the temperature range of 0 to 1,200°C, U.S. Geological Survey Water-Resources Investigations Report 94-4045, 85 pp., 1994.
- Hubbert, M. K., 1940, The theory of ground water motion, *Jour. Geol.*, v. 48, p. 785-944.
- Hubbert, M. K., Entrapment of petroleum under hydrodynamic conditions, *A.A.P.G. Bull.*, 37, 1954-2026, 1953.
- Hubbert, M. K., and W. W. Rubey, Role of fluid pressure in mechanics of overthrust faulting I. Mechanics of fluid-filled porous solids and its application to overthrust faulting, *G.S.A. Bull.*, 70, 115-166, 1959.
- Hunton, P. W., Fault severed aquifers along the perimeters of Wyoming artesian basins, *Ground Water*, 23(2), 176-181, 1985.
- Huyakorn, P. S., and G. F. Pinder, 1983, Computational methods in subsurface flow, Academic Press, New York, 473 p.
- Jackson, J., and D. P. McKenzie, 1983, The geometrical evolution of normal fault systems, *Journal of Structural Geology*, v. 5, p. 471-482.
- Jackson, J. A., and N. J. White, 1989, Normal faulting in the upper continental crust: observations from regions of active extension, *Journal of Structural Geology*, v. 11, p. 15-33.
- Jury, A. Gardner W. R. and W. H. Gardner, 1991, Soil Physics, 5th Edition, Wiley, 328 p.
- Kestin, J., Khalifa, H. E., and R. Corriea, 1981, Tables of the dynamics and kinematic viscosity of aqueous NaCl Solutions in the temperature range of 20-150 °C and the pressure range of 0.1-35 MPa, *Journal of Physical Chemistry Reference Data*, v. 10, p. 71-87.

- Konikow, L.F. and J.D. Bredehoeft. 1978. Computer model of two-dimensional solute transport and dispersion in ground water. U.S. Geological Survey Techniques of Water-Resources Investigations, Book 7, Chapter C2, 90 pp.
- Konikow, L. and J. D. Bredehoeft, 1992, Ground-water models cannot be validated, Advances in Water Resources, v. 15, p. 75-83.
- Konikow, L. F., Sanford, W. E., and P. J. Campbell, Constant-concentration boundary condition: Lessons from the HYDROCOIN variable-density ground waterbenchmark, Water Resources Research, v. 33, p. 2253-2261.
- Kuttan, K., Kulla, J. B., and R. G. Neumann, 1986, Freshwater influx in the Gippsland Basin: Impact on formation evalutation, hydrocarbon volumes, and hydrocarbon migration, APEA Journal, v. xx, p. 242-249.
- Lucia, F. J., 1995, Rock-fabric/petrophysical classification of carbonate pore space for reservoir characterization, Am. Assoc. Petrol. Geol. Bull. 79(9) 1275-1300.
- Luo, X., and G. Vasseur, Contributions of compaction and aquathermal pressuring to geopressure and the influence of environmental conditions, A.A.P.G. Bull., 76(10), 1550-1559, 1992.
- Mercer, J. Thomas, S. D., and B. Rose, 1982, Parameters and variables appearing in repository siting models, U.S. Nuclear Regulatory Commission, NUREG/CR-3086, 244 p.
- Mello A physical explanation for the positioning of the depth to the top of overpressure in shale-dominated sequences in the Gulf Coast basin, United States, Journal of Geophysical Research, v. 99, p. 2775-2789.
- Mello, U. T., Karner, G. D., and Anderson, R. N., 1994, A physical explanation for the positioning of the depth to the top of overpressure in shale-dominated sequences in the Gulf Coast Basin, United States, J. Geophys. Res., 99. 2775-2789.
- Marsily, G. de, Quantitative Hydrogeology, Marsily, G. de, Translator, 440 pp., Academic Press, New York, 1986.
- McCabe, C., and R. D. Elmore, The occurrence and origin of late paleozoic remagnetization in the sedimentary rocks of North America, Rev. Geophys., 27, 471-494, 1989.
- Nelson, P. H., Permeability-porosity relationships in sedimentary rocks, The Log Analyst, May-June, 38-62, 1994.
- Neuman, S. P., Theoretical derivation of Darcy's law, Acta Mechanica, 25, 153-170, 1977.
- Neuzil, C. E., Ground water flow in low-permeability environments, Water Resources Res., 22(8), 1163-1195, 1986.

- Neuzil, C. E., Low fluid pressure within the Pierre Shale: A transient response to erosion, Water Resources Res., 29(7), p. 2007-2020, 1993.
- Neuzil, C.E., Abnormal pressures as hydrodynamics phenomena, Am. Jour. Sci., v. 295, p. 742-786.
- Neuzil, C. E., How permeable are clays and shales?, Water Resources Res., 30(2), 145-150, 1994.
- Oreskes, N. Shrader-Frechette, K., and K. Belitz, 1994, Verification, validation, and confirmation of numerical models in the Earth sciences, Science, v. 263, p. 641-644.
- Person, M. and L. Konikow, 1986, Recalibration and predictive reliability of a solute transport model of an irrigated stream-aquifer system, Journal of Hydrology, 87, v., p. 145-165.
- Person, M., Raffensperger, J., Ge. S., and G. Garven, 1995, Basin-Scale Hydrogeological Modeling, Reviews of Geophysics, v. 34, p. 61-87.
- Person, M., D. Toupin, and P. Eadington, Effects of convective heat transfer on the thermal history of sediments and petroleum generation within continental rift basins, Basin Research, 7, 81-96, 1995.
- Reddy, J. N., 1984, An introduction to the finite element method, McGraw-Hill Book Company, 495 p.
- Reiter, M., M. W. Barroll, and S. M. Cather, Rotational buoyancy tectonics and models of simple half graben formation, *J. of Geophys. Res.*, 97(B6), 8917-8926, 1992.
- Rieke, H.H. and G.V. Chilingarian, Compaction of argillaceous sediments, 424 pp., Elsevier Scientific Publishing Company, 1974.
- Roberts, S. J. and J. A. Nunn, Episodic fluid flow from geopressured sediments, Marine and Petrol. Geol., 12, 195-204, 1995.
- Rubey, W. W., and M. K. Hubbert, Role of fluid pressure in mechanics of overthrust faulting II. Overthrust belt in geosynclinal area of western Wyoming in light of fluid-pressure hypothesis, G.S.A. Bull., 70, 167-206, 1959.
- Sanford, W. E., and L. F. Konikow, 1989, Simulation of calcite dissolution and porosity changes in saltwater mixing zones in coastal aquifers, Water Resources Res., 25(4), 655-667.
- Scheidegger, A. E., 1974, The physics of Flow Through Porous Media, 3rd Ed., Toronto, Univ. of Toronto Press, 353 p.
- Somerton, W. H., 1992, Thermal properties and temperature-related behavior of rock/fluid systems, Amsterdam, Elsevier, 257p.
- Smith, L. and D. S. Chapman, 1983, On the thermal effects of ground water flow. 1. Regional scale systems, Journal of Geophysical Research, v. 88, p. 593-608.

- Tissot, B. P., R. Pelet, and P. H. Ungerer, Thermal history of sedimentary basins, maturation indices, and kinetics of oil and gas generation, A.A.P.G. Bull., 71, 1445-1466, 1987.
- Tissot, B.P., 1969, Premieres donnees sur les mecanismes et la cinetique de la formation du petrole dans les sediments: simulation d'un schema reactionnel sur ordinateur. Revue de l'Institut Francais du Petrole, v. 24, p. 470-501.
- Tissot, B. and J. Espitalie, 1975, L'evolution thermique de la matiere organique des sediments: applications d'une simulation mathematique. Revue de L'Institut Francais du Petrole, v. 30, p. 743-777.
- Toupin, D., 1993, The effects of ground water flow patterns in evolving intracratonic sedimentary basins on heat flow and petroleum generation, MSc. Thesis, University of New Hampshire, 250 p.
- Turcotte, D. L. and G. Schubert, 1982, Geodynamics, John Wiley and Sons, New York, 450 p.
- Ungerer, P., J. Burrus, B. Doligez, P. Y. Chenet, and F. Bessis, Basin evaluation by integrated two-dimensional modeling of heat transfer, fluid flow, hydrocarbon generation, and migration, A.A.P.G. Bull., 74, 309-335, 1990.
- Ungerer, P., 1984, Models of petroleum formation: how to take into account geology and chemical kinetics. In: Thermal phenomena in sedimentary basins, edited by B. Durand, Paris, Technip, p. 235-246.
- Ungerer, P., J. Espitalie, F. Marquis, and B. Durand, 1986, Use of kinetic models of organic matter evolution for the reconstruction of paleo-temperatures: application to the case of the Gironville well (France). In: Thermal modeling in sedimentary basins, edited by J. Burrus, Paris, Technip, p. 531-546.
- Ungerer, P., and P. Pelet, 1987, Extrapolation of the kinetics of oil and gas formation from laboratory experiments to sedimentary basins. Nature, v. 327, no. 6117, p. 52-54.
- Vasseur, G., L. Demongodin, and A. Bonneville, Thermal modeling of fluid flow effects in thin dipping aquifers, Geophys. J. Inter., 112, 276-289, 1993.
- Wieck., J., M. Person, and L. Strayer, A new finite element model for simulating fault block motion and hydrothermal fluid flow within rifting basins, Water Resources Res., in press.
- Zheng, C. and G. D. Bennett, 1995, Applied contaminant Transport Modeling: Theory and Practice, Van Nostrand Reinhold, 440 p.

APPENDIX 1

DERIVATION OF TRANSPORT EQUATIONS

Fluid, solute and heat transport equations that describe processes within deforming sedimentary basins can be derived using various reference frames. In principle, the various approaches will yield the same results. Because it simplifies bookkeeping, RIFT2D uses a computational grid that deforms with the porous matrix; this way, the elements in the grid always contain the same "packet" of sediment or rock. This has been referred to as a Lagrangian approach (e.g. Bethke, 1985) because it follows the porous matrix as it deforms relative to an absolute, fixed coordinate system. The displacements relative to absolute coordinates are manifested through changes in dimensions of the elements and the corresponding changes in distance from the domain boundaries for each packet of porous medium. The transport equations, on the other hand, are developed with reference to the deforming coordinate system of the computational grid. Because of this we do not need to describe the advection, or movement of the porous medium. The equations used here to describe transport of water, solute and heat are therefore Eulerian in the sense that they describe movement relative to fixed points in the porous medium (and therefore relative to fixed points in the deforming coordinate system).

Transient ground water flow results from the interplay between the pore fluid and the porous matrix. Both hydrodynamics and deformation of the porous matrix play important roles. In RIFT2D we capture this interplay using a description of fluid transport based on poroelasticity. Developed by Biot (1941), and one of the most fundamental contributions to our understanding of transient ground water flow, poroelasticity provides a rigorous description of transient ground water flow in three dimensions. It also allows us to incorporate thermoelastic effects (porous medium deformation in response to temperature changes).

To simplify analysis, we make the assumption that deformation of the porous medium is limited to that in the vertical; there are no lateral deformations or strains. This is strictly true only in one dimensional systems, but is a good approximation for most (though not all) basins. Indeed, because RIFT2D calculates vertical deformation behavior from a user-specified porosity-depth relation, it can be argued that lateral deformations are incorporated implicitly. In any event, the approach used by RIFT2D reasonably approximates deformation due to transient flow and vertical load changes (such as by deposition and erosion) but cannot describe processes dominated by lateral deformation,

such as tectonic "squeezing." This limitation is shared by other basin simulators, such as that of Bethke et al. (1993).

The poroelastic approach is an infinitesimal-strain, elastic-based description of porous medium deformation. Basinal processes, such as sediment compaction over geologic time scales, clearly involves neither small strains nor elastic deformation. However, this is not as problematical as it appears. Although processes such as sediment compaction often result in large strains, or deformations, the strain during a single time step will generally be quite small and can be closely approximated by an infinitesimal-strain elastic description. Deformation as a nonelastic process is a more complex issue. Actual deformation of sediment and rock over geologic time involves a complex suite of processes. An approach widely used in practice, and adopted here, is to use porosity-depth relations as surrogates for explicit information relating deformation to effective stress, chemical and thermal conditions, and time. This has several implications that should be thoroughly understood, and is discussed in more detail in Chapter 3. The bottom line is that the elastic-based equations used in RIFT2D are able to describe long-term inelastic deformation of porous media by appropriate choice of parameters.

Conservation of fluid mass in a deforming porous medium can be described by:

$$\frac{\partial (\rho_f \phi)}{\partial t} + \nabla \cdot (\rho_f \vec{q}) = \rho_p q_p \quad (A1)$$

where ϕ is porosity, ρ_f is fluid density, \vec{q} is the Darcy velocity, ρ_p is petroleum density (oil or gas), and q_p is the petroleum production source term. The second term on the left hand side of equation A1 represents the net divergence of mass flux across a control volume while the first term on the left hand side of A1 represents the net change in fluid mass storage within the control volume due to fluid density and porosity fluctuations. The expression on the right-hand-side of A1 accounts for fluid production caused by petroleum generation. Using the chain rule of differentiation, we can expand this term as follows:

$$d(\rho_f \phi) = \phi d\rho_f + \rho_f d\phi \quad (A2)$$

For non-isothermal systems, Palciauskas and Domenico (1982) indicates that porosity changes can be expanded as:

$$d\phi = \left[\frac{1}{K} - \frac{1}{K_s} - \frac{\phi_o}{K_s} \right] dP - \frac{d\sigma_t}{(K - K_s)} + \phi_o \alpha_{Tp} dT \quad (A3)$$

where K is bulk modulus of compressibility, K_s is the bulk modulus of compressibility for the sediment grains, σ_t is the total stress, ϕ_o is the reference porosity (porosity at the land surface), P is fluid pressure, T is temperature, and α_{Tp} is the coefficient of thermal expansion of the pores. Changes in fluid density due to thermal expansion and pressure changes are given by:

$$dp_f = \frac{\rho_o}{K_f} dP - \alpha_{Tf} dT \quad (A3)$$

where K_f is the bulk modulus of compressibility of the fluid, α_{Tf} is the coefficient of thermal expansion of the fluids phase, ρ_o is the fluid density at reference state ($P=0$ Pa; $c=0$ mg/l; $T=10$ °C). Substituting A3 and A4 into A2 yields:

$$d(\rho_f \phi) = \left[\frac{1}{K} - \frac{1}{K_s} - \frac{\phi_o}{K_s} + \frac{\phi_o}{K_f} \right] dP - \frac{\rho_o}{3(K - K_s)} d\sigma_t - \rho_o \phi_o (\alpha_{Tf} - \alpha_{Tp}) dT \quad (A4)$$

The first term on the RHS of equation (A4) represents fluid mass changes due to changes in fluid mass due to pressure changes, the second term represents vertical stress loading caused by sedimentation or erosional unloading, the third term represents fluid mass change due to the thermal expansion of both the fluid and solid phases. The fluid flux, \vec{q} , in equation (A1) can be calculated using Darcy's Law:

$$\vec{q} = -\nabla_x \cdot \left[\frac{k}{\mu_f} (\nabla_x P + \rho_f g \nabla_x z) \right] \quad (A5)$$

Substituting (A5) and (A4) into (A1) yields:

$$\begin{aligned} & \left[\left(\frac{1}{K} - \frac{1}{K_s} \right) + \frac{\phi}{K_f} - \frac{\phi}{K_s} \right] \frac{\dot{Z}P}{\dot{Z}t} - \left(\frac{1}{K} - \frac{1}{K_s} \right) \frac{\dot{Z}\sigma_t}{\dot{Z}t} + \phi(\alpha_{Tf} - \alpha_{Tp}) \frac{dT}{dt} \\ &= \nabla_x \cdot \left[\frac{k}{\mu_f} (\nabla_x P + \rho_f g \nabla_x z) \right] + \rho_p q_p \end{aligned} \quad (A6)$$

We now define a modified specific storage, fluid compressibility and thermal expansivity terms for the porous media as follows:

$$S' = \rho_{fg} \left[\left(\frac{1}{K} - \frac{1}{K_s} \right) + \frac{\phi}{K_f} - \frac{\phi}{K_s} \right]$$

$$\beta = \frac{\rho_{fg}}{S'} \left(\frac{1}{K} - \frac{1}{K_s} \right) \quad (A7)$$

$$\Lambda = \alpha_{Tf} - \alpha_{Tp}$$

Substituting these expressions into (A6) yields:

$$\nabla_x \cdot \left[\rho_{fg} \frac{k}{\mu_f} (\nabla_x P + \rho_{fg} \nabla_x z) \right] + \rho_f g \rho_p q_p = S' \frac{\dot{Z}P}{Zt} - \rho_{fg} \phi \Lambda \frac{dT}{Zt} - S' \beta \frac{\dot{Z}\sigma_t}{Zt} \quad (A8)$$

An additional constraint arising from the compatibility relation in elasticity (e.g. Rice and Cleary, 1976) may be stated as:

$$\nabla_x^2 \sigma_t = \lambda \nabla_x^2 P \quad (A10)$$

where the dimensionless coefficient λ is defined as $\lambda = \frac{2(1-2v)}{3(1-2v)} \alpha$ and $\alpha = 1 - K/K_s$. For non-isothermal conditions in a medium which is linear thermoelastic (e.g. Boley and Weiner, 1960) the poroelastic constitutive relations take the form:

$$e_{ij} = \frac{1}{K} \left[\frac{1+v}{3(1-2v)} dS_{ij} - \frac{v}{3(1-2v)} d\sigma_{kk} \delta_{ij} - \frac{\alpha}{3} dP \delta_{ij} - K \alpha_T dT \delta_{ij} \right] \quad (A11)$$

where δ_{ij} is the Kronecker delta. For the case of unidirectional (vertical) strain, $\epsilon_{11} = \epsilon_{22} = 0$. With this constraint, and defining $\sigma_t = (\sigma_{11} + \sigma_{22} + \sigma_{33})/3$, A11 can be manipulated to yield:

$$d\sigma_t = \lambda dP + \frac{\zeta}{\beta} (1 - \lambda \beta) d\sigma_v + \frac{3}{\alpha} \lambda K \alpha_T dT \quad (A12)$$

where σ_{33} is now σ_v . When the system is homogenous and σ_v and T increase linearly with depth, the constraint provided by A12 ensures that A10 is satisfied., A complete description is thus

$$\nabla \cdot \left[\rho_{fg} \frac{k}{\mu} (\nabla P + \rho_{fg} \nabla z) \right] + g \rho_p q_p = S_s \frac{dP}{dt} - S_s \zeta \frac{d\sigma_v}{dt} - \rho_{fg} \phi \Lambda \frac{dT}{Zt} \quad (A13)$$

Noting that:

$$S_s = S' (1 - \lambda \beta)$$

$$\zeta = \frac{\beta(1 + v)}{[3(1 - v) - 2\alpha\beta(1 - 2v)]}$$

We can also recast the above equation in terms of hydraulic head noting that:

$$\begin{aligned} \nabla_x \cdot \left[\rho_f g \frac{\mathbf{K}}{\mu_f} (\nabla_x P + \rho_g \nabla_x z) \right] &= \nabla_x \cdot [\mathbf{K} \mu_r (\nabla_x h + \rho_r \nabla_x z)] \\ S_s \frac{dP}{dt} &= \rho_o g S_s \frac{dh}{dt} \\ \rho_r &= \frac{\rho_f - \rho_o}{\rho_o} \\ \mu_r &= \frac{\mu_o}{\mu_f} \end{aligned} \tag{A14}$$

Substituting these relations yields:

$$\nabla \cdot [\rho_f \mathbf{K} \mu_r (\nabla_x h + \rho_r \nabla_x z)] + \rho_p q_p = \rho_o S_s \frac{dh}{dt} - \frac{S_s \zeta}{g} \frac{d\sigma_v}{dt} - \rho_f \phi \Lambda \frac{dT}{Zt} \tag{A15}$$

However, if we assume that the grains are incompressible, then $K_s = \infty$. This implies that $\alpha = 1 - K/K_s = 1$ and:

$$\begin{aligned} S' &= \rho_f g \left[\frac{1}{K} + \frac{\phi}{K_f} \right] \\ \beta &= \frac{\frac{1}{K}}{\frac{1}{K} + \frac{\phi}{K_f}} \\ \lambda &= \frac{2(1 - 2v)}{3(1 - v)} \end{aligned} \tag{A16}$$

Thus:

$$\begin{aligned}
S_s &= S'(1 - \lambda\beta) \\
S_s &= S' - S'\lambda\beta \\
S_s &= \rho_{fg} \left[\frac{1}{K} + \frac{\phi}{K_f} \right] - \rho_{fg} \left[\frac{1}{K} + \frac{\phi}{K_f} \right] \left[\frac{2(1-2v)}{3(1-v)} \right] \left[\frac{\frac{1}{K}}{\frac{1}{K} + \frac{\phi}{K_f}} \right]
\end{aligned} \tag{A17}$$

Simplifying A17 yields:

$$\begin{aligned}
S_s &= \rho_{fg} \left[\frac{(1+v)}{3(1+v)} \frac{1}{K} + \frac{\phi}{K_f} \right] \\
S_s &= \rho_{fg} \left[\frac{1}{K'} + \frac{\phi}{K_f} \right]
\end{aligned} \tag{A19}$$

where K' is the one-dimensional modulus. We can also show that the dimensionless loading coefficient, ζ , can be simplified to

$$\zeta = \frac{\frac{1}{K}}{\frac{1}{K'} + \frac{\phi}{K_f}} \tag{A20}$$

The third term in our governing transport equation thus becomes

$$\frac{S_s \zeta}{g} \frac{\dot{Z}\sigma_v}{\dot{Z}t} = \frac{\rho_f \dot{Z}\sigma_v}{K' \dot{Z}t} \tag{A21}$$

Thus our governing transport equation becomes:

$$\nabla \cdot [\rho_f K \mu_r (\nabla_x h + \rho_r \nabla_x z)] + \rho_f \rho_p q_p = \rho_o S_s \frac{dh}{dt} - \frac{\rho_f}{K'} \frac{d\sigma_v}{dt} - \rho_f \phi \Lambda \frac{dT}{dt} \tag{A22}$$

Bredehoeft et al. (1994) present an expression for the gas source term

$$q_p = \frac{1}{V_k} \frac{\rho_k}{\rho_p} \frac{dV_k}{dt} - \frac{d\phi}{dt} \tag{A23}$$

The first term on the RHS of account for the addition of petroleum source while the second term account for the loss of porosity from the conversion of kerogen to petroleum. The second term can be related to the initial volume of kerogen:

$$q_p = \frac{1}{V_k} \frac{\rho_k}{\rho_p} \frac{dV_k}{dt} - \frac{\partial \phi}{\partial t} = \frac{1}{V_k} \frac{dV_k}{dt} \left[\frac{\rho_k}{\rho_p} - 1 \right] \quad (A23)$$

The volume of petroleum generated is inversely related to the kerogen transformation ratio:

$$\frac{1}{V_k} \frac{dV_k}{dt} = - \frac{dT_r}{dt} \quad (A24)$$

Resulting in our final expression for the source term:

$$q_p = - \frac{dT_r}{dt} \left[\frac{\rho_k}{\rho_p} - 1 \right] \quad (A25)$$

Substituting this into our governing transport equation:

$$\nabla_x \cdot [K \mu_r \rho_f \nabla_x (h + \rho_r)] = S_s \rho_o \frac{\dot{Z} h}{\dot{Z} t} - \frac{\rho_f}{K' \rho_s g} \frac{\dot{Z} \sigma_v}{\dot{Z} t} - \phi \rho_f \Lambda \frac{\dot{Z} T}{\dot{Z} t} + [\rho_k - \rho_p] \frac{\dot{Z} T_r}{\dot{Z} t} \quad (A26)$$

We now turn to the problem of determining values of the effective one-dimensional deformation modulus, K' , from the observed loss of porosity with depth. With the simplification of assuming that the solid grains are incompressible, equation (A3) can be simplified as

$$d\phi = - \frac{1}{K'} d\sigma_v + \frac{1}{K'} dP + \phi_o \alpha_T dT \quad (A27)$$

and equation (A12) can be rewritten as

$$d\sigma_t = \frac{2(1-2v)}{3(1-v)} dP + \frac{1+v}{3(1-v)} d\sigma_v + \frac{6(1-2v)}{3(1-v)} K' \alpha_T dT \quad (A28)$$

By substituting (A28) into (A27) and performing some rather involved algebraic manipulations one obtains

$$d\phi = -\frac{1}{K'} (d\sigma_v - dP) + \left[\phi_o \alpha_{Tp} - \frac{2(1-2v)}{(1-v)} \alpha_T \right] dT \quad (A29)$$

It can be demonstrated that for applications of interest the thermal term (the last term on the RHS of A29) can be considered to be a part of the mechanical loading, so it will be dropped to yield

$$d\phi = -\frac{1}{K'} (d\sigma_v - dP) = -\frac{1}{K'} d\sigma_e \quad (A30)$$

The relation between porosity and effective stress was earlier given by equation (28), that is

$$\phi = \phi_o \exp \left(-\beta \frac{\sigma_e}{g(\rho_s - \rho_f)} \right) + \phi_{ir} \quad (A31)$$

Defining the z coordinate as positive upwards, and taking the derivative of (A31) with respect to z, we obtain

$$\frac{d\phi}{dz} = -\beta \frac{d}{dz} \left(\frac{\sigma_e}{g(\rho_s - \rho_f)} \right) \phi_o \exp \left(-\beta \frac{\sigma_e}{g(\rho_s - \rho_f)} \right) \quad (A32)$$

Similarly, taking the derivative of (A29) with respect to z gives

$$\frac{d\phi}{dz} = -\frac{1}{K'} \frac{d}{dz} \left(\frac{\sigma_e}{g(\rho_s - \rho_f)} \right) \quad (A33)$$

Equating (A32) and (A33) yields the expression used to compute K', namely

$$\frac{1}{K'} = \frac{B\phi_o}{g(\rho_s - \rho_f)} \exp \left[\frac{-B\sigma_e}{g(\rho_s - \rho_f)} \right] \quad (A34)$$

APPENDIX 2

LIST OF NOTATION

- ∇_x – Gradient operator (m^{-1})
 \mathbf{K} – Hydraulic conductivity tensor (m^2)
 T – Temperature ($^\circ C$)
 C – solute mass fraction ($kg\ NaCl/kg\ H_2O$)
 P – Pressure conditions in the particular finite element of interest (M-Pa)
 h – Equivalent fresh water hydraulic head (m)
 v_s – Velocity of the solid phase in the z-direction (m/s)
 z – Elevation above datum (m)
 t – Time (s)
 ϕ – Porosity (m^3/m^3)
 ϕ_o – Porosity at the land surface (or sediment water interface; m^3/m^3)
 ϕ_{min} – minimum porosity (m^3/m^3)
 ϕ_{ir} – irreducible porosity (m^3/m^3)
 σ_e – effective stress (Pa)
 σ_{max} – maximum effective stress (Pa)
 K' – Porous media modulus of compressibility (Pa^{-1})
 K_f – Fluid modulus of compressibility (Pa^{-1})
 σ_T – Net downward load (fluid + sediment weight; Pa)
 β – Compressibility of fluid (1/m)
 β_{ul} – Compressibility of fluid (1/m)
 α_{Tf} – Coefficient of thermal expansion of the fluid phase ($1/^\circ C$)
 α_{Tp} – Coefficient of thermal expansion of the pores ($1/^\circ C$)
 ζ – Dimensionless loading coefficient
 T – Temperature ($^\circ C$)
 K_{xx}, K_{xz}, K_{zz} – Components of the hydraulic conductivity tensor (m/s)
 k_x, k_z – Intrinsic permeability in the x- and z-directions (m^2)
 ρ_o – Reference fluid density at $10^\circ C$ (kg/m^3)
 ρ_f – Density of the fluid phase (kg/m^3)
 ρ_s – Density of the solid phase (kg/m^3)
 ρ_p – Petroleum density (kg/m^3)
 ρ_k – Density of kerogen (kg/m^3)
 ρ_r – Relative fluid density (unitless)
 S_s – Specific storage coefficient (1/m)

- g – Acceleration due to gravity (m/s^2)
 μ_f – Fluid viscosity of the fluid ($\text{kg/m}\cdot\text{s}$)
 Λ – Thermal response coefficient ($1/\text{^\circ C}$)
 μ_o – Reference fluid viscosity of the fluid ($\text{kg/m}\cdot\text{s}$)
 q_x, q_z – Darcy velocity with respect to a moving coordinate framework (m/s)
 $|q|$ – Average Darcy velocity ($|q| = \sqrt{q_x^2 + q_z^2}$; m/s)
 $\lambda_{xx}, \lambda_{xz}, \lambda_{zz}$ – Components of the effective thermal conduction-dispersion tensor of the porous medium ($\text{W}/\text{^\circ C}\cdot\text{m}$)
 λ_f, λ_s – Thermal conductivity of the fluid and solid phase ($\text{W}/\text{^\circ C}\cdot\text{m}$)
 c_f – Specific heat capacities of the fluid phase ($\text{J}/\text{^\circ C}\cdot\text{kg}$)
 c_s – Specific heat capacities of the solid phase ($\text{J}/\text{^\circ C}\cdot\text{kg}$)
 h_f – Specific enthalpy of the fluid (J/kg)
 z_o – Land surface elevation (m)
 g – Gravitational constant (m^2/s)
 J_z – Basal heat flow
 $\frac{D(\cdot)}{Dt}$ – Material derivative $\left[\frac{D(\cdot)}{Dt} = \frac{\dot{Z}(\cdot)}{Zt} + v_s \cdot \nabla(\phi) \right]$
 P – Fluid pressure ($\text{kg/m}\cdot\text{s}^2$)
 \hat{h} – Finite element trial solution for hydraulic head (m)
 α_t, α_l – Transverse and longitudinal dispersivity (m)
 j – Spatial index
 k – Time step index
 q_{xi}, z_i – Spatial coordinates of the i^{th} vertices of the triangular elements ($i=1,2,3$; m)
 n – Weighting function (m)
 im – Line segments on either side of node i and m (m)
 ml – Line segments on either side of node m and l (m)
 J_{im} – Components of heat flux across the respective line segment im (W/m^2)
 J_{ml} – Components of heat flux across the respective line segment ml (W/m^2)
 A^e – Area of a triangular element ($A^e = \frac{b_1 \cdot c_2 - b_2 \cdot c_1}{2}$) (m^2)
 A – Constant that depends on the type of organic matter (referred to in the context of the Arrhenius equation as the pre-exponential factor) (sec^{-1})
 E_i – Activation energy required to break the bonds in the i^{th} fraction of kerogen (kcal/mole)
 R – Universal gas constant ($0.001987 \text{ kcal}/\text{K}\cdot\text{mole}$)
 k_i – Rate constant used in petroleum generation model (sec^{-1})
 x_i – Residual mass of kerogen (in mg/g total organic matter)

M – Mass of kerogen (in mg/g TOC)

TOC – Total organic carbon

M_{H_2O} α_s – Mass of water remaining in kerogen (mg/g)

$M_{H_2O}^o$ – Initial mass of water in kerogen (mg/g)

M_{CO_2} – Mass of CO_2 remaining in kerogen (mg/g)

$M_{CO_2}^o$ – Initial mass of CO_2 in kerogen (mg/g)

M_{CHn} – Mass of oil remaining in kerogen (mg/g)

$M_{CH_n}^o$ – Initial mass of oil in kerogen (mg/g)

M_{CH_4} – Mass of CH_4 remaining in kerogen (mg/g)

$M_{CH_4}^o$ – Initial mass of CH_4 in kerogen (mg/g)

T_r – Kerogen transformation ratio (m^3/m^3)

α_s – Salinity gradient with depth (in equivalent mass fraction kg NaCl/kg H_2O meter)

ρ_{oil} – Density of oil in the subsurface (kg/m^3)

ρ_{gas} – Density of gas in the subsurface (kg/m^3)

α – fault block rotation angle

γ – original fault dip

δ – total amount of rotation of fault block, kroneker delta function in Appendix 1

W_o^i – Old width of the i th fault block

W_n^i – New width of the i th fault block

Z_c^i – Centroid elevation of the i th fault block

X_c^i – Centroid position in the x -direction of the i th fault block

q_p – Rate of petroleum production (m^3/yr)

ρ_p – petroleum density (kg/m^3)

N, $kg\cdot m/s^2$; J, N-m; W, J/s

APPENDIX 3

RIFT2D INPUT DATA FILE DESCRIPTION

DATA FILE TITLE

<u>Line/ Item</u>	<u>Variable</u>	<u>Format</u>	<u>Description</u>
1	Title	A79	Data file title printed out to output and plot file.

SIMULATION CONTROL PARAMETER DATA

<u>Line/ Item</u>	<u>Variable</u>	<u>Format</u>	<u>Description</u>
2	Title	A79	Header Line
3	Title	A79	Header line containing variable names
4	NCOLS	I-Free	Number of nodal columns in finite element mesh.
4	IOUT	I-Free	Print out Flag: IOUT = 0: Only print out simulation control data and computed heads, temperatures, Darcy velocities, and petroleum generation parameters. IOUT = 1: Echo input data and print out computed heads, temperatures, Darcy velocities, and petroleum generation parameters. IOUT = 2: Echo input data; print out computed local and global finite element stiffness matrices; print out computed heads, temperatures, Darcy velocities, and petroleum generation parameters. It is usually sufficient to use either IOUT = 0, 1.
4	IPRINT	I-Free	Number of time steps between print outs of field variables to output file and graphics files of computed heads, temperatures, Darcy velocities, and petroleum generation parameters. IPRINT applies to units 8 and 9 (rift.out and rift_tec.dat).
4	ISKIP	I-Free	Number of nodes to skip when printing out computed heads, temperatures, Darcy velocities, petroleum generation parameters, etc. Using a large value of ISKIP (e.g., ISKIP = 10) greatly reduces the size of the output.
4	IPRFST	I-Free	Number of time steps before printed output begins. IPRFST applies to UNITS 8 and 11.
4	MAXIT	I-Free	Maximum number of solute transport time steps.

SIMULATION CONTROL PARAMETER DATA (continued):

<u>Line/ Item</u>	<u>Variable</u>	<u>Format</u>	<u>Description</u>
5	Title	A79	Header line containing variable names
6	IHEAT	I-Free	Flag to determine whether heat transport equation is solved.
			To solve the heat equation, set IHEAT=1. For isothermal calculations, set IHEAT=0.
6	IBRINE	I-Free	Flag to determine whether solute transport equation is solved. Set IBRINE=1 to solve for solute transport, set IBRINE=0 to neglect salinity affects.
6	ICOUP	I-Free	Flag to determine whether to solve the ground water flow and heat transport equations in a coupled manner (ICOUP=1). This should be done for free-convection problems. For forced convection, set ICOUP=0.
6	IFLOW	I-Free	Flag to determine whether to solve the ground water flow equation. Set IFLOW=1 to solve for ground water flow, IFLOW=0 if you don't want to compute hydraulic heads. Typically, this parameter (and IHEAT) is set to 0 when the user is creating a new data set and wishes to see what the mesh will look like.
6	IOIL	I-Free	Flag to determine whether to solve the kinetic equations for oil and gas generation. Set IOIL=1 to solve for petroleum generation, IOIL=0 if you don't want to solve for oil generation.
6	IPERM	I-Free	Flag to determine which permeability model to use. Set IPERM=1 for log-10linear permeability/porosity relation or IPERM=2 for Carmen-Kozeny permeability/grain size/porosity relationship.
6	IMTAG	I-Free	Flag to determine whether to read in 1 tag for every triangular element (IFLAG=1) or every other element (IFLAG=2) in I1 format. Since the format is I1, you may specify up to nine hydrostratigraphic units. By setting IFLAG=3, every other element tag is read in I2 format (thus the number of tags can range from 1-99).
6	IFLTAG	I-Free	Flag to determine which material tag represents the fault zone. The maximum permeability of this layer will be assigned parallel to the fault (subvertical). The tag should be less than or equal to NMAT.

SIMULATION CONTROL PARAMETER DATA (continued):

Line/ <u>Item</u>	<u>Variable</u>	<u>Format</u>	<u>Description</u>
7	Title	A79	Header line containing variable names
8	NTIME	I-Free	Number of time steps in the simulation.
8	DT	R-Free	Time step size (in years).
8	THETA	R-Free	Weighting factor for ground water flow and heat transport solution schemes. Set THETA=1 for fully implicit, THETA=0.5 for Crank–Nicholson, THETA=0, for fully explicit. To avoid numerical instabilities and to be able to choose a large time step size, it is recommended that a THETA value equal to or greater than 0.5 be used.
8	SGRAD	R-Free	Salinity gradient (in kg salt /kg solution-m NaCl solution) verses depth. SGRAD is only used if IBRINE=1. Sets initial salinity gradient for solute transport model.
8	NFLT	R-Free	Number of faults across the basin. If NFLT>0 then make sure to set ROTFLAG equal to either 1 (no rotation) or 2 (domino rotation).
8	GAMMA	R-Free	Weighting parameter for solute transport particle move (applied when IBRINE=1). Should be set between 0.2-0.8. Determines fractional distance a particle will be moved across an element in a given time step. If set less than one, will not allow particles to move beyond one element distance from initial position.
8	TBRSTR	R-Free	Time to commence solute transport calculations. If users wishes to commence solute transport calculations after some time period into the run, set TBRSTR to the time in years to start solute transport calculations.
8	DELZMN	R-Free	Prevents calculation of time step size for particle move (applied when IBRINE=1) if elemental thickness is less than DELZMN. Is intended to be implemented when new, thin elements are generated at the land surface.
9	Title	A79	Header line for output section
10-	BEC	R-Free	Exact number of elemental columns for each fault block (1 to NFLT+1).
10-	BER	R-Free	Maximum number of elemental rows for each fault block (1 to NFLT+1).

OUTPUT DATA

<u>Line/ Item</u>	<u>Variable</u>	<u>Format</u>	<u>Description</u>
11	Title	A79	Header line for output section
12	Title	A79	Header line containing variable names
13	PTEC	I-Free	Output flag to print TECPLOT formatted output. Set PTEC=1 to generate TECPLOT output files. The total number of time step output will be NTIME/IPRINT.
13	PEXP	I-Free	Output flag to write EXPLORER formatted output. Set PEXP=1 to generate EXPLORER output files. Set PEXP=0 to prevent file creation. The total number of time step output will be NTIME/IPRINT.
13	PSFC	I-Free	Output flag to print surface heat flow and vertical groundwater discharge data in TECPLOT format. Set PSFC=1 to generate surface heat flow output files. Set PSFC=0 to prevent file creation. The total number of time step printed will be NTIME/IPRFST. This writes to UNIT 50 (file name “sfc_tec.dat”).
13	PELEM	I-Free	Output flag for time dependent parameters for elements specified below by variable NREL. Set PELEM=1 to generate elemental output files. Set PELEM=0 to prevent file creation. Up to six elements may be specified using NNR. This writes to UNIT 66-71 (file names are “elem1_tec.dat, elem2_tec.dat, elem3_tec.dat, elem4_tec.dat, elem5_tec.dat, elem6_tec.dat”).
13	NNR	I-Free	Total number of elements for which time-dependent output is required. Be sure that PELEM=1 if NNR is non-zero. The total number of time steps will be printed NTIME/IPRFST. This writes to UNIT 60.
13	NUMWEL	I-Free	Number of nodal columns (up to 6) for which time dependent output is desired. The total number of time steps that will be printed is NTIME/IPRFST. This writes to UNIT 55-60. This TECPLOT formatted output will sequentially store all profiles and time steps in one file (“prf1_tec.dat to prf6_tec.dat”). Note that the header if NUMWEL=0, the two lines must be included in the data deck under the COLUMN OUTPUT DATA section (Title, WELLNM).
13	MSL	I-Free	Mean sea level elevation (in m) used in sine function boundary condition for flow equation when IHCHK=3.

ELEMENTAL OUTPUT DATA

<u>Line/ Item</u>	<u>Variable</u>	<u>Format</u>	<u>Description</u>
14	Title	A79	Header line containing variable names
15-	COUNTER	I-Free	Integer counter for user's convenience.
15-	NREL	I-Free	Element number for which time dependent output is required. The total number of time steps will be printed NTIME. This writes to UNIT 65-70.

COLUMN OUTPUT DATA

<u>Line/ Item</u>	<u>Variable</u>	<u>Format</u>	<u>Description</u>
16-	Title	A79	Header line containing variable names
17-	WELLNM	A20	Well or column name/identifier for column output.
17-	WELLID	I5	Column number for which depth dependent data is written to output file. Allows user to compare observed and computed pressures and temperatures in wells. The total number of time steps will be printed NTIME/IPRINT. This writes to UNIT 55-60.

NUMBER OF HYDROSTRATIGRAPHIC UNITS

<u>Line/ Item</u>	<u>Variable</u>	<u>Format</u>	<u>Description</u>
18	Title	A79	Header line
19	Title	A79	Header line containing variable names
20	NMAT	I-Free	Number of hydrostratigraphic units (aquifers, aquitards, and source rocks) for which distinct material properties will be read in.

POROUS MEDIA PROPERTY DATA: One set of properties for each of NMAT rock types.

<u>Line/ Item</u>	<u>Variable</u>	<u>Format</u>	<u>Description</u>
21	Title	A79	Header line describing rock unit (eg. aquifer)
22	Title	A79	Header line containing variable names
23–	PM1(n)	R-Free	First permeability–porosity coefficient of the n th hydrostratigraphic unit used by RIFT2D [$\log_{10}(k_x) = PM1 + PM2 \cdot PHI$ in m^2]. Only used in if log(k)/linear permeability model is used (IPERM=1).
23–	PM2(n)	R-Free	Second permeability–porosity coefficient of the n th hydrostratigraphic unit used by RIFT. If PM1 = -13 and PM2=0.0, then $k_x = 10^{-13} m^2$. Only used in if log(k)/linear permeability model is used (IPERM=1).
23–	ANS(n)	R-Free	Permeability anisotropy (k_x/k_z) of the n th hydrostratigraphic unit. If ANS = 10, then $k_z = k_x/10$.
23–	GDIAM(n)	R-Free	Characteristic grain diameter (in m) of n th hydrostratigraphic unit. Only used in if Carmen-Kozeny permeability model is used (IPERM=2).
24	Title	A79	Header line containing variable names
25–	TKF(n)	R-Free	Thermal conductivity of the fluid phase of the n th hydrostratigraphic unit (in $W/m \cdot ^\circ C$).
25–	TKS(n)	R-Free	Thermal conductivity of the solid phase of the n th hydrostratigraphic unit (in $W/m \cdot ^\circ C$).
25–	ALPHA(n)	R-Free	Thermal expansivity coefficient for the fluid phase of the n th hydrostratigraphic unit (in $1/\circ C$).

POROUS MEDIA PROPERTY DATA (continued)

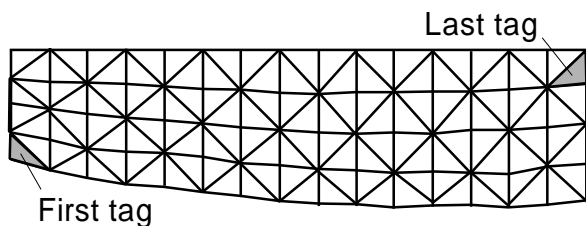
<u>Line/ Item</u>	<u>Variable</u>	<u>Format</u>	<u>Description</u>
26	Title	A79	Header line containing variable names.
27-	CVF(n)	R-Free	Heat capacity of the fluid of the n^{th} hydrostratigraphic unit (in calories/kg-°C).
27-	CVS(n)	R-Free	Heat capacity of the solid of the n^{th} hydrostratigraphic unit (in calories/kg-°C).
27-	LDIS(n)	R-Free	Longitudinal thermal dispersivity of the n^{th} hydrostratigraphic unit (in m).
27-	TDIS(n)	R-Free	Transverse thermal dispersivity of the n^{th} hydrostratigraphic unit (in m).
28	Title	A79	Header line containing variable names
29-	PHI_O(n)	R-Free	First coefficient in exponential porosity–effective stress relationship of the n^{th} hydrostratigraphic unit used by RIFT. Signifies the porosity at the land surface (m^3/m^3).
29-	BETA(n)	R-Free	Second coefficient porosity in exponential porosity–effective relationship of the n^{th} hydrostratigraphic unit used by RIFT (in 1/Pa). BETA corresponds to the natural log of the rate of change of porosity with depth of a sedimentary layer.
29-	PHI_IR(n)	R-Free	Irreducible porosity used in exponential porosity–effective relationship of the n^{th} hydrostratigraphic unit used by RIFT (in m^3/m^3). PHI_IR represents the minimum porosity at depth (dimensionless).
29-	BETA_UL(n)	R-Free	Second coefficient porosity in exponential porosity–effective relationship of the n^{th} hydrostratigraphic unit used by RIFT2D (in 1/Pa). BETA corresponds to the natural log of the rate of change of porosity with depth of a sedimentary layer. BETA_UL replaces BETA during uplift events account for hysteresis effects of loading/unloading. The parameter is only used when ICASE=3.
29-	DIF(n)	R-Free	Molecular diffusion coefficient of the n^{th} hydrostratigraphic unit (in m/yr^2).
29-	RHOS(n)	R-Free	Density of the solid of the n^{th} hydrostratigraphic unit (in kg/m^3).

POROUS MEDIA PROPERTY DATA (continued)

Line/ <u>Item</u>	<u>Variable</u>	<u>Format</u>	<u>Description</u>
30	Title	A79	Header line containing variable names
31-	PERCT1(n)	R-Free	Fraction of Type 1 organic of the n th hydrostratigraphic unit (PERCT1 + PERCT2 + PERCT3 = 1.0).
31-	PERCT2(n)	R-Free	Fraction of Type 2 organic of the n th hydrostratigraphic unit.
31-	PERCT3(n)	R-Free	Fraction of Type 3 organic of the n th hydrostratigraphic unit.
31-	TOC(n)	R-Free	Total organic matter (in g/kg of the n th hydrostratigraphic unit.

MATERIAL TAG DATA

<u>Line/ Item</u>	<u>Variable</u>	<u>Format</u>	<u>Description</u>
32	Title	A79	Header line
33-	MAT(n)	132I1	Porous material integer tag that specifies rock properties of triangular finite elements. Each line is intended to represent a row of one fault block (or an entire basin if NFLT=0). To read one tag per element column set IMTAG=1. To read two tags per element column set IMTAG=2 (one for each triangle). The material tag data is read in by the program from bottom to top from left to right of each fault block (or the entire sedimentary basin if NFLT=0). Thus, the first MAT tag read in corresponds to the element in the lower left-hand corner of a given fault block. The last MAT tag to be read in corresponds to the element in the upper right hand corner of a given fault block. If you have more than 132 nodal columns (and thus 132 columns of triangular element pairs) then you must continue the MAT tags for that sedimentary layer on the next line. You need BER rows of material tags in the data file. <i>Note that you must read in as many MAT tags as are needed to represent the maximum basin thickness during basin evolution.</i> The spare tags are used as additional sedimentary layers are deposited. Specifying too few elemental columns is a common cause of RIF2D run-time errors.



FAULT BLOCK CONTROL DATA

<u>Line/ Item</u>	<u>Variable</u>	<u>Format</u>	<u>Description</u>
34	Title	A79	Header line
35	Title	A79	Header line containing variable names
36	ROTFLAG	I-Free	Rotation control flag. If ROTFLAG=0 and NFLT is 0 then vertical subsidence occurs and layers may deform. If ROTFLAG=1 and NFLT>0, subsidence is accommodated by fault block motion using piano key tectonics (vertical direction only). Elements and sedimentary layers don't deform. If ROTFLAG=2 and NFLT>0, the domino-style subsidence occurs. Elements and sedimentary layers don't deform.
36	OMEGA	I-Free	Total rotation per tectonic time period (degrees). Note that this parameter controls basin deformation independent of the number of time steps or time step length.
36	DELZ	R-Free	Element thickness (m) for each element. This parameter is only used when ROTFLAG>0.
36	INIT_ROWS	I-Free	Initial number of element rows as the start of the start of the simulation. This parameter is only used when ROTFLAG=0. If ROTFLAG=0, then DELZ is used to specify element thickness in each column. The thickness of the initial elements in a column using INIT_ROWS is based on initial thickness of the column and the initial number of rows specified (ZMAX(n) - ZMIN(n))/INIT_ROWS). This variable must be set to 2 or greater when ROTFLAG=0.
37	Title	A79	Header line containing variable names
38-	COUNTER	I-Free	Counter; 1 entry for each fault block required
38-	CENTZ(n)	R-Free	Vertical depth of centroid for n th fault block below the land surface (in m).

TECTONIC TIME PERIOD CONTROL DATA

<u>Line/ Item</u>	<u>Variable</u>	<u>Format</u>	<u>Description</u>
39	Title	A79	Header line
40	Title	A79	Header line containing variable names
41–	VZTIM2– VZTIM7	R-Free	Time in years to when a change in the boundary conditions should occur for sediment compaction (ie. tectonic subsidence, uplift, and erosion), ground water flow (ie. water table configuration), and heat transfer (ie. surface temperature and basal heat flow) equations. Set these variables to a very large value (eg. larger than DT•NTIME) if you don't wish to change the boundary condition data during the simulation.
42	Title	A79	Header line containing variable names
43–	VZTIM8– VZTIM13	R-Free	Time in years to when a change in the boundary conditions should occur for sediment compaction.

BASIN SUBSIDENCE/UPLIFT CONTROL DATA

<u>Line/ Item</u>	<u>Variable</u>	<u>Format</u>	<u>Description</u>
44	Title	A79	Header line
45	Title	A79	Header line containing variable names
46	Title	A79	Fault block header
47-	COUNTER	I-Free	Counter. NCOL entries required.
47-	X(n)	R-Free	Horizontal position of n^{th} nodal column in meters from left edge of the basin. Two nodal columns (in the same position) must be defined for each fault plane.
47-	VZTBASE(n)	R-Free	Initial tectonic subsidence rate for n^{th} nodal column in m/yr. If VZTBASE(n) is negative, subsidence will occur. If VZTBASE(n) is positive, uplift will occur (Fig. 7).
47-	VZTINC(n)	R-Free	Incremental change in tectonic subsidence rate such that $VZT(n) = VZTBASE(n) + VZTINC(n)$ (in m/yr ²).
47-	VER(n)	R-Free	Erosion rate at the land surface in m/yr This is only applied with ICASE(n)=3.
47-	ZMAX(n)	R-Free	Land surface elevation (in m above datum) above datum at start of simulation for n^{th} column in meters.
47-	ZMIN(n)	R-Free	Elevation (in m above datum) of the base of basin at start of simulation for n^{th} column in meters.
47-	ICASE(n)	I-Free	Flag to specify type of tectonic boundary condition applied to n^{th} column. If ICASE=0, the land surface node is pinned and all nodes below the land surface move up or downwards depending on the value of VZT(n). Under this condition, the grid does not deform. Setting ICASE=1 is similar to ICASE=0 except that calculated porosity changes will deform the grid. If ICASE=2, then the entire column of nodes moves up or down without sediment compaction. Note that the heads along the column are adjusted (increased) if uplift occurs to account for changes in elevation head. If ICASE=3, then erosion occurs at the land surface. The erosion rate is determined by the (positive) value of VER(n).
47-	GRDFAC(n)	I-Free	Grid multiplier that determines the width of new elements generated at the land surface. The critical width [ZCHK(n)] can be estimated in the following manner for a nodal column: $ZCHK(n) = VZT(n) \cdot GRDFAC(n) \cdot DT$. Thus choose a relatively large value of GRDFAC(n) for a coarsely discretized grid and a small value of GRDFAC(n) for a finely discretized solution domain. For example, if we desire a elemental width of 100 m, and we have a time step size of 10,000 years and a subsidence rate of 10^{-5} m/yr, the GRDFAC should be set to 1000. It is highly recommended to use uniform values of GRDFAC for a given tectonic time period. Also, the above discussion only applies when

ROTFLAG=0 and ICASE<2. If ROTFLAG>0, then the mesh thickness is controlled by a DELZ described above.

WATER-TABLE BOUNDARY CONDITION DATA

<u>Line/ Item</u>	<u>Variable</u>	<u>Format</u>	<u>Description</u>
48	Title	A79	Header line
49	Title	A79	Header line containing variable names
50–	IHCHK	I-Free	Integer flag to determine whether to vary imposed water table boundary conditions through time. If IHCHK=1, then HEAD(n)=Z(n) at the land surface (this is often specified with ICASE=2 or 3). If IHCHK=2, then HEAD(n) = HDBASE(n) at the land surface. If IHCHK= 2, then a linear boundary condition is used (see eq. 5.1) over a tectonic time period. IF IHCHK=3, a sine function boundary condition is used (equation 5.2).
50–	THA	R-Free	Time of start of tectonic time period when imposed water table boundary conditions
50–	THB	R-Free	Time of end of tectonic time period when imposed water table boundary conditions
51	Title	A79	Header line containing variable names
52–	COUNTER	I-Free	Nodal column number; NCOLS - NFLT entries required.
52–	HDBASE(n)	R-Free	Initial water table elevation for nodal column in meters.
52–	HDINC(n)	R-Free	Multiplier to adjust linear and sine function water table boundary condition (see equation 5.1 and 5.2; has units of m/yr).

BASEMENT HEAT FLOW BOUNDARY CONDITION DATA

<u>Line/ Item</u>	<u>Variable</u>	<u>Format</u>	<u>Description</u>
53	Title	A79	Header line
54	Title	A79	Header line containing variable names
55-	IJCHK I-Free		Integer flag to determine whether to vary imposed heat flux boundary conditions through time. If IJCHK=1, then a linear boundary condition is imposed (equation 5.1). If IJCHK=2, a sine function boundary condition is used (equation 5.2) and if IJCHK=3, an exponential boundary condition is employed (equation 5.4).
55-	TJA	R-Free	Time of start of tectonic time period when imposed heat flux boundary condition is desired (years).
55-	TJB	R-Free	For IJCHK=2, is the period (in years) for sine function boundary condition. If IJCHK=3, is the denominator in the exponential decay equation for basal heat flow (see equation 5.4).
56	Title	A79	Header line containing variable names
57-	COUNTER	I-Free	Nodal column number; NCOLS entries required.
57-	J1BASE(n)	R-Free	Initial basement heat flux across line segment L1 defined in Figure 2.7 in RIFT2D manual in mW/m ² .
57-	J2BASE(n)	R-Free	Initial basement heat flux across line segments L2 defined in Figure 2.7 in RIFT2D manual in mW/m ² .
57-	J1INC(n)	R-Free	Incremental change in basement heat flux across line segment L1 in mW/yr-m ² that over a time step.
57-	J2INC(n)	R-Free	Incremental change in basement heat flux across line segment L2 defined in Figure 2.7 J2INC has units of mW/yr-m ² over a time step.

SURFACE TEMPERATURE BOUNDARY CONDITION DATA

<u>Line/ Item</u>	<u>Variable</u>	<u>Format</u>	<u>Description</u>
58	Title	A79	Header line
59	Title	A79	Header line containing variable names
60–	ITCHK	I-Free	Integer flag to determine whether to vary imposed temperature boundary conditions through time. If ITCHK=1, then a linear boundary condition is used (eq. 5.1) at the land surface. If ITCHK=2, then a sine function boundary condition is used (eq. 5.3).
	TTA	R-Free	Time of start of tectonic time period when imposed temperature boundary condition is desired.
	TTB	R-Free	Period for sine function boundary condition. Only implemented with ITCHK=2.
61–	COUNTER	I-Free	Nodal column number; NCOLS entries required.
62–	TPBASE(n)	R-Free	Initial land surface temperature for nodal column n in °C.
62–	TPINC(n)	R-Free	Incremental change in temperature boundary condition at the land surface node in °C/yr.

SURFACE SOLUTE BOUNDARY CONDITION DATA

<u>Line/ Item</u>	<u>Variable</u>	<u>Format</u>	<u>Description</u>
63	Title	A79	Header line
64	Title	A79	Header line containing variable names
65-	COUNTER	I-Free	Nodal column number; NCOLS entries required.
65-	CNBASE(n)	R-Free	Land surface solute concentration in mass fraction (mass solute/mass solution).
65-	NEVAP(n)	I-Free	Integer material tag for solute concentration boundary condition to be specified at the land surface using the value of CEVAP. If the element at the surface along a particular column has the material tag matching NEVAP, then the associated concentration (CEVAP) will be imposed along that column. If NEVAP=0, CNBASE is used instead regardless of what layer is at the land surface. This might be used if a playa layer is at the land surface during a period of basin evolution.
65-	CEVAP(n)	R-Free	Land surface solute concentration associated with material tag NEVAP in mass fraction.
65-	NCLAY(n)	I-Free	Integer material tag for which solute concentration should be specified for a subsurface layer which the user wishes to specify along a nodal column. NCLAY can be used to represent brine formation associated with the dissolution of an evaporite bed
65-	CLAY(n)	R-Free	Associated concentration to be specified for a given subsurface layer (e.g. evaporite bed). The solubility of a given evaporite mineral is often used for CLAY.

CHANGES TO BOUNDARY CONDITION DATA:

Boundary condition data may be modified during the simulation up to 12 times (VZTBM2- VZTBM13) to allow the user to adjust tectonic, hydraulic, and thermal boundary conditions. The input format is almost identical to the above input boundary condition data except that some variables are removed. The variables are described in more detail in the above portion of APPENDIX 3. This data is read in subroutine BCREAD.

MESH BOUNDARY CONDITION DATA

<u>Line/ Item</u>	<u>Variable</u>	<u>Format</u>	<u>Description</u>
66	Title	A79	Header line
67	Title	A79	Header line containing variable names
68-	Counter	I-Free	Nodal column number. NCOL lines required.
68-	VZTBASE(n)	R-Free	Initial tectonic subsidence/uplift rate for nodal column in m/yr.
68-	VZTINC(n)	R-Free	Incremental change in tectonic subsidence rate in m/yr ² .
68-	VER(n)	R-Free	Erosion rate at the land surface in m/yr described above.
68-	ICASE(n)	I-Free	Flag to specify type of tectonic boundary condition to apply for n th nodal column.
68-	GRDFAC(n)	I-Free	Grid multiplier that determines the width of new elements generated at the land surface before described above.

WATER TABLE BOUNDARY CONDITION DATA:

<u>Line/ Item</u>	<u>Variable</u>	<u>Format</u>	<u>Description</u>
69	Title	A79	Header line
70	Title	A79	Header line containing variable names
71	IHCHK	I-Free	Integer flag to determine type of water table boundary condition to apply (described above).
71	THA	R-Free	Time of start of tectonic time period.
71	THB	R-Free	Period of sine function boundary condition (applied when IHCHK=3).
71	Msl	R-Free	Sea level elevation used to impose sinusoidal head boundary condition when IHCHK=3.
72	Title	A79	Header line containing variable names
72	Counter	I-Free	Nodal Column number. NCOLS-NFLT entries required.
72	HDBASE(n)	R-Free	Initial water table elevation for nodal column in meters.
72	HDINC(n)	R-Free	Incremental change in water table boundary condition in m/yr.

SURFACE SOLUTE BOUNDARY CONDITION DATA:

<u>Line/ Item</u>	<u>Variable</u>	<u>Format</u>	<u>Description</u>
73	Title	A79	Header line
74	Title	A79	Header line containing variable names
75	COUNTER	I-Free	Nodal column number; NCOLS entries required.
75	CNBASE(n)	R-Free	Land surface solute concentration specified (mass solute/mass solution).
75	NEVAP(n)	I-Free	Integer material tag for solute concentration boundary condition to be specified at the land surface using the value of CEVAP (described above).
75	CNBASE(n)	R-Free	Land surface solute concentration associated with material tag NEVAP in mass fraction .
75	NCLAY(n)	I-Free	Integer material tag for which solute concentration should be specified for a subsurface layer which the user wishes to specify along a nodal column.
75	CLAY(n)	R-Free	Associated concentration to be specified for a given evaporite layer. The solubility of a given evaporite mineral is often used for CLAY.

FAULT BLOCK ROTATION CONTROL DATA:

<u>Line/ Item</u>	<u>Variable</u>	<u>Format</u>	<u>Description</u>
76	Title	A79	Header line
77	Title	A79	Header line containing variable names
78	OMEGA	I-Free	Total rotation per tectonic time period (degrees).
78	IPRINT	R-Free	Number of time steps between printing output.
79	Title	A79	Header line containing variable names
80-	COUNTER	I-Free	Counter; 1 entry for each fault block (NFLT+1).
80-	CENTZ(n)	R-Free	Vertical depth of centroid for n th fault block in m.

MATERIAL TAG DATA:

<u>Line/ Item</u>	<u>Variable</u>	<u>Format</u>	<u>Description</u>
81	Title	A79	Header line
82-	MAT(n)	132I1	Porous material tag that specifies rock properties of triangular finite element (described above).